

**TUC – TECHNICAL UNIVERSITY OF CRETE  
SCHOOL OF MINERAL RESOURCES ENGINEERING**

Master thesis

**Evaluation of Plio-Pleistocene formations in Katakolon  
(Greece) as sources of biogenic gas**

---

Makri Vagia Ioanna

Examination committee

---

Prof. N. Pasadakis      Supervisor

Dr. D. Marinakis

Dr. K. Nikolaou

Chania, 2018

*A MSc thesis submitted in partial fulfilment of the requirements for the degree  
of Master of Science in Petroleum Engineering*

*The MSc Program in Petroleum Engineering of the Technical University of  
Crete was attended and completed by Mrs. Makri Vagia Ioanna due to the  
HELPE Group Scholarship award*

© Copyright by Makri Vagia Ioanna

All Rights Reserved

## **Acknowledgments**

This dissertation has been carried out at TUC in cooperation with Energean Oil & Gas. I would like to express my sincerest gratitude to my supervisor, Professor Nikolaos Pasadakis for his invaluable suggestions and support throughout the entire project.

I would also like to thank Energean Oil & Gas, especially Mr. Panagopoulos George for following up on the dissertation and providing data as well as for his continuous support, valuable advices and thoughtful comments.

I do also wish to express my appreciation to Dr. Konstantinos Nikolaou who guided me through my BSc thesis and whose assistance, comments and suggestions have always been helpful.

Finally, I am grateful to my family for their patience, support and encouragement throughout my studies.

## ABSTRACT

Katakolon oil and gas field is geographically located in Greece, more specifically in the North-Western Peloponnesus both onshore and offshore, while geologically it lies in the external-central Ionian zone. It is a small, yet relatively known field with proven reserves.

Several exploration wells have been drilled in the wider area, facing oil and gas flowing from different layers. Mainly methane hydrocarbon shows appear in the onshore area which is mainly associated with biogenic gas while in the offshore area the gas shows are predominantly catagenetic associated with condensate.

The main purpose of this study is the thermal maturity modelling of source rocks in both offshore and onshore locations, in terms of gas generation. Several 1D models are created to model these petroleum systems at individual well point locations throughout the field, utilizing PetroMod 2017.1, Schlumberger software. The examined petroleum systems refer to an onshore petroleum system with Plio-Pleistocene source rocks, prone to biogenic gas generation as well as to an offshore petroleum system with Triassic source rocks, prone to both oil and gas generation.

Biogenic gas generation seems to be favoured regarding all the prevailing conditions in the onshore models. Rapid sedimentation, low geothermal gradient, shallow burial depth and the immaturity of the source rocks reinforce the modelling result of ongoing biomethane generation and expulsion. Still, in one of the onshore wells (MY-1) erosion events affect negatively the generation of biomethane.

Different case scenarios in terms of source rock characteristics are examined for the offshore Katakolon models, since the evaporites have not been fully penetrated yet. Calibration has been performed for all the models, showing the chief importance of the overburden sediment amount and of the paleo-heat flow trend to the maturation of the underlying source rocks.

A picture of maturity and generation potential at each point location is drawn indicating that source rock layers in the offshore West Katakolon field lie in the catagenesis stage. Generation of hydrocarbons has begun from around 200Ma, while gas expulsion in most case scenarios is not initiated prior to the trap formation. Even though gas expulsion is not possible from all the studied case scenarios, the gas entrapment is achieved from the ones that are, since the trap formation takes place between Langhian and early Zanclean (16-5Ma).

## Table of Contents

Introduction.....	1
1.1. Study area.....	1
1.2. Katakolon gas field.....	1
1.3. Biogenic and thermogenic gas in the wider Katakolon area .....	2
1.4. Main purpose.....	2
Geological setting.....	3
2.1. Tectonic evolution .....	3
2.2. Geostratigraphy of the Ionian zone.....	5
Oil and gas generation.....	10
3.1. Petroleum systems.....	10
3.2. Organic matter maturity evolution.....	10
3.3. Thermal maturity.....	11
Theoretical background of 1D maturity modelling .....	13
4.1. Fundamentals.....	13
4.2. Software input.....	14
This study .....	19
5.1. Introduced data.....	19
5.2. Model frame.....	20
5.3. Rock-Eval analysis.....	21
Onshore models.....	22
6.1. Depositional environment.....	22
6.2. Calibration parameters .....	23
6.3. Input data .....	24
6.4. ALF-1 model .....	26
6.4.1. Calibration of the final model.....	26
6.4.2. Timing of biomethane generation and expulsion .....	28
6.5. MY-1 model.....	32
6.5.1. Calibration of the final model.....	32
6.5.2. Timing of biomethane generation and expulsion .....	34
6.6. Conclusions .....	37
Offshore models .....	39
7.1. Case scenarios .....	39
7.2. Calibration parameters .....	40
7.3. Input data .....	40

7.4.	WK-1 models.....	41
7.4.1.	Calibration of the final model.....	41
7.4.2.	Timing of HC generation and expulsion.....	45
7.5.	WK-2 model.....	48
7.5.1.	Model frame.....	48
7.5.2.	Model input.....	49
7.5.3.	Calibration of the final model.....	50
7.5.4.	Timing of HC generation and expulsion.....	52
7.6.	Case study.....	55
7.6.1.	Model frame.....	55
7.6.2.	Timing of HC generation and expulsion.....	57
7.7.	Discussion.....	61
7.7.1.	Appendix A.....	63
7.7.2.	Appendix B.....	64
	West Katakolon 2D modelling.....	66
8.1.	2D model.....	66
8.2.	Discussion.....	68
	References.....	70

## List of Figures

Figure 1: Map of the geotectonic units of Western Greece where the study area is indicated by the red border (modified after Marnelis et al., 2007).....	1
Figure 2: Geological map of Western Greece and adjacent regions, from Maravelis et al. (2012). .....	4
Figure 3: Generalized lithostratigraphic column of the Ionian zone (modified after Karakitsios and Rigakis, 2007 and Maravelis et al., 2014).....	9
Figure 4: Organic matter maturity evolution through diagenesis, catagenesis and metagenesis, from Bahlurbg and Breitzkreuz (2004) .....	13
Figure 5: Location map of the examined point locations (wells) in the West Katakolon area. ....	19
Figure 6: Burial history preview of the WK-1 model. ....	21
Figure 7: Temperature profiles of the onshore wells. ....	23
Figure 8: VR calibrations, ALF-1 model. ....	27
Figure 9: Temperature profile, ALF-1 model .....	28
Figure 10: Source rock's TR (%), ALF-1 model.....	29
Figure 11: Biomethane generation rate per TOC mass, ALF-1 .....	30
Figure 12: Expulsion of biomethane, ALF-1 .....	30
Figure 13: Biomethane generation rate per TOC mass, ALF-1 .....	31
Figure 14: Expulsion of biomethane, ALF-1 .....	31
Figure 15: VR (%Ro) calibration, MY-1 model. ....	33
Figure 16: Effective porosity calibration, MY-1 model.....	34
Figure 17: Biomethane generation rate per TOC mass, MY-1 .....	35
Figure 18: Biomethane expulsion, MY-1 .....	35
Figure 19: Biomethane generation rate per TOC mass, MY-1 .....	36
Figure 20: Biomethane expulsion, MY-1 .....	36
Figure 21: Source rocks' TR (%), MY-1 model.....	37
Figure 22: Temperature profile, WK-1. ....	40
Figure 23: Maturity (%Ro) final calibration fit, WK-1 models. ....	42
Figure 24: Mean maturity time plot (%Ro), WK-1 models .....	42
Figure 25: BHT trend, WK-1 models. ....	44
Figure 26: Temperature distribution through the burial history of WK-1 point location. ....	44
Figure 27: Generation rate of gas per TOC mass utilizing Perpper&Corvi_TIIS. ....	46
Figure 28: Gas expulsion, utilizing Perpper&Corvi_TIIS. ....	46
Figure 29: Generation gas rate per TOC mass, utilizing Burnham_TIII. ....	47
Figure 30: Gas expulsion, utilizing Burnham_TIII.....	47

Figure 31: Burial history, WK-2 model.....	49
Figure 32: Maturity (%Ro) trend with respect to depth.....	50
Figure 33: Maturity and Temperature time plots of the Evaporitic formation.....	50
Figure 34: Gas generation rate of the deepest evaporitic part, WK-2.....	53
Figure 35: Gas generation rate of the middle evaporitic part, WK-2.....	53
Figure 36: Expulsion onset of the deepest evaporitic part, WK-2.....	54
Figure 37: Expulsion onset of the middle evaporitic part, WK-2.....	54
Figure 38: Burial history Preview, case study.....	55
Figure 39: Maturity (%Ro) trend with respect to depth.....	56
Figure 40: Maturity progress time plot for both evaporites and Vigla shale member.....	56
Figure 41: Distribution of temperature through the entire burial history.....	57
Figure 42: Generation rate of gas per TOC mass utilizing Perpper&Corvi_TIIS and 4000m thick flysch.....	59
Figure 43: Gas expulsion onset, TIIS kinetics, 4000m thick flysch deposition.....	59
Figure 44: Generation gas rate per TOC mass utilizing Burnham_TIII and 4000m thick flysch deposition.....	60
Figure 45: Gas expulsion onset, TIII kinetics, 4000m thick flysch deposition.....	60
Figure 46: Plots indicating the hydrocarbon generation type for the onshore models (left column), offshore models (right column).....	63
Figure 47: 2D model of the West Katakolon field, modified after Xenopoulos and Roussos (2007) and Maravelis et al. (2014).....	66
Figure 48: Source rock TR (%) distribution in West Katakolon offshore field.....	67
Figure 49: Source rock's expulsion onset in West Katakolon offshore field.....	68

## List of Tables

Table 1: Geochemical parameters describing the level of thermal maturation.....	12
Table 2: General interpretation scheme for vitrinite reflectance and compensated kerogen types for the main stages of HC generation, modified from Dembicki, (2009).....	17
Table 3: Rock-Eval analysis data of Pliocene and Triassic outcrop samples, taken from a neighbouring location of the Katakolon onshore area.....	22
Table 4: Boundary conditions of the ALF-1 model.....	25
<b>Table 5:</b> Sublayer source rocks' characteristics.....	28
Table 6: General picture of the onshore models' main input.....	64

## ABBREVIATIONS

**BCS:** Refers to the Best Case Scenario of the WK-1 and WK-2 models

**BHT:** Bottom-Hole Temperature (BHTs: plural)

**BPSM:** Basin Petroleum System Modelling

**FM:** Formation (fms: plural)

**HC:** Hydrocarbons

**HF:** Heat Flow ( $\text{mW/m}^2$ )

**HI:** Hydrogen Index ( $\text{mgHC/gTOC}$ )

**MCS:** Refers to the Middle Case Scenario of the WK-1 and WK-2 models

**OI:** Oxygen Index

**PI:** Productivity Index [ $S1/(S1+S2)$ ]

**PS:** Petroleum System

**PSM:** Petroleum System Modelling

**PWD:** Paleo-Water Depth

**RE:** Rock-Eval analysis

**SWIT:** Sediment Water Interface Temperature ( $^{\circ}\text{C}$ )

**TOC:** Total Organic Carbon (wt.%)

**TR:** Transformation ratio. It reveals the relative percentage conversion of organic matter present in the source rock formation which is converted to hydrocarbons.

**VR:** Vitrinite reflectance. It is a measure of the percentage of incident light that is reflected from the surface of vitrinite particles in a sedimentary rock given in units of reflectance, %Ro.

**WCS:** Refers to the Worst Case Scenario of the WK-1 and WK-2 models



# Chapter 1

## Introduction

### 1.1. Study area

Geographically, the study area is located in western Greece and more specifically, in the north-western Peloponnesus. Geologically, is located in the outer Hellenic arc, which comprises the south branch of the Alpine orogenic system (Kamperis et al, 2000). From middle-upper Miocene, subduction of the African plate under the Euro-Asian plate takes place in the wider area, resulting compression stresses and the subduction of the examined Ionian zone under the most internal (eastern) zones.

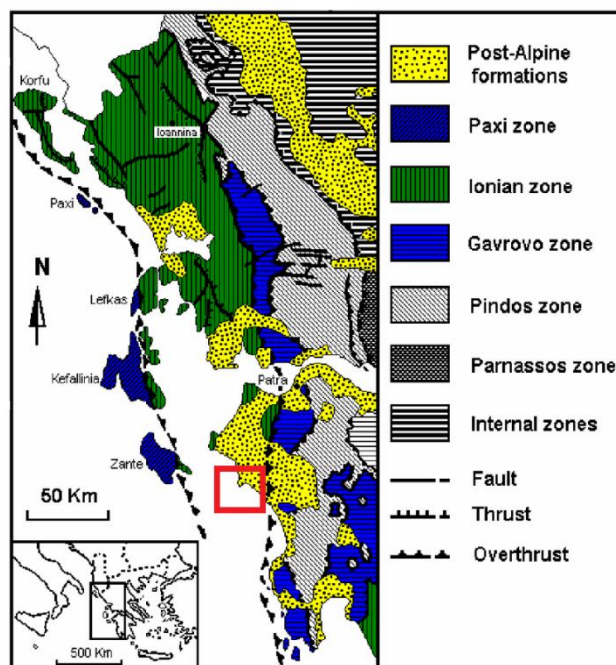


**Figure 1:** Map of the geotectonic units of Western Greece where the study area is indicated by the red border (modified after Marnelis et al., 2007).

### 1.2. Katakolon gas field

In the onshore area of Katakolon, during 1980 a small gas field was discovered that gave some very promising gas horizons reported from two different wells (KA-101 and KA-102). Wells drilled in most of NW Peloponnesus have indicated HC gas shows and the main concentrations are found in Plio-Pleistocene sediments and more specifically Peristeri and Vounargo formations, described in the

post-Alpine/orogenic sequence section. In the late Cenozoic sediments, most of the gases found are dry, although most of the gas seeps in the area are wet gases (Rigakis et al, 2001).

As reported by Rigakis et al. (2001), most offshore gases found in the West Katakolon oil field, tested by the wells, which will be discussed later on, appear to be catagenetic associated with condensate. The same happens with gases located in the evaporitic formation and sometimes this type of gases are found in shallower depositions, such as the Neogene sediments. However, this is possible only in case of tectonism. Whilst there is lack of isopic data, West Katakolon gases can be roughly classified in biogenic and catagenetic.

### **1.3. Biogenic and thermogenic gas in the wider Katakolon area**

Gas seepages throughout the Katakolon bay (onshore and offshore) intrigued the scientists' interest and are considered to be one of the biggest thermogenic seepage zones in Europe (Etiope et al., 2013), yet the biggest methane seep in Greece. As reported by Kamperis et al. (2001), most of the onshore located gases in the Late Cenozoic clastic sediments are dry, while the gases associated to the pre-Neogene basement, either the carbonatic or the Triassic evaporites are characterized as catagenetic, thus wet gases.

As Kokinou et al. (2005) and Kamperis et al. (2000) have suggested, the gases found in the Plio-Pleistocene sediments from the onshore wells are of microbial origin and they are characterized as biogenic gas. This type of gas in this area is the most obvious in terms of generation, since all the requirements are met. In further detail, the burial depth is less than 2000m, the recorded temperature gradient is far below the mean average one, rapid sedimentation has occurred in anoxic environment and also the reported  $C1/(C2+C3)$  ratio is more than 1000 in all the Cenozoic clastic sediments. Hereby, the generation of biogenic gas is favoured under the prevailing conditions during Plio-Pleistocene.

According to a study conducted by (Etiope et al., 2013) that utilises isopic data, it is suggested that the wider Katakolon area is related to a petroleum system of a Triassic source rock. This opinion is intensified by means of present gas seepages, which with respect to Etiope and Ciccioli (2009) reveal a similarity to the global average ratios of thermogenic seeps. However, the originating source rock of this thermogenic gas is still under research, yet the organic rich Triassic organic rich intercalations and the Vigla shale member are two source rock candidates.

### **1.4. Main purpose**

In the present study, two petroleum systems are examined; one of Plio-Pleistocene age in which the generation of biogenic gas is investigated and one with Triassic source rocks with all the reservoir

formations entrapped in a pseudo anticline of Mio-Zanclean age, while case studies with Triassic and upper Cretaceous source rocks are also investigated. The application of petroleum system modelling is used to examine the paleo-conditions in both locations and determine whether they had the potential for hydrocarbon generation.

This dissertation is divided in three main parts. Firstly, a theoretical part in order to ensure the comprehension of both the geology of the area and the organic matter's maturation process. Secondly, PSM is carried out for the onshore region, examining the source rock maturities, aiming to answer if the Plio-Pleistocene succession is able to produce biogenic gas. Then, PSM is also carried out for the offshore region where the maturities of the Triassic and upper Cretaceous potential source rocks are examined; the main objective of this part is to examine the potential of these source rocks in terms of thermogenic gas generation. Finally, the maturity of the Triassic source rocks is further examined by utilising 2D BPSM.

1D maturity modelling is carried out in PetroMod 2017.1, Schlumberger software with the use of data provided by Energean Oil & Gas. More specifically, these data refer to geochemical analyses which are prepared by: Robertson research International limited for the WK-1 well, the Public Petroleum Enterprise for the WKA-2 well which is interpreted by Rigakis in 1984, the Core laboratories in 1987 for the ALF-1 well with a temperature profile created by Schlumberger through logging, the Rompetrol for MY-1 well and for SK-1 is prepared by BeicipFranlab in 1982.

## **Chapter 2**

### **Geological setting**

#### **2.1. Tectonic evolution**

Greece is subdivided in geotectonic terranes, which are further divided into isopic zones as they were named by Aubouin (1959) and are found to be parallel to the deformation which will be discussed later on. This isopic zone division is based on their paleogeographic position, the formations from which they are constituted, as well as their evolution through geological time. The wider area of Katakolon, which is located in NW Peloponnesus (western Greece), is exclusively composed of Ionian zone formations, as part of the external/central Ionian zone. This zone is the most external zone of Greece after the Paxi and before Gavrovo and Tripoli zones, which altogether constitute the Hellenide fold-and-thrust belt. It is part of the H1 external geotectonic terrane according to D. Papanikolaou (1989, 1997) and in a wider view Ionian is thrust over the Paxi zone to the west and flanked by the Gavrovo zone to the east.

Developed during the collision and further convergence of the Eurasian and African-Arabian Plate, Hellenide fold-and-thrust belt was created during Mesozoic. Deformation associated with this convergence was expressed as a progressive westward migrating ‘deformation front’, which compressed the previous predominantly extensional basin and platform morphology (IGRS-IFP, 1966; Clement et al., 2000). Prior to this, starting from the Triassic period, Western Greece was part of the Apulian continental block on the southern passive margin of Tethys (Karakitsios and Rigakis, 2007) with a most probable Hercynian basement.

At a mega scale (hundreds of kilometres), the entire Alpine belt is thought out to be the inverted margin of the Neotethyan Ocean as a result of the collision of Apulia and Eurasian plates (de Graciansky et al., 1989). On a smaller, yet mega scale (few tens of kilometres), the various sub basins of the Hellenic Tethyan margin have been inverted to produce the main Hellenic thrust sheets or folded zones. This occurred successively from Eastern to Western zones, thus from internal to external respectively (Karakitsios, 1995).

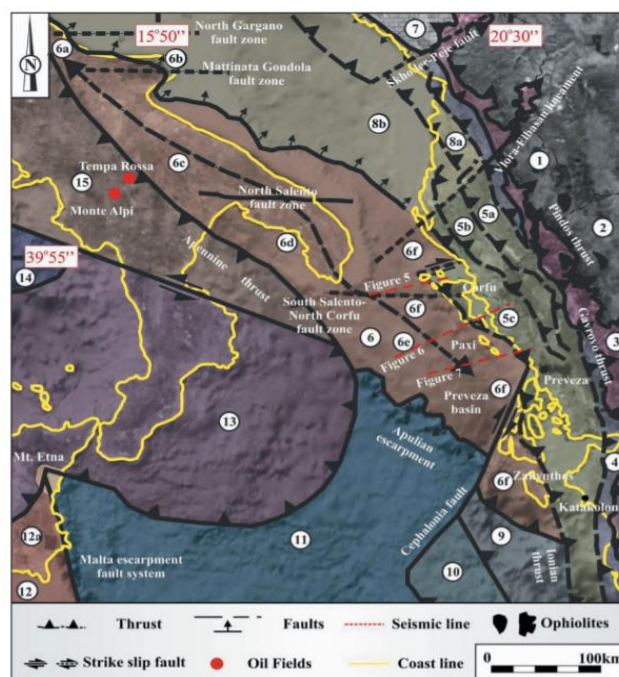


**Figure 2:** Geological map of Western Greece and adjacent regions, from Maravelis et al. (2012).

The yellow line marks the coastline while the red dashed lines mark the seismic reflection profiles. 1) Internal Albanides, 2) Internal Helenides, 3) Pindos zone (Krasta), 4) Gavrovo zone (Kruja), 5a) Internal Ionian zone, 5b) Middle Ionian zone, 5c) External Ionian zone, 6) Apulian platform, 6a) Plateau Rospo, 6b) Gargano promontory, 6c) Murge ridge, 6d) Salento peninsula, 6e) Apulia plateau, 6f) Pre-Apulian (or Paxi) zone 7) Albanian Alps, 8a) Dures basin, 8b) Ionian-Albania basin, 9) Hellenic trench, 10) Mediterranean ridge, 11) Ionian abyssal plain, 12) Africa, 12a) Hyblean plateau, 13) Calabrian arc, 14) South Tyrrhenian Sea, 15) South Apennine

Thrusting commenced in Greece during Liassic, when the most internal oceanic terranes started obduction on the most internal platform terrane which was at that time part of the Eurasian plate. Migrating to the West, the most Eastern Hellenides started being thrustured during the Upper Cretaceous (Maastrichtian) which is considered to be the beginning of the Alpine orogeny. Progressively thrusting reached the Ionian zone in early Miocene times (Smith and Moores, 1974; Robertson and Dixon, 1984). During early Miocene, thrust movements which are the aftereffect of compressional events, affected the already deposited stratigraphy and structure style due to the westward merging of the Ionian Zone (Kamperis et al., 1996). Continuous regional compression resulted in uplift of the Ionian Zone (Kamperis et al., 1996; Zelilidis et al., 2003), delimiting the beginning of its main orogenesis stage during late Miocene, when tectonic structures were developed in the wider area.

## **2.2. Geostratigraphy of the Ionian zone**

This study focuses on the investigation of the central Ionian zone, in the wider Katakolon area. Hence, its geostratigraphy has to be described and further analysed.

The Ionian zone comprises of three distinct stratigraphic sequences (Karakitsios, 1995); A pre-rift sequence, a syn-rift sequence and a post-rift sequence, reflecting the evolution of a first created neritic platform into a pelagic basin.

### **Pre-rift sequence**

The pre-rift sequence consists of the oldest known formations of this zone, namely the Triassic evaporates, the Foustapidima limestone and the Pantokrator limestone sequences. The bottom most known formation is the Triassic evaporitic sequence with a deposition that lasted from lower to middle Triassic. Their thickness is estimated to be more than 1500m, mainly consisting of halite, anhydrite and potassium salts most interbedded with dolomites and with alternating sulphate and carbonate sediments, which were probably deposited in a “sabkha cotier” environment and are only known from borehole data (Jenkins, 1972, Karakitsios, 2007-1)

The Triassic Breccias are evaporites dissolution collapse breccias (Karakitsios and Pomoni – Papaioannou, 1998) and their origin is mainly affiliated with the atmospheric exposure (Karakitsios, 2007-1). These processes are believed to be the reason of the organic richness preservation within the Triassic breccias. Along the sedimentological and diagenetical evolution during Triassic which had a synchronously repeating character, dolomites and dolomitic limestones were deposited and they are found today laminated to evaporites. Following this scenario, it can be accepted that the preservation

of this organic matter was favoured due to evaporitic sedimentation accompanied by eustatic sea level changes (Herbin et al., 1995).

The Triassic evaporites are the bottom most known sequence of the Ionian zone; although the presence of a Hercynian basement is believed to lie below them, yet there is no borehole data. Foustapidima limestones which are located exactly below the Pantokrator limestones overlie this evaporitic sequence having a Ladinian to Rhetian age (Karakitsios and Tsaila-Monopolis, 1988), yet in this study their deposition is assumed to have lasted from Carnian to Rhaetian. Foustapidima limestone deposition is followed by the shallow marine Pantokrator limestones of early Liassic age (Hettangian to Sinemurian) (Aubouin, 1959; IGRS-IFP, 1966; Karakitsios and Tsaila-Monopolis, 1988; Karakitsios, 1990, 1992). The depositional environment of the last mentioned Liassic sequence, is neritic (intertidal environment), regarding the algae and the found sedimentary structures (Karakitsios, 2007-1).

During Liassic, large accommodation space was being created due to strong subsidence which was filled by prolific carbonate sediments, resulting in the build-up of a shallow-water sequence, more than a 1000m thick (Karakitsios 2007-1). As a result the maximum probable pre-rift sequence thickness consisted of carbonate and evaporitic series reaching a maximum thickness of 4200m.

### **Syn-rift sequence**

Exactly after the completion of the pre-rift sequence deposition, beginning during Pliensbachian, extension occurred, culminating in a deep sea marine basin, delimitating the beginning of the syn-rift period. These syn-rift formations correspond to the general deepening of the Ionian area which results in the formation of the so called Ionian basin, which was followed by the internal syn-rift differentiation of the Ionian basin marked by smaller paleogeographic units (Karakitsios, 2007-1). These paleogeographic units were recorded in the prismatic synsedimentary wedges of the syn-rift formations and are aged from Toarcian to Tithonian comprising the deepest part of this half-graben.

The directions of the present synsedimentary structures (e.g. slumps and synsedimentary faults) indicate that deposition was controlled both by extension related tectonism; a result of the Neotethys Ocean opening and halokinesis of evaporites in the base of the Ionian zone (Karakitsios, 1995). The presence of extensional tectonic structures can be translated as the result of the divergence between the Gondwana and Eurasian tectonic plates which probably occurred during late Triassic to Jurassic.

However, in this study syn-rift deposits are not examined due to the fact that they were not penetrated by any of the wells in the wider Katakolon area as it is discussed in the first chapter.

## **Post-rift sequence**

The post-rift sequence begins with the pelagic Vigla limestones deposition from early Berriassian (Karakitsios, 1992; Karakitsios and Koletti, 1992). The Vigla limestones in the examined cases are found to directly overlie the pre-rift sequence due to the absence of the syn-rift phase. As a consequence, the base of Vigla limestones represents the break-up unconformity of the post-rift sequence in the Ionian Basin (Karakitsios and Rigakis, 2007). The deposits of Vigla limestones illustrate a general deepening of the entire basin (Karakitsios, 1992) and their introduced thickness has the mean value of 500m, according to Karakitsios (1995).

Following the Vigla formation, Senonian limestones were deposited, during the upper Cretaceous; From Coniacian to Maastrichtian. This sequence comprises of limestones with globotruncanidae and rudists fragments, illustrating a marine depositional environment. Moreover, its facies distribution reflect the Ionian Basin's separation into a complex structural basin topography consisting of a central topographically higher region and two surrounding talus slopes with higher sedimentation rates (IGRS IFP, 1966). The clastic material provided in the Ionian basin was originated from the Paxi and Gavrovo neritic platforms, located on the East and on the West side of the Ionian basin respectively.

Overlying the Senonian limestones, Paleocene and Eocene limestones were deposited as it is demonstrated by their name, from Paleocene to Eocene and more specifically from Danian to Priambonian. Sediment supply from the adjacent areas during this period provides the Ionian basin with microbreccious or breccious elements. The main facies during this period are platy sublithographic limestones with Globigerinidae and siliceous nodules, analogous to those of the Vigla limestones, lacking however continuous cherty beds. Their greatest possible thickness is 700m according to Karakitsios (2007), although in this study a value of 400 m is chosen for the unique presence of Eocene limestones.

Carbonate platforms, continued to provide the study area with clastic carbonate material. Turbidites accumulated across the Eocene – Oligocene boundary and they conformably overlie the Eocene limestones (Karakitsios and Rigakis, 2007), yet they are not penetrated by any of the wells in the study area and thus it is assumed that they have been eroded during the main erosion event which is believed to have taken place from Langhian ( $\pm 16$ Ma) to Zanclean ( $\pm 5$ Ma) eroding also carbonate formations. Previous studies indicate that in the central Ionian zone the flysch and the molasse are almost 1500m thick.

PERIOD	EPOCH	AGE	LITHOLOGY		THICKNESS (m)		RIFT PHASE
QUART.	Pleis.	Zanclean	Deltaic	Keramidia	<2300		POST-RIFT
				Vounargon			
NEOGENE	Plioc.			Peristeri			
				Pr Helias			
PALEOGENE	Mioc.	Aquitanian	Molasse		400	NP	
		Chatian	Flysch (turbidite sequence)		1000		
	Eoc.	Priambonian	Micro-breccious limestones		400		
		Pal.	Maastrichtian	Senonian limestones		200	
CRETACEOUS	Upper	Coniasian	Vigla limestones <i>shale member</i>		500		
		Turonian					
JURASSIC	Late	Tithonian	Pelagic facies		200	NP	
		Mid	Pliensbachian				
	Early	Sinemurian	Pantokrator limestones		1500		
		Hettangian					
TRIASSIC	Late	Rhaetian	Foustapidima limestones		200		
	Mid	Ladinian	Evaporites		2500		
				<i>Organic rich intercalations</i>			
	Early	Scythian					

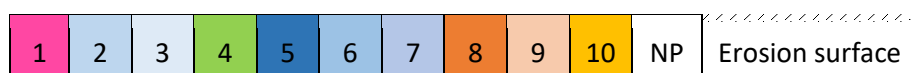


**Figure 3:** Generalized lithostratigraphic column of the Ionian zone (modified after Karakitsios and Rigakis, 2007 and Maravelis et al., 2014).

1) Deltaic sequence mostly composed of claystones, sandstones, limestones and some lignite layers; 2) Sandstones, shales and conglomerates; 3) Turbidites; 4 and 5) Pelagic limestones with clastic material; 6) Pelagic cherty limestones (shale member: cherty beds with clays, sometimes shaly); 7) Syndimentary pelagic formations; 8) platform limestones; 9) platy black limestones; 10) Anhydrites, salt, gypsum (Shale layers: dolomites and shales).

### **Post-Alpine/Orogenic sequence**

The formations following the molassic sequence are dated from Pliocene to Pleistocene and with the Oligocene-Miocene formations comprise the post-Alpine sequence of the Ionian zone. This succession suggests that the sedimentation took place in a mostly fluvial environment (Kamperis and Ioakim, 1992; Maravelis et al. 2014).

The relation of the lithostratigraphic units allows distinguishing nine lithologically distinct formations, yet only four of them were penetrated by wells in the West Katakolon and are examined in this study. These formations are: “Profitis Helias”, “Peristeri”, “Vounargo”, and “Keramidhia”, as presented in lithostratigraphic column (figure 3).

The above mentioned formations are described in detail below, according to Kamperis (1987).

- The “Profitis Helias” formation consists of thick silt-sand layers which upwards pass into greyish lacustrine or brackish clays with relative thin sands. Lithologically this formation consists mostly of clays.
- The “Peristeri” formation consists mainly of thick conglomerates with lens shaped sands intercalated in clays.
- The “Vounargo” formation consists of alternation of silt sands and silty clay which were deposited in a wide variety of shallow marine lagoonal and lacustrine environments.
- The “Keramidhia” formation consists of blue clays intercalates with lens-shaped sands and lignites (shallow marine and lagoonal origin).

The upper Cenozoic succession of the western Peloponnesus area show an extremely complex pattern of predominantly terrigenous-clastic deposits, with repeated observed changes in marine influence and in sediment supply of fluvio-lacustrine and lagoonal paleogeographic configuration (Kamperis and Ioakim, 1992). Moreover, during the late Pleistocene (Tyrrhenian) new sea transgression caused the deposition of shallow marine sediments on the western area.

The Plio-Pleistocene sedimentation can probably delineate the post-Alpine sedimentation. During the early Pliocene compressive phase, inverse tectonic movements resulted in normal movements along pre-existing reverse faults creating high angle reverse faults which are believed to post-date the Vounargo fm (Early Pleistocene).

## **Chapter 3**

### **Oil and gas generation**

#### **3.1. Petroleum systems**

As it is defined from Allen and Allen (2005), “A petroleum system comprises a pod of mature source rock and all of the migration paths, reservoir rocks, caprocks, and traps that can be charged by that source rock to produce oil and gas accumulations”.

The source rock, the reservoir rock, the seal rock and the overburden rock comprise the petroleum system elements while the trap formation, generation, migration, accumulation and preservation are the main processes that make the petroleum system functional under the right timing. Source rock could justly be recognized as the most essential element of a petroleum system, although without the proper biological productivity the optimum conditions for its formation are not possible to prevail.

#### **3.2. Organic matter maturity evolution**

Following the deposition of organic rich sediments, organic matter undergoes three main transformation phases which will be described according to Tissot and Welte (1984) and North (1985). Firstly is the *diagenesis stage* which occurs in the first stages of sediment burial while the conditions are still mild microbial processes, taking place at less than 2000m depth and at temperatures below 60 °C.

Bacteria which are present at these conditions assist on biogenic decay leading to the conversion of some accumulated organic matter into biogenic gas which is mainly methane (CH<sub>4</sub>). During further sediment burial temperature increases, leading to the diminishing of bacteria, water expulsion and finally to the breakdown of proteins and carbohydrates into kerogen (insoluble - in common organic solvents- sedimentary organic matter) and bitumen (soluble -in common organic solvents- sedimentary organic matter) due to the organic reactions.

As temperature and depth increase, the kerogen enters the mature *catagenesis stage*, also called “cracking”. Under thermal degradation, kerogen’s composition starts to change, by producing hydrocarbons; oil and gas. With this continuous process, at some point the oil generating capacity becomes depleted and instead, gas and light hydrocarbons condensate phase start being formed (Dembicki, 2017). Oil can be generated under specific conditions that constitute the so called “Oil window”.

Along the “oil window”, liquid oil generation is accompanied with gas formation and the more mature “wet gas zone” where cracking generates light hydrocarbons with increasing proportion of methane (Tissot and Welte, 1984) and significant ethane, propane and heavier HC amounts. This stage is defined by a maximum temperature of 175 °C and depth of 6000 m. Above 200 °C all the produced hydrocarbons are converted into methane and graphite and further on they become unstable.

Catagenesis stage is followed by metagenesis stage which is the final phase of organic matter transformation. During this stage, the conditions, namely the pressure and the temperature are too high that border on low grade metamorphism. “Dry gas window” where dry gas is generated, is located into this transformation phase. Dry gas consists of mainly methane, thus having the same form with microbial gas. At the end of this stage, graphite is the only remaining due to the depletion of hydrogen and the domination of carbon.

### **3.3. Thermal maturity**

These two words refer to the generation of oil, wet gas and finally dry gas as a result of organic matter transformation under temperature driven reactions through geological time. The boundaries of each stage are presented below in a table modified after Magoon and Dow (1994).

*Thermally immature source rocks* are the ones able to produce microbial (biogenic) gas, since they have undergone only the diagenesis stage and the organic matter is hydrogen-rich due to aliphatic structures. Biogenic gas has been generated with microbial activity having a key role to the breakdown of organic matter (*Schlumberger oilfield glossary*), thus it is mainly composed of methane; a by-product of anaerobic microbial metabolism. It is clean energy and an abundant source on Earth, which occurs under specified conditions and circumstances provoking its exploration importance. In this study, the source which is going to be examined is the so called “Primary” biomethane.

Thermally mature source rocks are rich in aromatic structures which reflect the loss of hydrogen and they correspond to the “oil window”. By the postmature stage, source rocks refer to the “gas window”

consisting of both wet and dry gas zones, able only for hydrocarbon gases generation having an organic matter full in aromatic structures.

Thermogenic gases are a result of high temperature oil and kerogen cracking, through late catagenesis stage. It can be dry or it can contain significant amounts of ethane, propane etc. that define it as wet gas. Thermogenic gas can be either primary or secondary, hence with a direct organic matter thermal cracking origin or with oil thermal cracking origin respectively. Its generation apparently begins with a maturity of 0.80%Ro, while most of it is generated later on with increased maturity. Thermal maturation of organic matter is described below in detail.

Potential (quantity)	TOC (wt.%)	Rock-Eval (mg/g rock)		Bitumen (ppm)	Hydrocarbons (ppm)
		S1	S2		
<b>Poor</b>	<0.5	<0.5	<2.5	<500	<300
<b>Fair</b>	0.5-1	0.5-1	2.5-5	500-1000	300-600
<b>Good</b>	1-2	1-2	5-10	1000-2000	600-1200
<b>Very good</b>	2-4	2-4	10-20	2000-4000	1200-1400
<b>Excellent</b>	>4	>4	>20	>4000	>2400

Kerogen (quality)	(mgHC/gTOC)	S2/S3	Atomic H/C	Main product at peak maturity
<b>I</b>	>600	>15	>1.5	Oil
<b>II</b>	300-600	10-15	1.2-1.5	Oil
<b>II/III</b>	200-300	5-10	1-1.2	Oil/Gas
<b>III</b>	50-200	1-5	0.7-1	Gas
<b>IV</b>	<50	<1	<0.7	None

Maturity	Ro (%)	Maturation			Generation	
		Tmax (°C)	TAI	Bitumen/TOC	(mg/g rock) Bitumen	S1/(S1+S2) PI
<b>Immature</b>	0.2-0.6	<435	1.5-2.6	<0.05	<50	<0.1
<b>Mature</b>						
<b>Early</b>	0.6-0.65	435-445	2.6-2.7	0.05-0.1	50-100	0.1-0.15
<b>Peak</b>	0.65-0.9	445-450	2.6-2.7	0.15-0.25	150-250	0.25-0.4
<b>Late</b>	0.9-1.35	450-470	2.9-3.3			>0.4
<b>Postmature</b>	>1.35	>470	>3.3			

**Table 1:** Geochemical parameters describing the level of thermal maturation (Modified after Magoon and Dow, 1994).

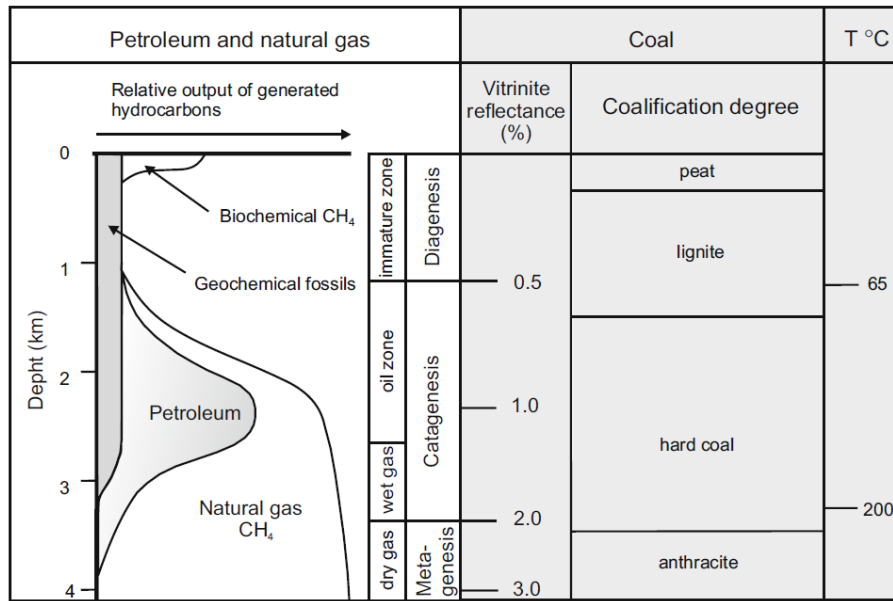


**Figure 4:** Organic matter maturity evolution through diagenesis, catagenesis and metagenesis, from Bahlurbg and Breitzkreuz (2004)

## Chapter 4

### Theoretical background of 1D maturity modelling

#### 4.1. Fundamentals

The modelling of a basin development and evolution as well as its hydrocarbon potential can be split in three separate, yet interrelated parts; The *burial history* of the area under consideration, its *thermal history* through geological time and finally the *HC generation, migration and/or accumulation*. Basin modelling has the ability to simulate the hydrocarbon-generation process, to calculate the volume of the generated hydrocarbons, as well as the fluid flow in order for the entrapment locations and accumulations to be predicted.

This study will provide a useful insight into the HC potential of two different formations in the Katakolon area by examining their generation potential. PetroMod's 1D modelling is utilised and it examines a given point location.

In order to construct an accurate PS model five main steps are considered to be made. (1) *The ages and lithologies determination for each formation interval*, (2) *the tectonic events*, (3) *the petroleum system elements*, (3) *the source rock parameters*, (4) *the boundary conditions* and finally (5) *the*

*calibration of the model.* A basic principle used for the reconstruction of the basins' evolution is *backstripping* which infers to the sedimentation removal in order to get a most clear analysis of the tectonic subsidence as well as of compaction and its outcomes. An outcome of compaction is porosity which according to Athy (1939) and Hedberg (1936) decreases exponentially with depth in normally pressured sediments and it has the following form:

$$\Phi = \Phi_0 * e^{-cz} \quad (1)$$

Where  $\Phi_0$  is the initial porosity,  $c$  is the slope determining coefficient and  $z$  is the depth. It therefore helps creating a more precise burial history which is vigorous for the model and its outcomes.

## **4.2. Software input**

### **Main input**

First of all, the deposited formations (*lithologies*) with their evolution through time (*ages*) have to be introduced as accurately as possible. These input data are the basis of the model providing the burial history upon which the potential hydrocarbon generation will be examined. Secondly, *tectonic events* have also to be inserted in detail (e.g. erosion, hiatus), by means of type and duration and in case of an erosion event, the eroded thickness has to be specified. Likewise, *petroleum system elements* of the examined petroleum system have to be introduced as they have a key role in the critical moment determination of the HC generation and migration.

Their acting periods are presented in a petroleum system events chart, accompanied with the critical moment. This is the time of hydrocarbons generation, migration and accumulation that occur in the examined petroleum system, when an accumulation area already exists. Even though this moment is at the discretion of the modeller, in the following models is set based on the deposition of the younger layers.

Other crucial parameters are the source rock properties and its reaction kinetics. Total organic carbon (TOC) which is measured through combustion and Hydrogen index (HI) which is obtained through RE pyrolysis are the so called source rock characteristics. Furthermore, TOC can be a proxy of the total amount of organic matter present in the sediment (Ronov, 1958). These input parameters are necessary in order to simulate the organic matter degradation reaction that leads to hydrocarbon generation. As far as the generation kinetic models are concerned, there is a variety of available

kinetic models which can be used for the selected source rock, although the user can define his own kinetic algorithm and assign it to the source rock of his model.

## Boundary conditions

The quality of the simulation result and the accuracy of the output model are strongly dependent on the boundary conditions; the *PWD*, the *HF* and the *SWIT*. By introducing these conditions into the software, the basic energetic conditions are defined for temperature and source rock burial history and thus for the maturation of organic matter through geological time. They are introduced in the model either as user-defined values or by using PetroMod's default models and they comprise the input for heat, pressure and fluid flow calculation through geological time (Petrobuilder 3D User Guide, PetroMod, Schlumberger, 2014).

Through geological time, *SWIT* could be automatically calculated by the software based on Wygrala (1989) model. This model's algorithm extracts a standard temperature at sea level over geological time based on present day geographic location, providing the *SWIT*. The last boundary condition, *HF*, refers to the process of transferring heat from the Earth's interior to its surface, in this case from the base to the top of the sedimentary column. It is believed to be the most important parameter that controls the basin's thermal regime through geological time. In case it is only conduction related, *F* is the product of thermal conductivity and geothermal gradient across a layer formation (Deming, 1994).

$$Q = \lambda * \frac{\Delta T}{\Delta Z} \quad (2)$$

Where  $Q$  ( $\text{W/m}^2$ ) is the heat flow,  $\lambda$  ( $\text{W/m/K}$ ) is the conductivity and  $\frac{\Delta T}{\Delta Z}$  ( $\text{K/m}$ ) is the geothermal gradient. Equation (2) shows that heat flow can be calculated in a point location of an existing borehole where temperature and conductivity data are available. Estimations of heat flow are used for temperature calculation which is possible through equation 3.

$$\rho C_p \left[ \frac{\partial T}{\partial t} + v * \nabla T \right] = \nabla * (k \nabla T) + A \quad (3)$$

Where  $\rho$  is the density,  $C_p$  is the specific heat,  $A$  is the heat generation and  $v$  is the velocity of the moving material (Carslaw and Jaeger, 1959). This equation balances the change in the heat content of a body with the heat transferred by conduction, brought in by material motion and generated within the body (Stein C.A., 1995). However, temperature calculation according to equation (3) is a non-unique inverse problem which has a lot of uncertainties regarding the physical properties of each formation and the thermal effects drawn by the solid state convection in the mantle (Richter, 1989).

What is more, the abundance of the naturally occurring radioactive elements in the Earth's crust constitutes a significant heat source which affects the surface heat flow, yet it is not easy to be determined. Thus, an accurate paleo-heat flow trend cannot be calculated solely from conductivity and thermal gradient.

In any case, paleo-heat flow is commonly difficult to define, although utilising the McKenzie (1978) crustal heat flow model, HF is automatically calculated. This model incorporates the rift periods, the distribution of beta-crust stretching factors through time, the crust and mantle thickness and a constant base temperature corresponding to the original lithosphere thickness.

Boundary conditions are vital for the temperature model generation. Temperature is simulated based on the upper boundary condition (SWIT), the lower boundary condition (basal heat flow) and the thermal conductivity of the layers within the model.

It is important to point out that according to related studies, in contrast to erosion events, thickening of the continental crust results in decrease of the surface heat flow while erosion events augment the surface heat flow. If this augmentation is neglected, as it was stated on the past (e.g Lachenbruch 1968, 1970), it will lead to misinterpretation (England, Richardson, 1980).

Another fact of vital importance is the so called "*thermal blanketing*". According to this effect, when deposition of low thermal conductivity sediments takes place, surface heat flow temporarily decreases. The latter effect is believed to occur during the Cenozoic clastic sedimentation, where hundreds of meters of sediment are deposited within a small time interval.

### **Calibration parameters**

The final model is a result of precise several calibration iterations. Even though Rock-Eval pyrolysis data (e.g. Tmax, OI etc.) and many more parameters can be introduced and used as calibration data, in this study, VR and BHT are used for the calibration of thermal history, while in one of the wells where porosities are provided they also contribute to a better calibration fit achievement.

*Bottom-hole temperatures (BHTs)* are basically provided by borehole data. By adjusting the tectonic events and lithologies, calibration could be achieved. Additionally, HF is a very good calibration parameter.. As it is stated in Naidu et al. (2017) study, present heat flow is most proper to be used for BHT calibration, while paleo-heat flow for calibration of kerogen maturity indicators (VR). Similarly, in this study present-day HF is introduced to adjust the thermal model and find the acceptable fit between measured and calculated BHT with an outcome of a trustworthy present-day heat flow of the point location under consideration.

*Vitrinite reflectance (VR)* is the most common kerogen maturity indicator with respect to whether the examined organic matter has generated or could potentially generate hydrocarbons, indicating always the maximum temperature conditions the rock has undergone. It is a parameter which is used along with BHTs to optimise the thermal history models.

Kerogen type	Ro %	Gas prone generation	Ro%	Oil prone generation	Ro %
I	0.7	Immature	< 0.8	Immature	<0.6
II	0.4	Early gas	0.8 - 1.2	Early oil	0.6-0.8
III	0.45-0.5	Peak gas	1.2 - 2	Peak oil	0.8-1
IV	0.8	Late gas	>2	Late oil	1-1.35
				Wet gas	1.35-2
				Dry gas	>2

**Table 2:** General interpretation scheme for vitrinite reflectance and compensated kerogen types for the main stages of HC generation, modified from Dembicki, (2009).

Strictly speaking, vitrinite is a maceral originating from land plants (type of woody kerogen) which changes consistently when heat supply is present and its reflectance illustrates the rock's maturity. The maturity (VR) trend is modelled utilising the Easy%Ro model of Sweeney and Burnham (1990) which is a simplified version of VITRIMAT model (Sweeney and Burnham, 1989), applicable for VR values ranging from 0,28% to 4.5%.

This model uses an Arrhenius first-order parallel-reaction approach (4) with a common frequency factor (A) and a simple exponential relation. By representing each parallel reaction with a kerogen's chemical bond breaking, it provides the opportunity of maturity calculation with changing time and temperature with a distribution of activation energies. Time and temperature are the two most vital variables in this equation.

$$dw/dt = -kw \quad (4)$$

Where

$$k = Ae^{\left(\frac{-E}{RT}\right)} \quad (5)$$

Where  $k$  is the reaction rate,  $w$  is the amount of unreacted component,  $A$  is the frequency factor,  $E$  is the activation energy,  $R$  is the universal gas constant and  $T$  is the temperature.

Despite the linear relation of the reaction processes with time as it is seen in the equation above, the reaction progresses exponentially with temperature leading to the conclusion that temperature plays a vital role in the reaction processes (Dembicki, 2017).

The fraction of the reactant converted (TR) which is defined as the amount of reactive kerogen that has been converted to hydrocarbons, divided by the total amount of reactive kerogen initially available is expressed as percentage (Dembicki, 2017) and it is presented below:

$$F = TR = 1 - \frac{w}{w_0} = 1 - \sum_i f_i [w_i/w_{0i}] \quad (6)$$

Where  $w_{0i}$  is the initial concentration for component  $i$ ,  $w_0$  is the initial concentration of the total reactant and  $f_i$  is the weighting coefficient for the parallel reaction components.

Transformation ratio “F” is calculated in a constant heating-rate segments manner by using formulas described from Braun and Burnham (1987). After TR calculation, VR can be calculated as an exponentially correlated value with the TR in the interval 0.20% to 4.66% (Kauerauf, 2007), as follows:

$$\%Ro = 0.20 \left(\frac{4.66}{0.20}\right)^{TR} \quad (7)$$

Even though paleo-heat flow is used to achieve a decent calibration fit of the maturity trend, tectonic events are also of vital calibration importance. Measured VR trends commonly have offsets at erosional discordances as the uplifted layers have already experienced a heating period with a corresponding increase in maturity (Kauerauf, 2007), which can be used as calibration indicator. As it is demonstrated by previous studies (e.g. Wangen et al., 2007) paleo-heat flow is related to VR values as they are both function of time and temperature.

## Chapter 5

### This study

#### 5.1. Introduced data

In this study, four point locations are examined, given the borehole data from four penetrated locations in the area. Two of them are located onshore: “MY-1” and “ALF-1” wells and the other two are located offshore: “WK-1” and “WK-2” wells. For the onshore areas, ALF-1 offers the most information while MY-1 well provides a rough lithological approximation and four VR values. The same scenario applies for WK-1 and WK-2 wells where WKA-2 provides RE data and WK-1 provides TOC, some HI, OI and VR data.

Considering the fact that these wells are separately located very close to each other (ALF-1 with MY-1 and WK-1 with WK-2) it is assumed that the two onshore and the two offshore wells have the same characteristics and thus, the provided data are shared. The onshore wells share the same RE data and almost the same lithological input, while VR values and BHT were introduced separately.

For the offshore wells, WK-2 RE data are introduced in the WK-1 model, VR is introduced according to WK-1 and the lithological input is introduced separately according to well formation tops. Additionally, VR trend is used to calibrate the models and thus to predict the paleo-conditions.

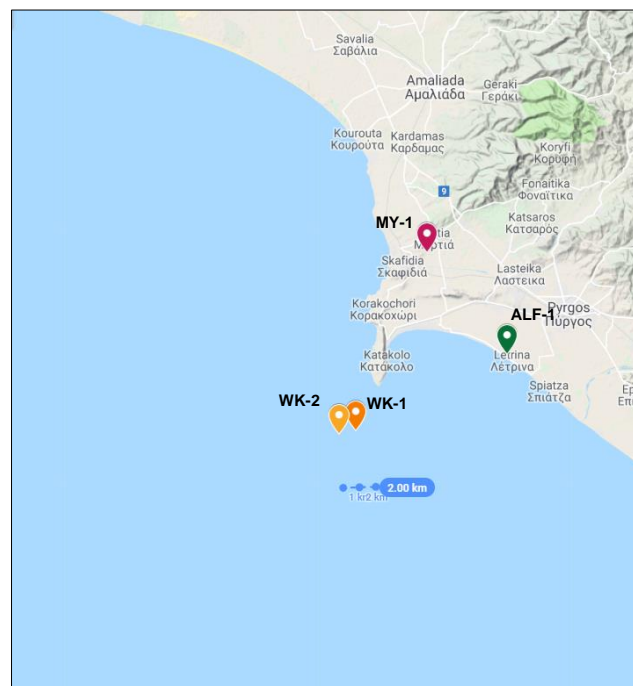


**Figure 5:** Location map of the examined point locations (wells) in the West Katakolon area.

## 5.2. Model frame

These aforementioned studied, together with the well formation tops, suggest that the wider area of Katakolon does not include syn-rift sediments as described in [figure 3](#) and therefore in this study a *non-synrift approach* is suggested.

More specifically, it is assumed that this area has not undergone a syn-rift phase, although during this period it was subjected to uplift and erosion of the already deposited Pantokrator limestones was taking place. Once the erosion was completed, thermal subsidence occurred.

In a wider picture, evaporites were deposited during Triassic with a maximum thickness of 2500m, followed by Foustapidima limestones of 200m and 1500m of Pantokrator limestones. The aforementioned erosion event took place from 190 to 145Ma, thus exactly after the Pantokrator deposition. With respect to the general assumption of a non syn-rift phase, it is assumed that during this erosion, 500m of the Pantokrator limestones were eroded leading to a final thickness of 1000m. The following thermal subsidence was accompanied by the deposition of pelagic limestones (Vigla, Senonian and Eocene) which from 33 to 16Ma were overlaid by a 1000m thick flysch and 400m thick molasse. Completed at 16Ma, this succession started being eroded until 5Ma, when the Plio-Pleistocene sedimentation began and its deposition lasts until the present day.

Noteworthy is the character of the recent erosion (16 to 5Ma) which in the onshore area is considered to have eroded all the carbonate series (a total of 3700m), leading to the overlying of the Triassic evaporites by the Plio-Pleistocene sequence. In the offshore case, the erosion has not affected the whole carbonate section; in the WK-1 point location, the flysch, the molasse and some Eocene limestones are eroded, thus a total thickness of 1600m. Accordingly, in the WK-2 point location it seems that a total thickness of 2200m has been eroded and at present time Plio-Pleistocene sediments overlie the Vigla formation.

This period (16 to 5Ma) led to the entrapment of the pre-Cenozoic section by a pseudo-anticline formation generated through this erosion accompanied by tectonic tresses. This trapping character is further completed by the deposition of the clastic Plio-Pleistocene sediments of a most-like sealing character.

Finally yet importantly, it is evident that the onshore and offshore models should have the same burial history ([figure 6](#)), thus almost the same lithostratigraphy. According to this fact, even if the absent formations have been thrust away or the Triassic evaporites are present in this area due to thrusting events, erosion is assumed for both cases. This stems from the fact that thrusting details, age and origin are not known.

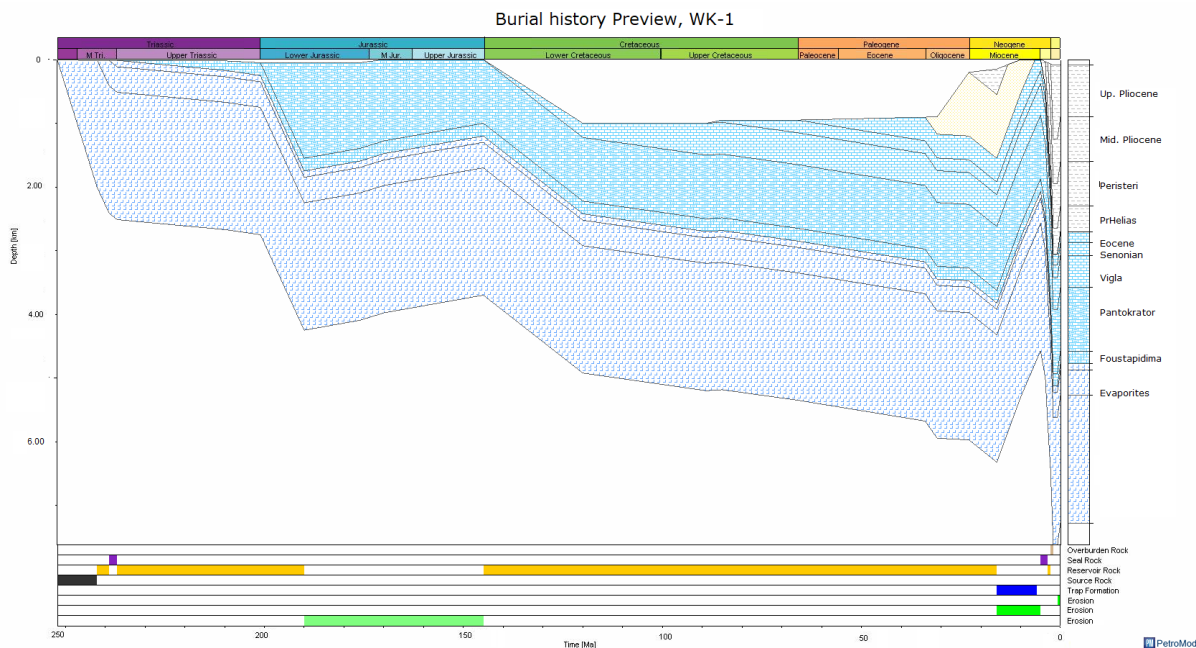


**Figure 6:** Burial history preview of the WK-1 model.

### 5.3. Rock-Eval analysis

To achieve a further comparison and evaluation of the possible source rocks, some samples of neighbouring areas are examined through RE pyrolysis and further determination of TOC in the department's research centre. During this analysis the sample is weighted, splintered until fine-grained, sieved and then heated into a RE pyrolysis oven in the absence of oxygen.

Parameters measured through this pyrolysis include the TOC, the free HC in the rock (S1), the remaining HC generative potential of the rock (S2) in mgHC/gTOC, the temperature reached during the maximum hydrocarbon pyrolysis yield and the amount of CO<sub>2</sub>/g rock yield (S3) during kerogen's thermal breakdown.

Following the RE pyrolysis, some parameters are also measured. The amount of oxygen relative to the organic carbon of the sample (OI) or in other words the relative oxygen richness, the amount of hydrogen relative to the organic carbon amount present in the sample, thus the hydrogen richness (HI) and the maturity of a homogenous source (PI).

More specifically, seven samples were pyrolysed, over which only three provided proper results. Two of them are taken from Pliocene outcrops while the third one is taken from a Triassic outcrop from a neighbouring area. What is more, kerogen classification diagrams are constructed from data obtained

from the above-mentioned geochemical analyses from all the wells as well as from this RE pyrolysis and are plotted and presented in [appendix A](#).

In general, the results show that the analysed samples are generally of type III, while type II-III is also abundant, yet only in the offshore data. Hence, onshore source rocks can be classified as gas prone type III, while for the Triassic source rocks a precise conclusion cannot be created. However, previous studies indicate the presence of type II-S oil and gas prone Triassic source rocks in this area.

Age	SMPL	Qty (mg)	S1	S2	S3	PI	Tmax	TOC	HI	OI
						(S1/ S1+S2)			S2/ (TOC*100)	S3/ (TOC*100)
<b>Plio.</b>	BK_1	59.9	0.17	4.25	2.54	0.04	421	4.22	101	60
<b>Plio.</b>	BK_2	63.3	0.02	0.51	1.46	0.03	424	0.86	59	170
<b>Triassic</b>	TR_1	64.7	0.03	0.02	0.54	0.17	427	0.99	14	55

**Table 3:** Rock-Eval analysis data of Pliocene and Triassic outcrop samples, taken from a neighbouring location of the Katakolon onshore area.

## Chapter 6

### Onshore models

#### 6.1. Depositional environment

In these models, the examined petroleum system is of Plio-Pleistocene age and its source rock layers have probably been deposited in deltaic settings, regarding their lithologies and geochemical characteristics. Hence, a mainly fluvial transported organic matter as well as from coastal swamps that are dominated by terrestrial higher plant material is considered (Barker, 1982), possible to generate and deposit also coal in the proximal delta area.

Regarding the compositions provided by the geochemical analysis of the ALF-1 well, there is combined marine and terrestrial organic matter contribution. Encountering the fact that fluvial environments may contribute to the marine organic input into the system creating similar to upwelling reducing conditions, the presence of both environment phases is not unreasonable.

In more detail, two cores taken from the Plio-Pleistocene succession which were geochemically evaluated have revealed a combination of depositional environments. Taking into account the *ph/pr* ratio which is one of the most common correlation parameters used as a depositional environment

indicator (Peters et al., 2005) gave values between 1.4 and 2.2, revealing an aquatic depositional environment (reducing conditions) and a fluviomarine and a coastal swamp respectively, according to Lijmbach (1975). In relation to the normal alkanes examined from these depths, the inference drawn about the depositional environment is in correspondence with the conclusions made.

## 6.2. Calibration parameters

In the matter of the ALF-1 well, the thermal gradient is considered to be fairly low, reaching  $1.47^{\circ}\text{C}/100\text{m}$ . In the same way, MY-1 has a geothermal gradient of  $1.65^{\circ}\text{C}/100\text{m}$ , thus both onshore wells exhibit low temperatures, fairly below the mean geothermal gradient ( $2.5^{\circ}\text{C}/100\text{m}$ ). Still, the calculation of the geothermal gradients in these point locations is problematic. On the other hand, the geothermal gradient of a neighbouring onshore well is calculated to be  $2.15^{\circ}\text{C}/100\text{m}$ .

What is more, a static temperature of  $60^{\circ}\text{C}$  which is measured at a TVD of 2304m in the MY-1 well is believed to be erroneous with a bigger one to prevail at that depth according to provided data.

Whilst in any other case this reduced geothermal gradient could be a drawback in the maturity of the organic matter, in this case it constitutes one of the main characteristics. In the following plot, static temperatures of MY-1 well, and maximum measured temperatures of the ALF-1 are displayed, accompanied by the mean geothermal gradient of the neighbouring well.

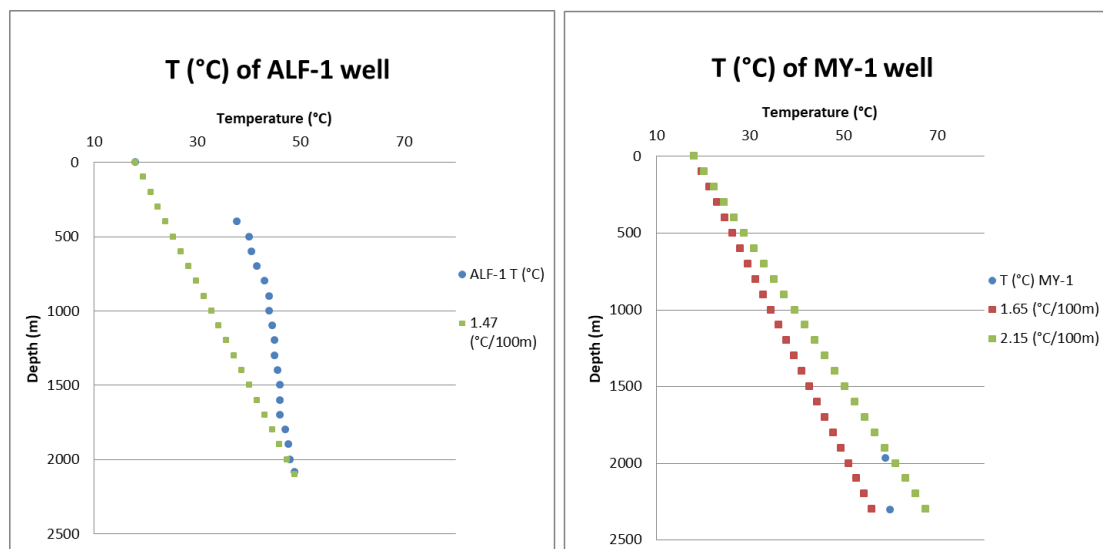


**Figure 7:** Temperature profiles of the onshore wells.

Thermal gradients for each well and the thermal gradient of a neighbouring onshore LAS-1 well ( $2.15^{\circ}\text{C}/100\text{m}$ ) are plotted.

In general, temperature plays a significant role in the organic matter's maturation and VR is strictly an indicator of this maturity stage. Maturation of ALF-1 ranges from 0.19%Ro to 0.32%Ro while of MY-1 samples ranges from 0.36%Ro to 0.45%Ro. When dealing with immature source rocks, VR is a poor indicator as stated by Cvetković (2016), although in this case both VR sample groups even with that difference among them lead to the same conclusion.

Having as a maximum VR a value less than 0.50%Ro and a maximum temperature less than 65°C, it is accepted that these sediments lay on the immature zone, undergoing the diagenesis stage (figure 4, table 2).

While TOC content takes values below 1.70%, some coaly layers in Vounargo and Peristeri reach 6.33% and 32.78% respectively; Also, Tmax and PI range below 440°C and 0.40 respectively, confirming the source rocks' immaturity.

A peculiar phenomenon is the exaggerated Oxygen index values and the extremely low HI values. According to a study made by Katz (1983), very high oxygen indices result from the fact that as carbonate minerals decompose during RE, the matrix properties are reflected instead of kerogen's properties that are contained within the rock matrix. The same scenario applies for the low hydrogen indices that result from the hydrocarbon retention on mineral grains (Espitalie et al., 1980; Katz, 1983). Both scenarios are generated from low TOC sediment samples of less than 2% and thus some values resulting from RE analysis are misleading.

### **6.3. Input data**

#### **Main input**

Intentionally the Plio-Pleistocene lithostratigraphy is introduced in detail, with respect to the cutting's lithological information obtained from these two onshore wells. The depositional period for each layer was introduced regarding the total depositional period of each formation. Source rock layers are selected in terms of lithology and TOC content. Finally, tectonic events are introduced as a result of multiple calibration iterations

Also, despite the fact that Pr. Helias fm has not been reported in the ALF-1 well, it has been introduced in both models since it is present in most of the onshore wells. In any case, this does not have to be misleading since the lithologies and the source rock characteristics are introduced with respect to the penetrated layers, as described in the above-mentioned geochemical studies.

## Boundary conditions

Fossilised organisms and lithologies concerning the general lithostratigraphy of the Ionian zone are the main factors for PWD selection, while the present-day water depth is provided by *Energean oil & gas*. SWIT is calculated based on Wygrala (1989) as described [above](#) and as far as HF is concerned, it is introduced in reference to many sources.

First of all, Mavromatidis (2009) has suggested a  $50\text{mW/m}^2$  for the pre-rift phase,  $80\text{mW/m}^2$  for the syn-rift phase and  $35\text{mW/m}^2$  for the post-rift phase. Secondly, Fytikas and Kollios (1979) have created a preliminary heat flow map of Greece which proposes a present day heat flow ranging from 28 to  $40\text{mW/m}^2$ . Finally the introduced values are a combination of the aforementioned, illustrated in the following table (table 4), concerning the ALF-1 model.

Values of HF change when considering the MY-1 well. This happens chiefly due to the increased maturity which will be discussed later on. After the Miocene erosion event, the HF remains at  $40\text{mW/m}^2$  until the end of the Keramidhia erosion at 0.10Ma when it decreases to present-day HF of  $28\text{mW/m}^2$ .

Age (Ma)	PWD(m)	Age (Ma)	SWIT(°C)	Age (Ma)	HF (mW/m <sup>2</sup> )
0.00	0.000	0.00	17.79	0.00	28.00
10.00	0.000	5.00	18.88	4.00	28.00
16.00	0.150	10.00	20.00	5.00	40.00
23.00	0.200	16.00	20.94	16.00	34.00
31.00	0.900	23.00	22.22	123.25	55.62
66.00	0.950	31.00	23.52	137.75	65.00
85.00	0.950	66.00	25.84	145.00	65.00
89.00	1.000	85.00	28.40	149.50	65.00
120.00	1.000	89.00	28.95	190.00	31.79
145.00	0.000	120.00	30.00	240.00	50.00
170.00	0.000	145.00	28.48	252.00	50.00
176.00	0.050	170.00	25.00		
201.00	0.050	176.00	24.81		
210.00	0.020	201.00	24.79		
252.00	0.010	210.00	25.63		
		252.00	25.98		

**Table 4:** Boundary conditions of the ALF-1 model.

## **Kinetic model selection**

For each onshore model, kinetic model named “Biogenic reactions” is chosen for each source rock layer. This kinetic reaction model is responsible for the simulation of biomethane generation after some biogenic reactions which generate predominantly methane.

As it is mentioned above, biogenic gas is generated by anaerobic biomass decay in shallow burial depths and in these models the generation method is selected to be a Gaussian distribution. Several methods can be used, yet in this one the reaction is based on the maximum temperature attained, following a Gaussian distribution with given mean and standard deviation.

The generation occurs proportionally to the trend with increasing temperature from 20°C to 80°C, reaching its maximum (per unit temperature increase) at the mean temperature of 50°C and it decreases thereafter, with respect to the distribution (Kinetics editor information, Schlumberger PetroMod software 2013).

## **6.4. ALF-1 model**

### **6.4.1. Calibration of the final model**

Crucial in the onshore model’s calibration seems to be the detailed introduced lithology as well as the erosion and hiatus events that take place. Approaching the real geo-lithostratigraphic frame of the model as much as possible, the model tends to be more accurate.

Nevertheless, modification of the HF values is attained, yet is not possible to extract a unique paleo-heat flow history from just a VR signal. Vitrinite Reflectance measurements do not provide a continuous curve along depth, but an optimal continuous curve of the model can be fitted to the measurements. The challenge is then to obtain the paleo heat flow values that reproduce the VR data represented by the curve (Wangen et al., 2007).

Several calibration iterations lead to the conclusion that the specific lithology does have a small, yet significant effect on the calibration. A *hiatus event* is assumed to have taken place during 1.80Ma to 0.78Ma which is the period of Keramidhia deposition that does not occur in this location.

Moreover, paleo-heat flow seems to be a chief calibration parameter. The maturity trend (figure 8) is not possible to have resulted through any other process except from the low thermal conditions; even by a hiatus event. However, present-day HF cannot deviate from the range of 27 to 40mW/m<sup>2</sup>. In any case, the generated VR curve has a maximum fitting value of 0.34%Ro respecting a post-orogenic HF of 27mW/m<sup>2</sup>.

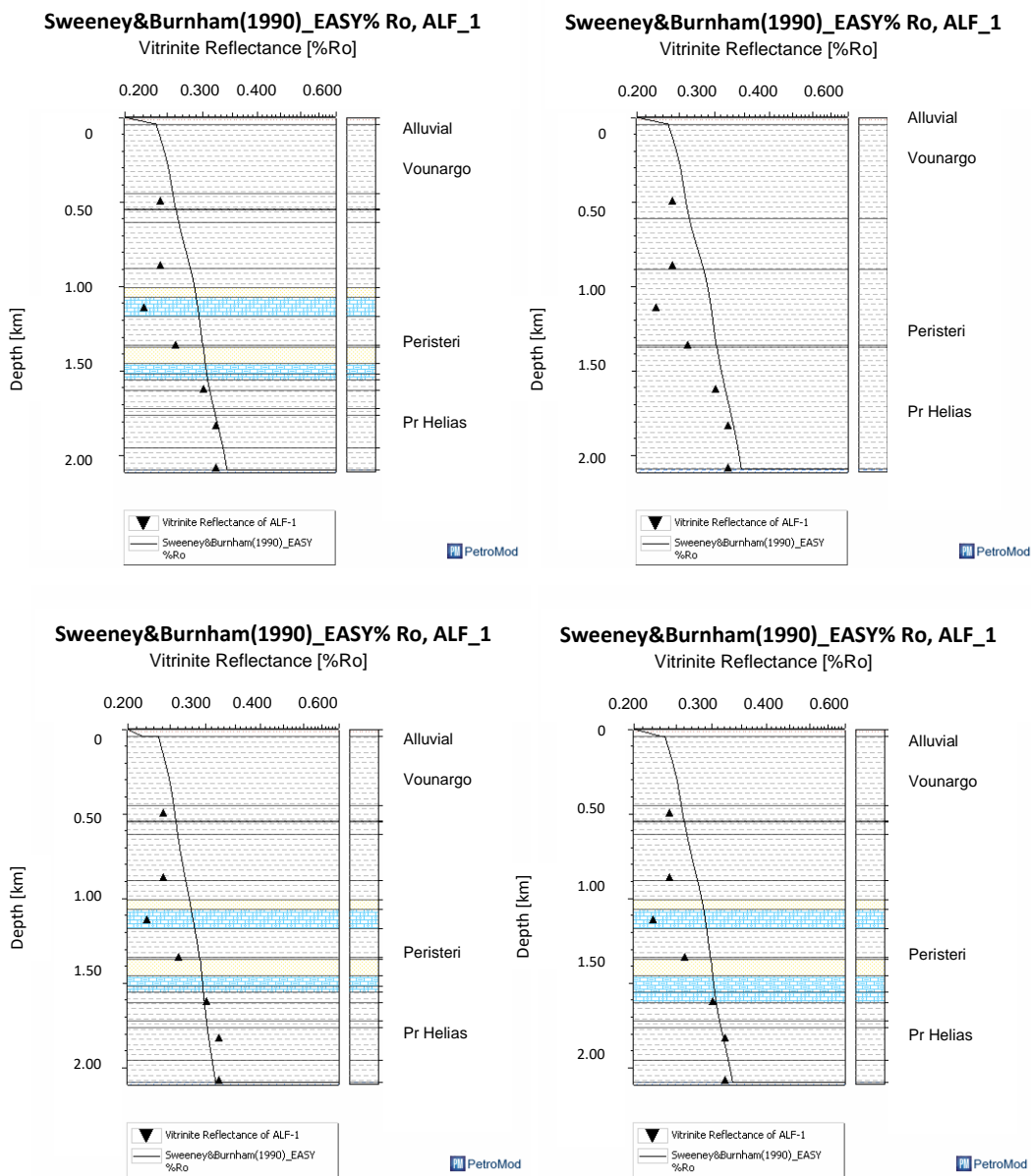


**Figure 8:** VR calibrations, ALF-1 model.

Post-orogenic HF= 28 mW/m<sup>2</sup> (above left), Post-orogenic HF= 28 mW/m<sup>2</sup> and generic lithostratigraphy (above right), Post-orogenic HF= 23 mW/m<sup>2</sup> and detailed lithostratigraphy (below left), Post orogenic HF=27mW/m<sup>2</sup> (below right) - final model. In all cases a hiatus event from 1.80Ma to 0.78Ma is encountered.

Following the paleo-conditions calibration according to VR values, the present-day heat flow is also calibrated according to the BHT and vice versa. Whilst the best temperature calibration is attained by utilising a present day HF value of 23mW/m<sup>2</sup>, it does not seem rational regarding the available

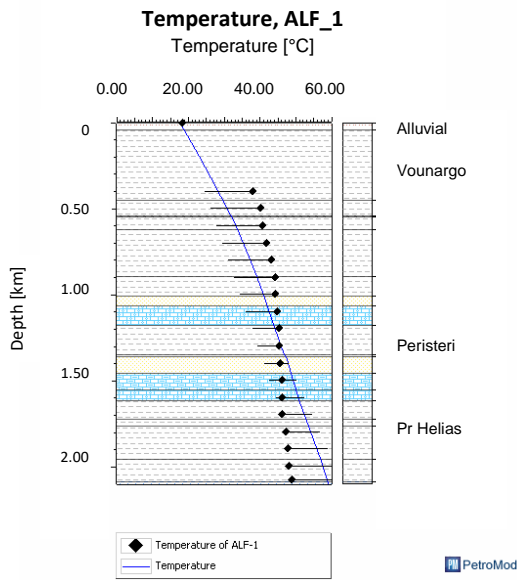


**Figure 9:** Temperature profile, ALF-1 model

information. Even though HF limitations have been assumed for this study, BHTs seem to be problematic. Thus, for the onshore models the present day heat flow is assumed to be 27mW/m<sup>2</sup>, which generates a temperature profile with a maximum-depth temperature of 62.5°C (figure 9).

The modelled temperature curve corresponds to a linear temperature gradient of 2.15°C/100m when assuming a T<sub>surf</sub> of 18°C.

It appears that the generated curve obtains an acceptable fit with LAS-1 temperature gradient, while in order for this curve to fit the ALF-1 measurements a 23mW/m<sup>2</sup> present-day HF is needed, leading to the conclusion of probably erroneous measurements.

### 6.4.2. Timing of biomethane generation and expulsion

In this chapter, five potential source rocks are examined. The first three refer to clay layers interbedded in the pr. Helias, Peristeri and Vounargon fms and the last two on coaly layers interbedded in Vounargon and Peristeri fms, having the following characteristics:

Sublayer	TOC (wt.%)	HI (mgHC/gTOC)
Vounargon	0.31	131
Peristeri	0.80	22.60
Pr. Helias	0.50	31
Vounargon coal	6.33	52
Peristeri coal	32.78	105

**Table 5:** Sublayer source rocks' characteristics

In view of the figures below, generation rate seems to be ongoing. Considering a detailed lithology as proposed previously, the generation is separated in three stages, all of them governed by expulsion. For all five layers, the *first stage* occurs during 3.00-1.80Ma, the *second stage* from 1.80Ma to 0.80Ma, while the third stage lasts from 0.80Ma till present time.

As it will be discussed in the conclusion section, the TR is a generation and expulsion indicator since all of the generated methane is believed to have been expelled from the beginning of its generation. The distribution of this parameter is displayed below along the burial history.

Peak generation rate of biogenic gas is reached regarding a temperature of 50°C. In this model, this temperature is almost reached by the source rock layers during their peak generation, at 1.80Ma. Even though the temperatures of the shallower layers are lower, they still lie within the Gaussian distribution temperature range.

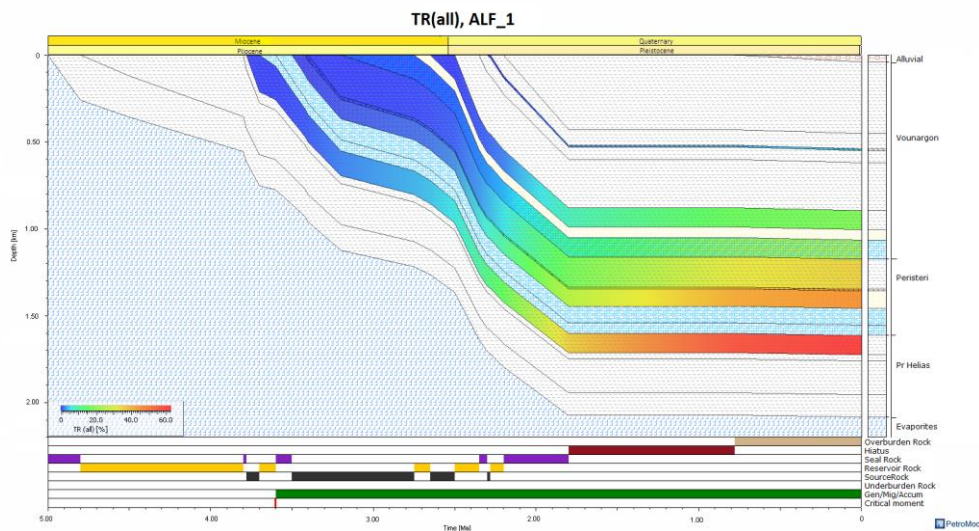
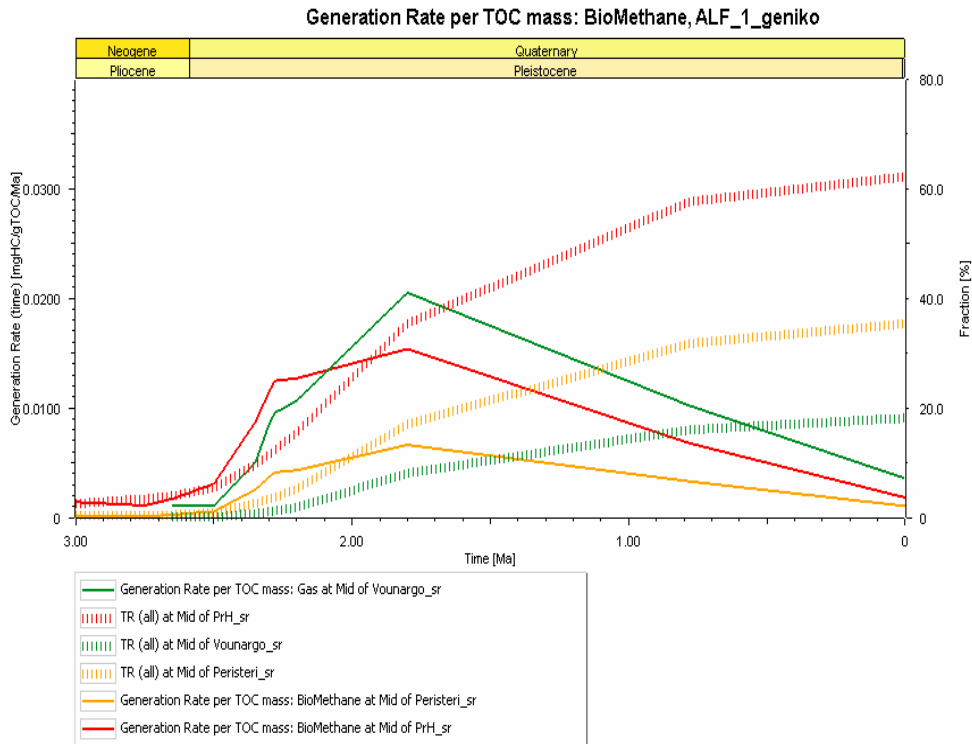
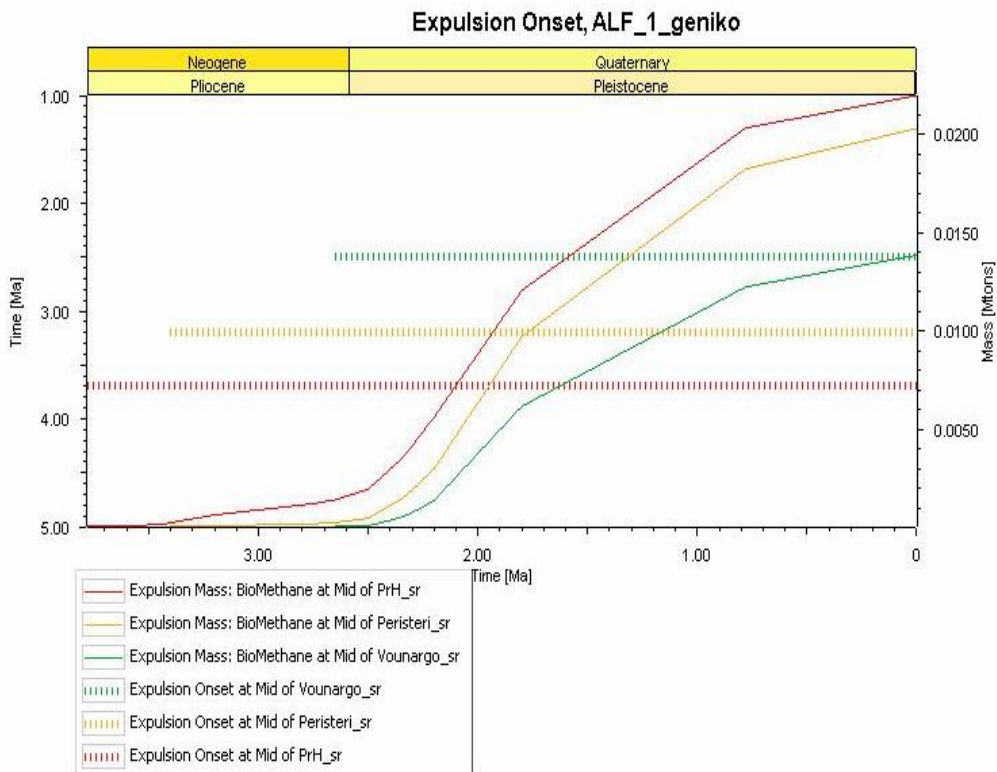


**Figure 10:** Source rock's TR (%), ALF-1 model



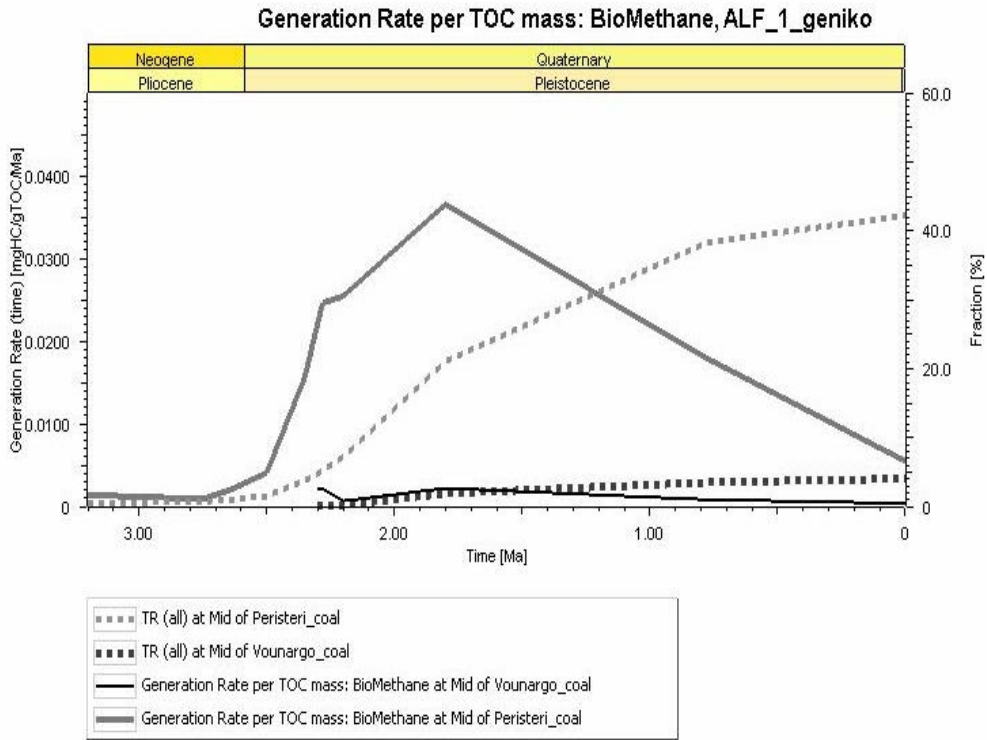
PetroMod

**Figure 11:** Biomethane generation rate per TOC mass, ALF-1



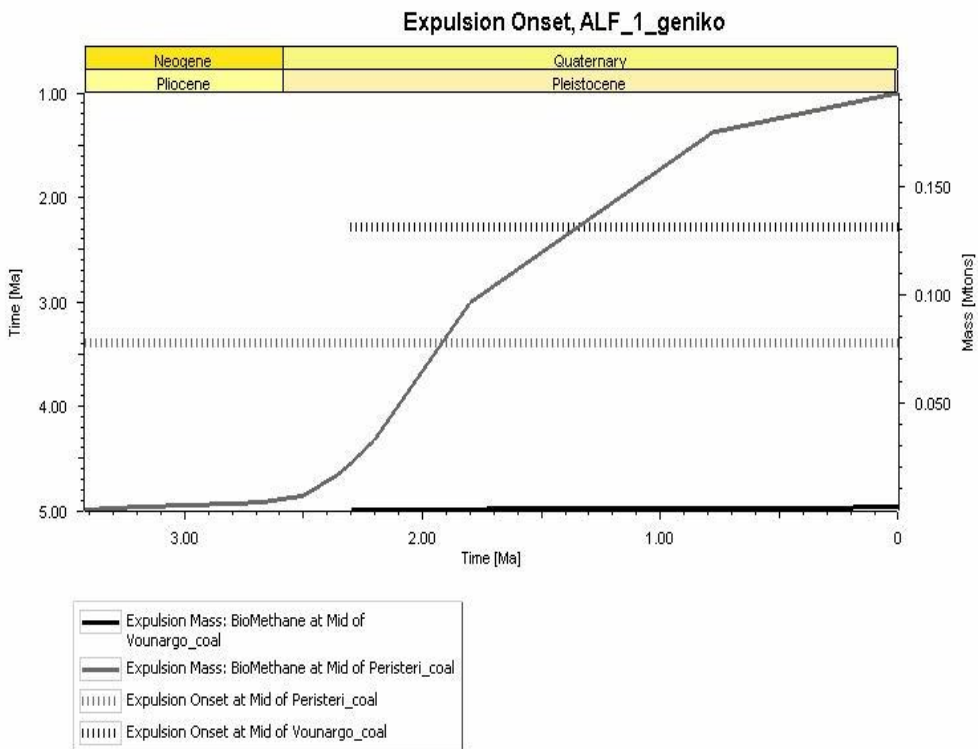
PetroMod

**Figure 12:** Expulsion of biomethane, ALF-1



PetroMod

**Figure 13:** Biomethane generation rate per TOC mass, ALF-1



PetroMod

**Figure 14:** Expulsion of biomethane, ALF-1

## 6.5. MY-1 model

### 6.5.1. Calibration of the final model

Detailed lithology is also used in this model and the main input is similar to ALF-1 model, yet with some differences. Even though these two point locations are very close to each other, MY-1 sediments' maturity seems to be higher. A possible explanation for this distinct difference could be the deeper burial depth achieved through vast overburden load deposition.

As it is already mentioned, erosion events are notably effective in terms of thermal maturation. By taking into account the same to the ALF-1 parameters, MY-1 does not achieve a calibration fit, only in case of massive recent erosion.

The final calibration of the model shows that the maximum VR has a value of 0.42% at the Miocene's unconformity depth. By utilizing a present day HF of  $27\text{mW/m}^2$ , the temperature at 2304m MD is  $61^\circ\text{C}$ .

Despite the fact that a present day HF of  $30\text{mW/m}^2$  generates a temperature which is in accordance with the described problematic measurements described in the [calibration parameters](#) section, no detailed data are available and thus a present-day HF of  $28\text{mW/m}^2$  is utilized for this model.

Accordingly, the last case seems to be the most valid one since it incorporates the same conditions as the ALF-1 model, yet altered due to the ongoing erosion that is assumed to have taken place before and after Keramidhia sedimentation. The iteration procedure is displayed in figure 15.

Coupled with the available porosity measurements, the final model is further calibrated (figure 16). Further changes have an effect only in the eroded thickness and the HF. Of course, in any case the aforementioned modifications are done comparing in situ and neighbouring formation thicknesses. In light of the latter, the average eroded thickness is estimated to be 520m of the Keramidhia fm, eroded within the last 0.78Ma and 200m of the Vounargon fm, eroded from 1.80Ma to 1.60Ma.

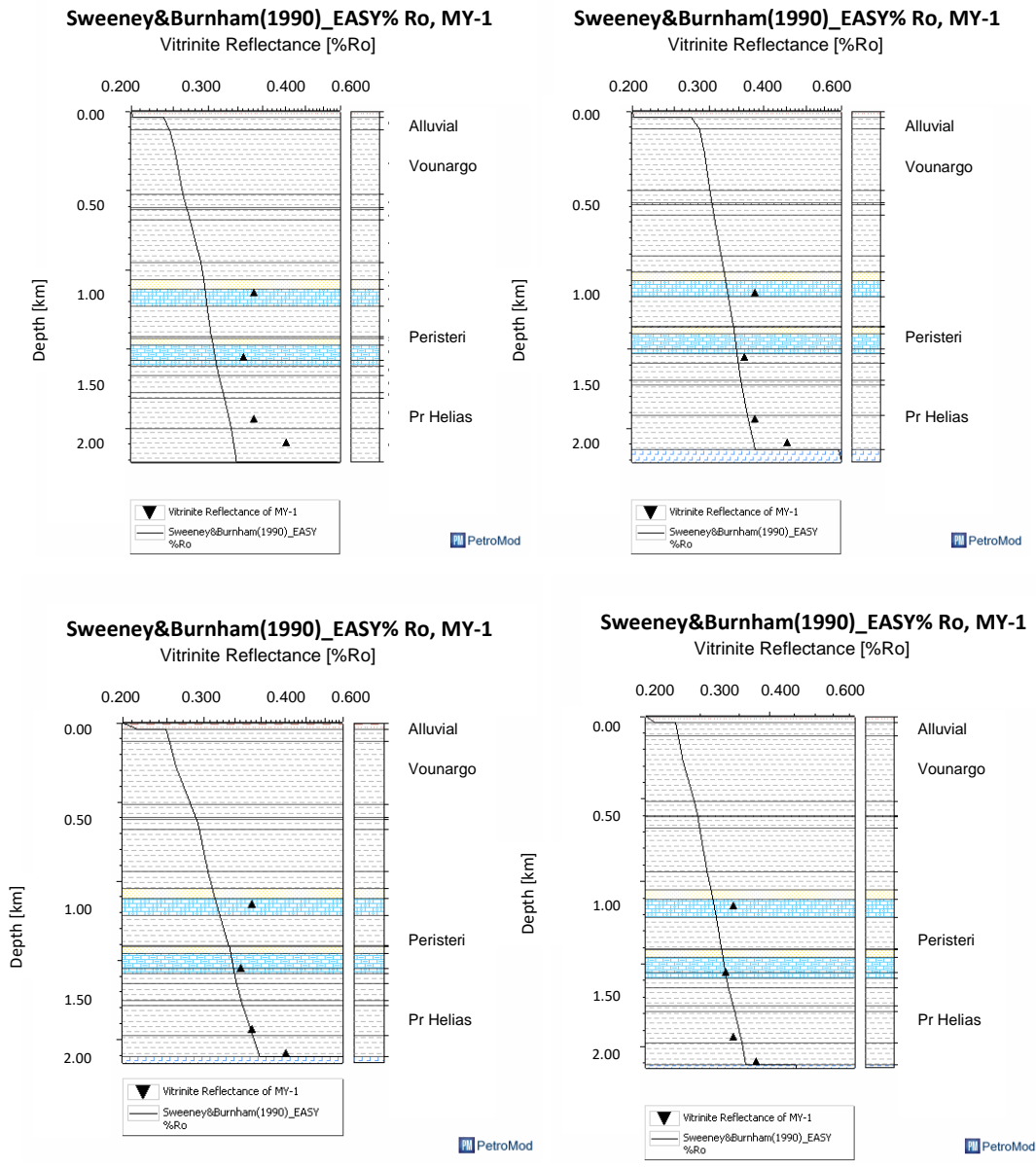


**Figure 15:** VR (%Ro) calibration, MY-1 model.

Post-orogenic HF=28mW/m<sup>2</sup> and erosion thickness of Keramidhia=300m and of Vounargo=100m (above left), Post-orogenic HF=28mW/m<sup>2</sup> and erosion thickness of Keramidhia=3000m and of Vounargo=100m (above right), Present-day HF=30mW/m<sup>2</sup>, during post-orogenic erosion HF=35mW/m<sup>2</sup>, erosion thickness of Keramidhia=520m, and of Vounargo=100m (below left), present day HF=28mW/m<sup>2</sup>, post-orogenic erosion HF=40mW/m<sup>2</sup>, Keramidhia erosion amount=520m, Vounargo erosion amount=200m – final model (below right).

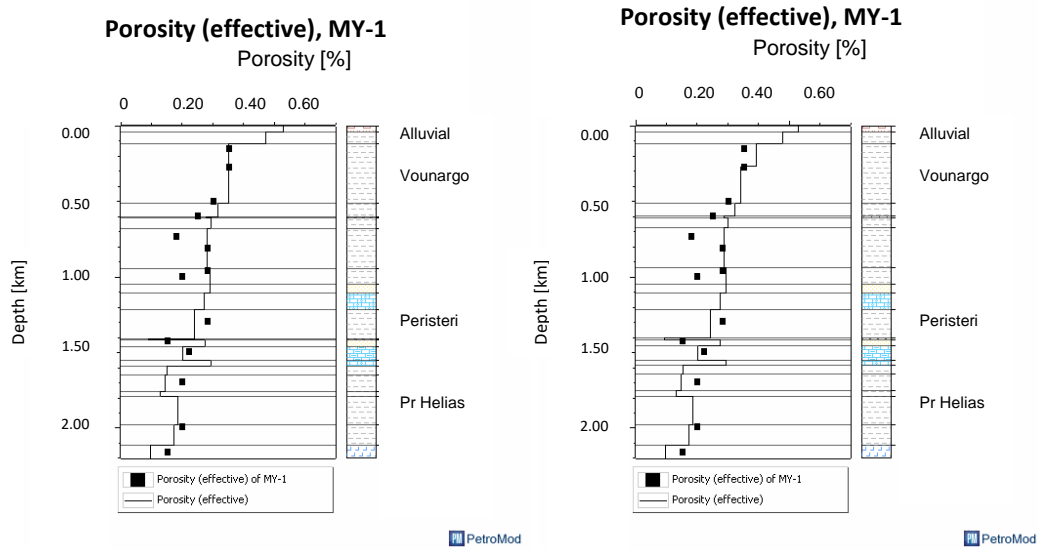


**Figure 16:** Effective porosity calibration, MY-1 model.

Keramidhia erosion of 520m thickness and Vounargo erosion of 200m –final model (left), Keramidhia erosion thickness of 500m and Vounargo erosion of 200m (right)

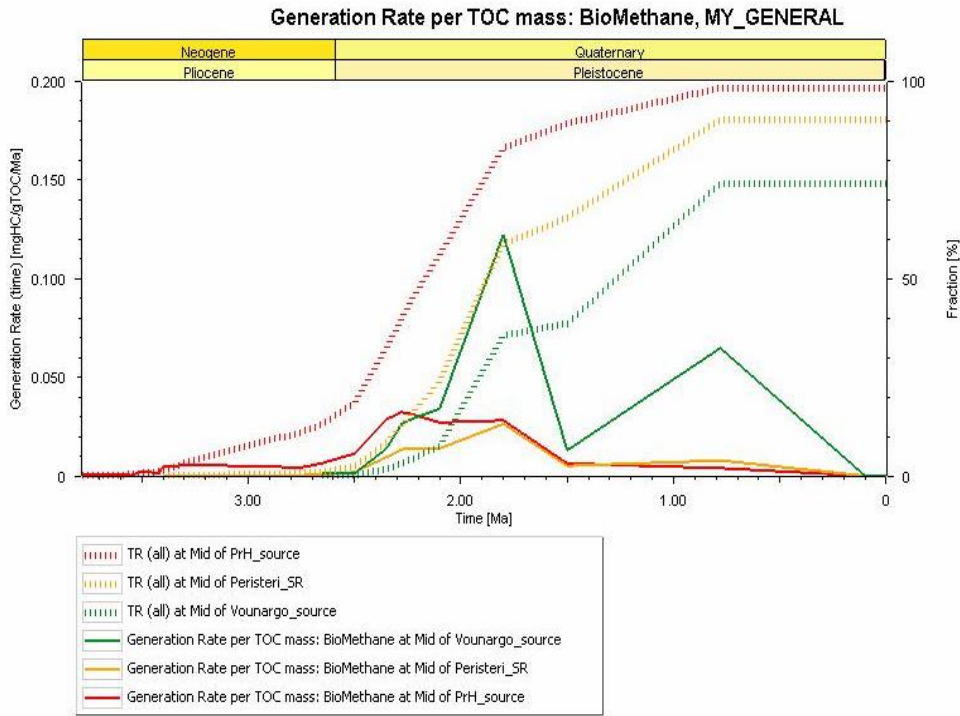
### 6.5.2. Timing of biomethane generation and expulsion

Regarding both VR and porosity calibration, the achieved calibration fit is acceptable. The generated TR (%) burial plot representing each source rock layer (figure 21) shows that HF has a chief impact on the transformation of the organic matter.

In a general sense, the generation stages are the same when comparing the onshore models. However, there are some notable differences which can be seen in the figures below, while the aforementioned erosion states are assumed.

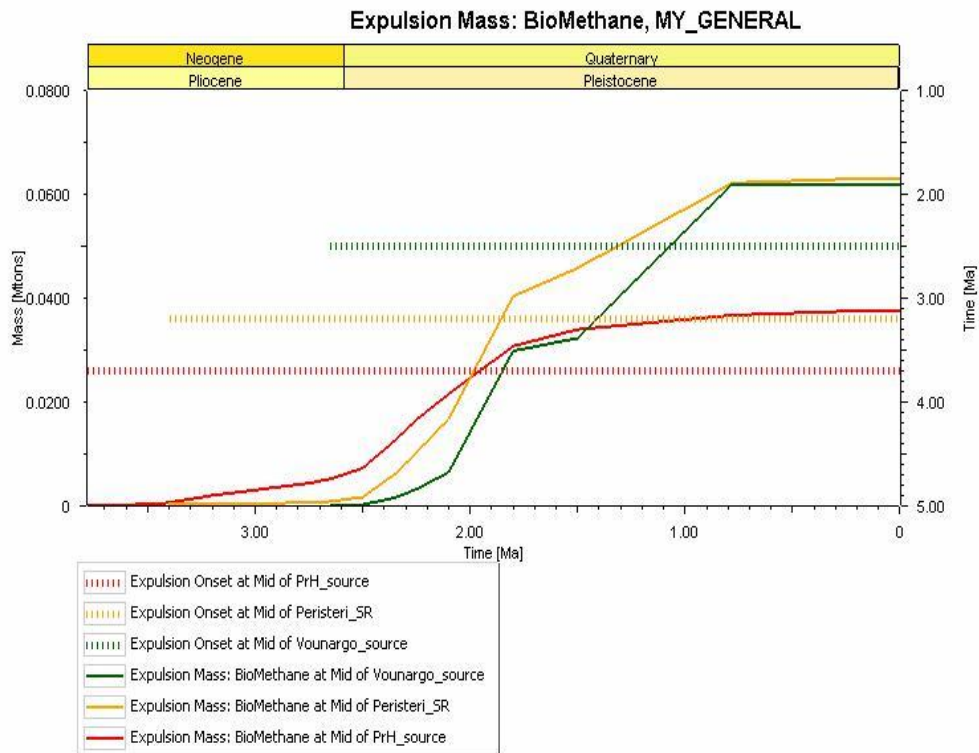
Notwithstanding the increased HF that facilitated the generation and expulsion, expulsion continues while generation seems to be currently ceased. This probably comprises the main result of that turbulent period when erosion was the chief ongoing event, eroding a vast amount of sediments away.

As well as in the ALF1-model, all the encountered source rock layers lie within the Gaussian distribution temperature range and peak generation rate is reached during the peak temperature of the distribution.



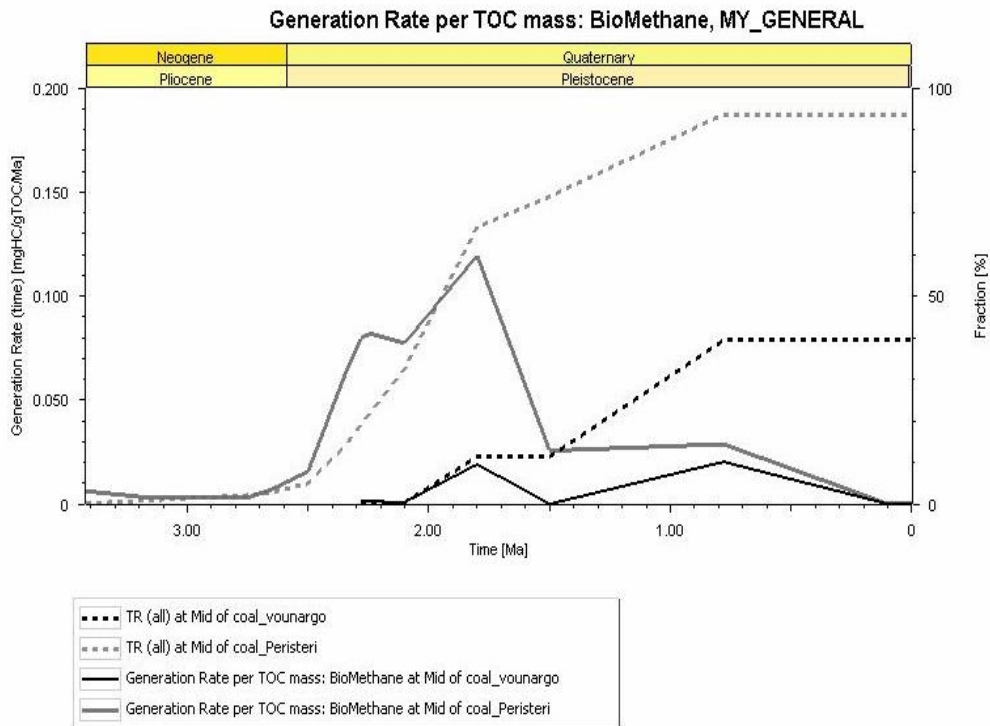
PetroMod

**Figure 17:** Biomethane generation rate per TOC mass, MY-1



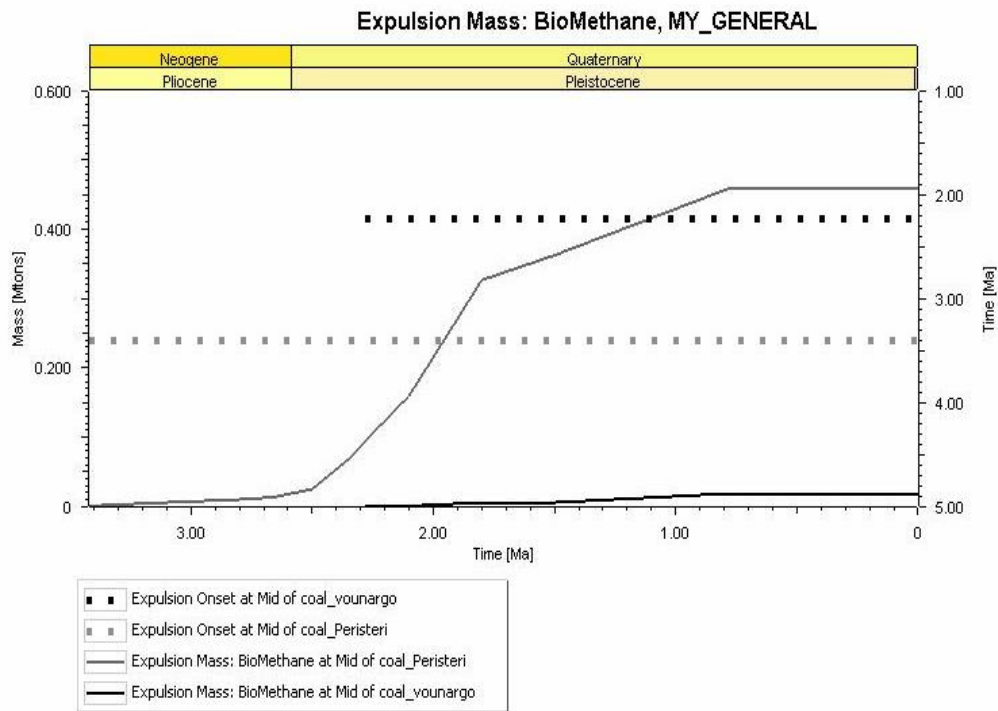
PetroMod

**Figure 18:** Biomethane expulsion, MY-1



PetroMod

**Figure 19:** Biomethane generation rate per TOC mass, MY-1



PetroMod

**Figure 20:** Biomethane expulsion, MY-1

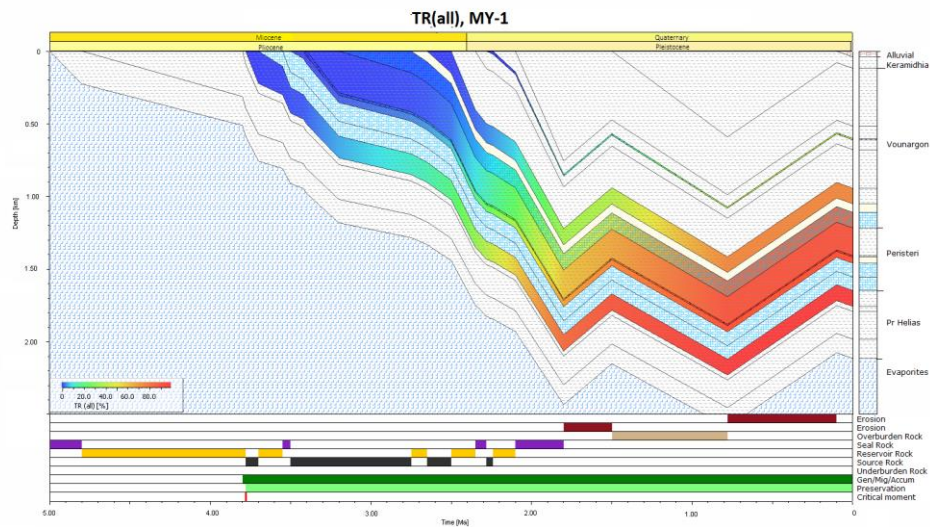


Figure 21: Source rocks' TR (%), MY-1 model

## 6.6. Conclusions

Very low maturities are observed in the ALF-1 model, lying within the lowest part of the Vounargon fm as illustrated in the VR trend. These very low VR values may indicate a HF reduction and thus a lower geothermal gradient. Regarding their position, laying in-between two low conductive coal layers, this scenario seems realistic.

One might argue that the generated maturity trend is not precisely calibrated. However, with these two coal layers taken into account and respecting the fact that the modelling is done for the examination of the potential biogenic gas generation, this calibration is satisfactory.

When talking about bacterial gas, TR indicates the expulsion of the bacterial methane (Troskot-Corbic et al. 2009), reaching in these case percentages of 90% in MY-1 source rock layers and 60% in the ALF-1 model.

Whilst this difference in MY-1 model maturation could result through massive overburden paleo-deposition, could also be an outcome of a heat pulse; still it cannot be assumed without any relative data.

While present-day HF is restricted in the same limits for both onshore models, an overburden paleo-deposition of 520m and 200m regarding the Keramidhia and the Vounargon fms respectively as well

as their further erosion is assumed for the finest maturity calibration. The erosion of Vounargon fm takes place between 1.80-1.50Ma and of Keramidhia fm between 0.78Ma till present time.

A principal result of this paleo-deposition is the increase in the underlying sediments' maturity and thus an augmented generation rate. Despite this, MY-1 model's generation is currently ceased. The aforementioned events seem to be the chief factors of this rapid organic matter transformation but they are also responsible for the expulsion break in the MY-1 point location. Hence, may the expulsion amount be larger in this case, yet its generation ability has to be recovered.

Coupled with the VR values obtained from the calibration procedure, all the above-mentioned results lead to the biogenic gas presence. Not only these results, but also the sedimentation rate, the low prevailing temperatures, the shallow burial depths and the low measured VR values result in an immature diagenesis phase during which the generation of biogenic gas is favoured.

A problem which is possible to be faced in such a lithostratigraphy where evaporites underlie other formations is the sulphur ions present in the evaporites. In this case are present and may convert the Plio-Pleistocene methane into H<sub>2</sub>S (Rice and Claypool, 1981). However, according to the available studies, there is no sulphur action in the Plio-Pleistocene sequence and thus the presence of the evaporites does not seem to have a negative effect on gas accumulation. Instead of this, this evaporitic dome may help the gas accumulation by assisting to the trap generation during its uplift movements (Rigakis et al., 2001).

Last but not least, the suggestion that gases found in the Plio-Pleistocene clastic sequence in the onshore Katakolon bay are of biogenic origin is reinforced by this study; suggesting that a decent amount of biomethane has been generated, an important amount has been eroded and also a vast amount still is expelled and escapes to the surface probably accompanied by deeper catagenetic gases, most likely by virtue of tectonism.

## Chapter 7

### Offshore models

#### 7.1. Case scenarios

The main issue addressed in this chapter is the thermogenic gas generation. A number of studies have investigated its source in Western Greece, concluding that it should probably originate from the Vigla shale member, Posidonia shales or the Triassic source rock intercalations.

Since the syn-rift phase and the Vigla shale member are not present in the external-central Ionian zone, the offshore models' study focuses on the generation potential of the Triassic source rocks. What is more, the Vigla source rock's potential is examined later on in a case study.

In the West Katakolon offshore case, the reservoir rocks are marine carbonates which are entrapped by the pseudo-anticline. During the Miocene erosion, 1000m thick flysch, 400m molasse and a little amount of Eocene limestones seem to have been eroded away. Following this event, the Plio-Pleistocene sedimentation took place which has more like a sealing character, assisting to the preservation of the generated and expelled HC.

Taking into account that the Triassic evaporites have never been entirely drilled, the creation of an exact image is not the case. Consequently, three case scenarios are created regarding the WK-1 and WK-2 wells which examine the hydrocarbon generation potential from the Triassic organic rich intercalations which are examined as part of the evaporites' lithological mixture.

These case scenarios are namely the Best case scenario (BCS), the Mean case scenario (MCS) and the Worst case scenario (WCS) and their dividing characteristics are the TOC (%) and the HI (mgHC/gTOC) of the source rocks.

These parameters are introduced according to the cutting samples of a neighbouring well (SK-1) regarding the BCS and the WCS and from the RE analysis ([table 3](#)) for the MCS, yet a little bit modified, while their classification is done regarding their TOC content. Thus, they are categorized as follows:

- BCS: TOC = 3.85% and HI = 189 (mgHC/gTOC),
- MCS: TOC = 1% and HI = 50 (mgHC/gTOC) and
- WCS: TOC = 0.5 % and HI = 25 (mgHC/gTOC)

## 7.2. Calibration parameters

On the question of temperature, the measured BHTs from the WK-1 well are also very low reaching a maximum of 66°C at a MD of 3040m. Regarding a linear thermal gradient of 1.65°C/100m, the mean linear temperature profile of the post-evaporitic sequence can be delineated, revealing a very low thermal profile, easily compared to the onshore conditions.

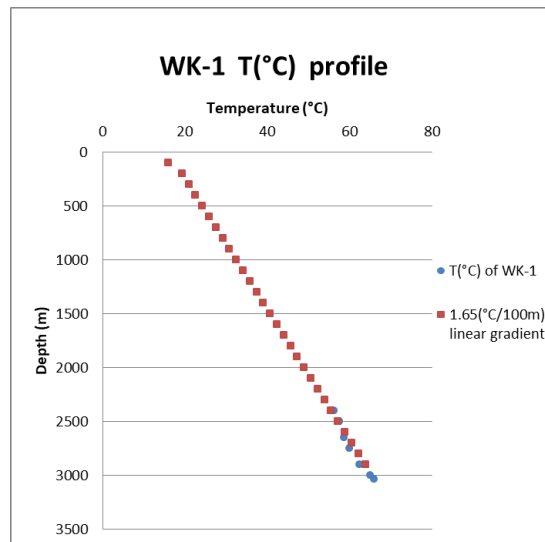


**Figure 22:** Temperature profile, WK-1.

Widely used as a strict maturity indicator, VR values vary from 0.33%Ro to 0.57%Ro within the post-Vigla section. With reference to these values, the calibration of the offshore models is achieved.

On the subject of maturity, RE analysis parameters suggest that the organic matter which is examined from the WK-2 well cuttings is a gas and/or oil source mostly of type III kerogen while type II-III is also existent. Exceptions do exist, yet all the data are presented in [appendix A](#). The presence of very low and very high values of HI and OI respectively is of importance since they are misleading, so they are not taken into account when it comes to the interpretation of the data.

## 7.3. Input data

### Main input data

Much attention has been given to the introduced formations. Even though detailed lithology is not available, a more generic case has been drawn. The lithologies of the penetrated formations (clastics,

Eocene, Senonian, Vigla and Pantokrator limestones) are known, while the evaporites' lithology is introduced regarding the SK-1 well cuttings.

The under investigation Triassic intercalations, are not differentiated as software's input, yet they are distributed within evaporites as part of the lithological mixture.

While in the onshore models the clastic sequence is introduced in detail, in the following models it attains a more generic description. The main input table is presented in [appendix B](#).

## **Boundary conditions**

Boundary conditions of the offshore models are considered to be almost the same with the onshore ones as illustrated in [table 4](#). In more detail, PWDs are the same with only exception the present-day depth which is 87m for the WK-1 model and 250m for the WK-2 model. Furthermore, SWIT is introduced automatically based on the Wygrala (1989) model and the paleo-HF comprises of the same values as in the onshore models except from the Miocene erosion during which the HF reaches  $45\text{mW/m}^2$ .

## **Kinetic model selection**

The hydrocarbon generation from the Triassic evaporites is determined by Pepper&Corvi(1995)\_TII-S(A) kinetic model as it is suggested by previous studies, while Burnham(1989)\_TIII is also examined. These two generation kinetic models have been chosen according to the available data and their correspondence between the age and lithology of the source rocks. Previous studies suggest that the HC source rock's kerogen is of type II-S due to the sulphur content, making it the main candidate of this modelling procedure.

## **7.4. WK-1 models**

### **7.4.1. Calibration of the final model**

Considering the fact that the examined petroleum system lies below the Miocene unconformity, the amount of the paleo-deposited sediments has a major impact on the thermal maturation of the underlying source rocks as a result of the heating period that they could have experienced.

In the maturity depth plot (figure 23), a localized decrease in VR values can be spotted in the shallow part of the clastic section. However, in this study whatever the localized VR deviation, only the main

part of the VR trend is considered in order to calibrate the model and establish a valid maturity interpretation.

The evaporites formation attains a maximum maturation of 1.72%Ro at present time which concerns the formation’s deepest part. In addition, the figure 24 represents the maturity at the middle of the source rock formation providing the mean source rock’s maturity framework.

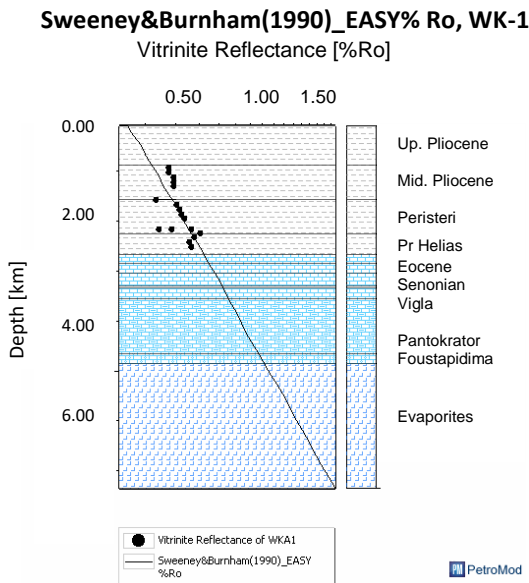


**Figure 23:** Maturity (%Ro) final calibration fit, WK-1 models.

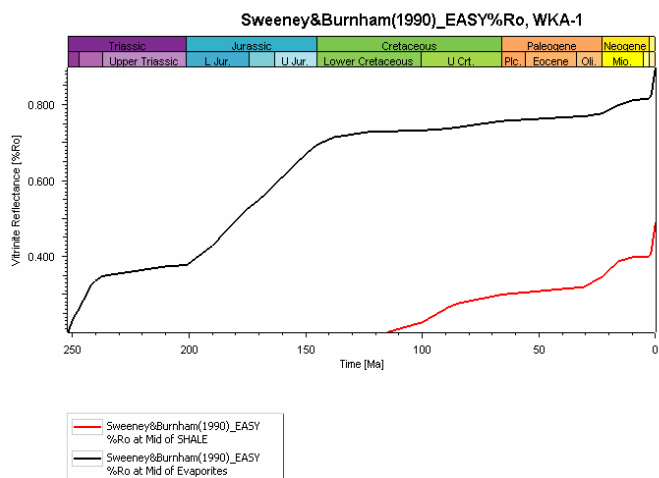


**Figure 24:** Mean maturity time plot (%Ro), WK-1 models

Conversely, BHT is calibrated by the present-day HF and vice versa. Eventually, the present day HF turns out to be 24mW/m<sup>2</sup> when considering a perfect maturity trend fit, although all the available data suggest a heat flow of 28mW/m<sup>2</sup>, thus a temperature equal to 72°C at the unconformity depth.

The maximum difference between these two scenarios is of maximum 10°C which is not problematic neither irrational regarding the value of uncertainty of the measurements. In any case, the available BHTs seem to be problematic.

Another noteworthy information is the fact that since the evaporites may act both as reservoir and source rock, they are separated into three different layers in the input data. The bottom-most is the source rock with 2000m thickness, the middle one is the reservoir rock with 400m thickness and the top one comprises the seal rock with a 100m thickness.

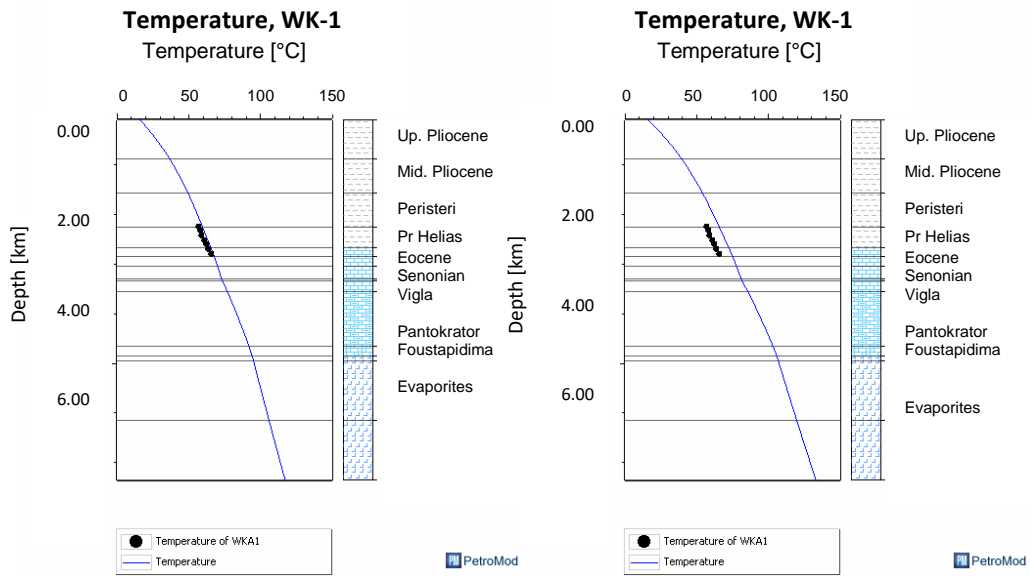


**Figure 25:** BHT trend, WK-1 models.

Present-day HF=24mW/m<sup>2</sup> (left), present-day HF=28mW/m<sup>2</sup> (right)

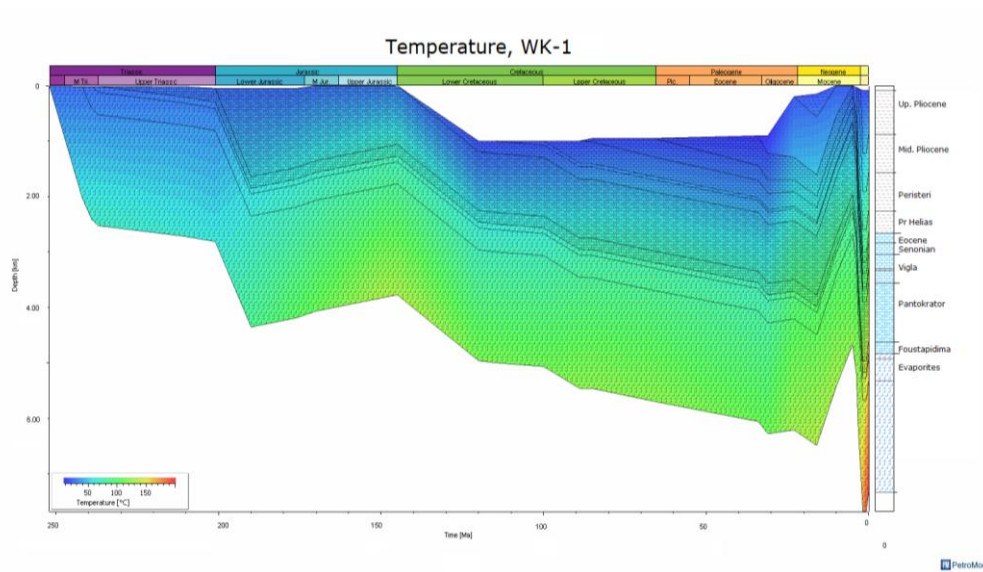


**Figure 26:** Temperature distribution through the burial history of WK-1 point location.

#### 7.4.2. Timing of HC generation and expulsion

The modelled HC generation of the studied WK-1 case scenarios show that the Triassic source rocks have generated HC. Taking into account a flysch thickness of 1000m, a molasse thickness of 400m and two different generation kinetic models, the generation stages take place as follows.

Considering an oil and gas prone source rock (*Pepper&Corvi\_THS kinetic model*), the *first stage*, in other words the early generation phase took place during 200 to 120 Ma. During this period the TR attains a maximum value of 50% while mean maturity ranges between 0.39 and 0.72%Ro. The *second stage* lasts from 120Ma to 5Ma. The TR ranges between 50 and 80% and the maturity between 0.72 and 0.80%Ro. The third stage takes place during the last 5Ma reaching a maximum TR of 98% and a VR of 0.95%Ro.

The *earliest expulsion onset*, reached by the deepest part of the formation is set at 170Ma both for oil and gas phase. At that time, the temperature is almost 110°C, the maturity 0.67%Ro and the TR 35%, illustrating an early thermogenic gas phase.

When a *mean expulsion onset* is considered, in other words the expulsion originating from the middle depth inside the SR, the onset is estimated at 2.50Ma. However, gas is being expelled from 1.80Ma given the maturity of 0.95%Ro and 156°C illustrating a thermogenic gas phase, yet a more mature one when compared to the aforementioned case.

These two expulsion phases represent the BCS solely since the other two scenarios are not yet able to expel any gas, as illustrated in the figures below.

From the perspective of a gas prone type III kerogen, the *first stage* of generation occurs from 175 to 120Ma with a maximum TR of 10% and VR varying from 0.63 to 0.72%Ro. The *second stage*, from 120 to 5Ma has maturity values from 0.78 to 0.85%Ro and TR from 10 to almost 20%. During the *third stage*, 5Ma to present time, TR ranges between 18 and 70% while maturity attains values between 0.83 and 0.90%Ro.

Expulsion onset has been reached from the beginning of generation (175Ma) from the BCS with 0.61%Ro and 103°C. In the other cases, MCS expulsion is estimated to start at 2.43Ma with 1.00%Ro and 118°C while the WCS expulsion has just started.

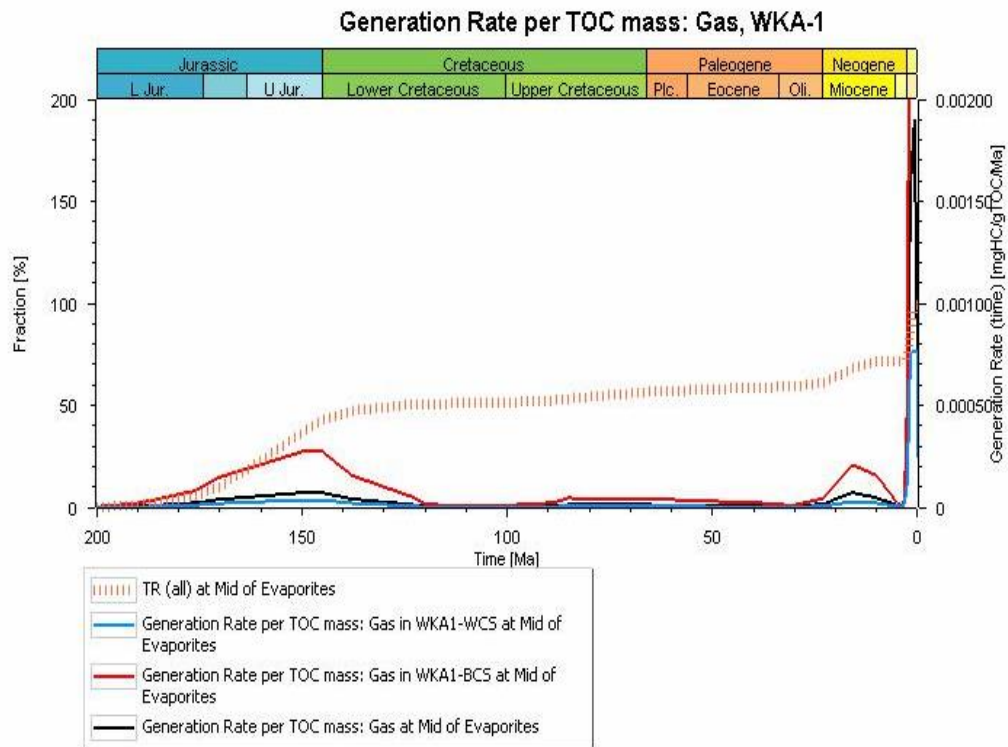


**Figure 27:** Generation rate of gas per TOC mass utilizing Perpper&Corvi\_TIIS.

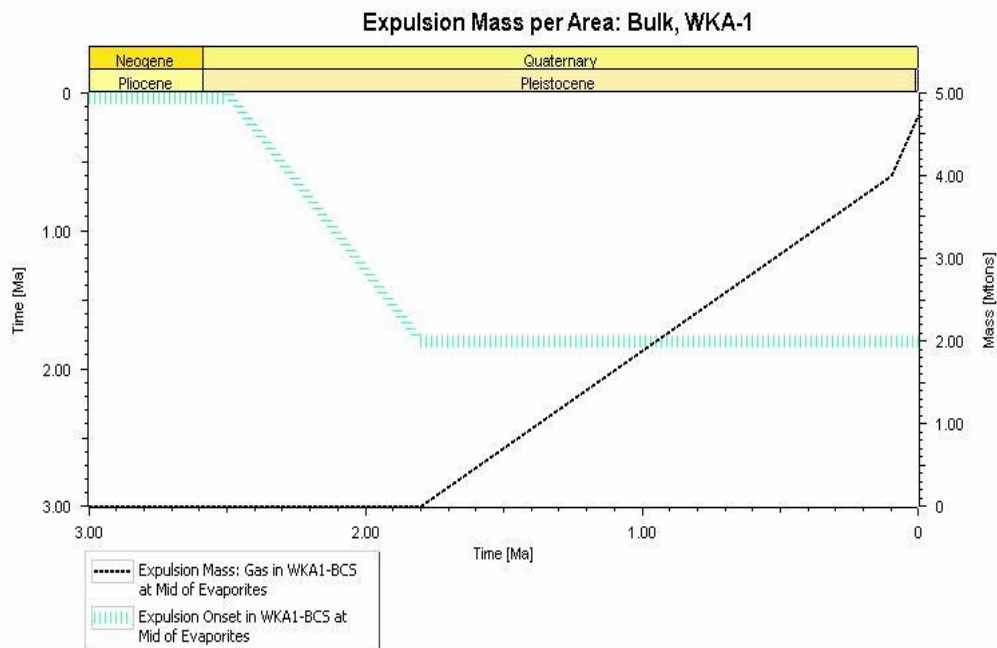
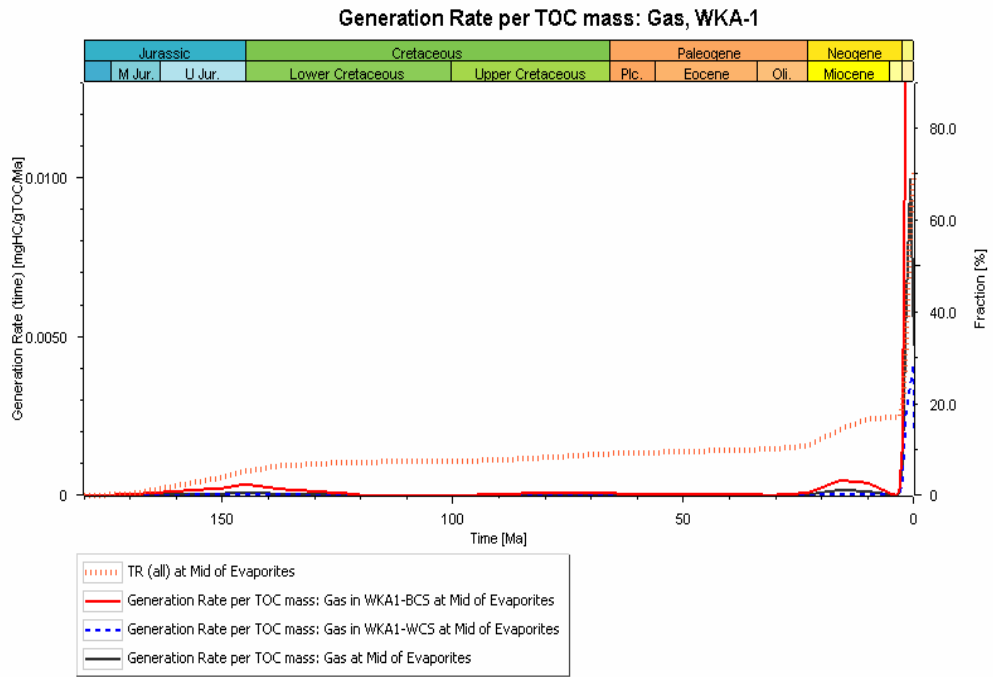
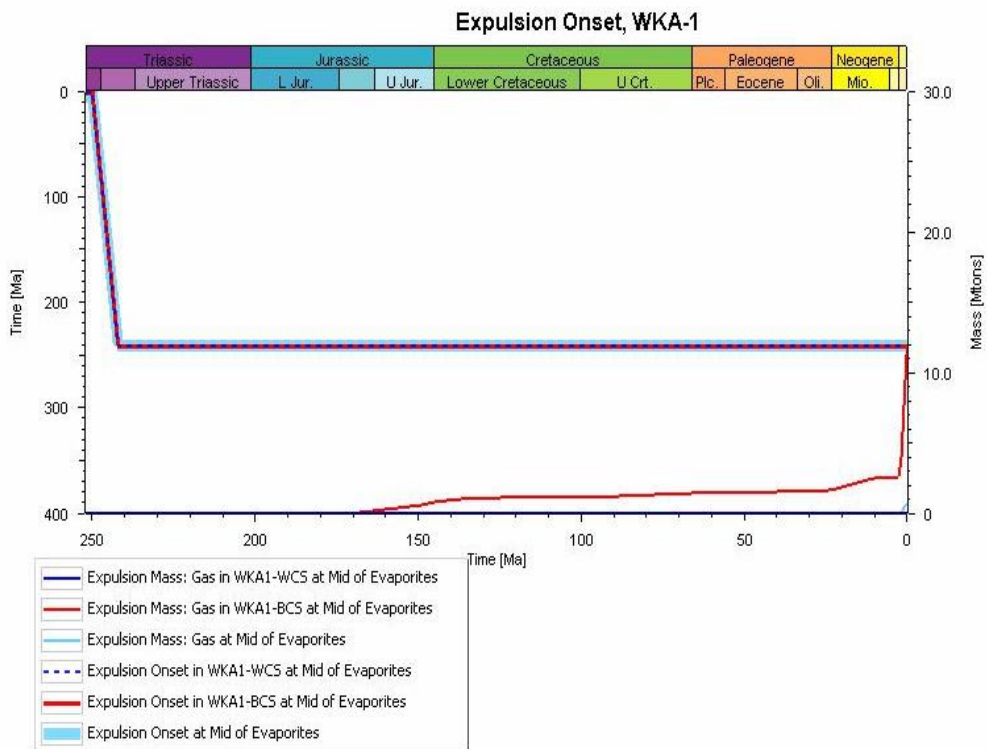


**Figure 28:** Gas expulsion, utilizing Perpper&Corvi\_TIIS.



PetroMod

**Figure 29:** Generation gas rate per TOC mass, utilizing Burnham\_TIII.



PetroMod

**Figure 30:** Gas expulsion, utilizing Burnham\_TIII.

Noteworthy is the calculation of the generation mass which is a result of a series of calculations as presented below that incorporate source rock's HI, TOC, reference simulation cell volume, formation thickness and formation density. Without a doubt, uncertainties are present in these calculations since exact lithological information are not available.

$$M(gTOC) = \left[ \frac{TOC(w\%)}{100} \right] * d \left( g/cm^3 \right) * V(cm^3) \quad (8)$$

Where  $\rho$  is the density and V is the volume of the formation. The mass of HC generated per gram of organic carbon is estimated through equation 9.

$$R \left( mg/gTOC \right) = HI_0 \left( mgHC/gTOC \right) - HI_I \left( mgHC/gTOC \right) \quad (9)$$

Where  $HI_0$  is calculated from the software regarding the S2 and TOC, while  $HI_I$  is taken from pyrolysis data. Finally, the total mass of HC generated is determined from the following equation.

$$HCG(kgHC) = R \left( mg/gTOC \right) * M(gTOC) * 10^{-6} \left( kg/mg \right) \quad (10)$$

## 7.5. WK-2 model

### 7.5.1. Model frame

The location of this well (WK-2) is of major importance for the West Katakolon offshore field. It penetrates the whole clastic sequence up until some hundred meters within the Pantokrator limestones. The crucial part here, is that the clastic sealing section overlies unconformably the Vigla formation, leading us to the conclusion that all the in between section has been eroded.

Generally the burial history is the same to the WK-1. However, during the Miocene erosion not only 1600m have been eroded but 2200m including the Eocene, Senonian and some amount of the Vigla limestones.

Furthermore regarding the fact that the real thickness of the Triassic SR is not known, although it is believed to exceed 1500m, it is introduced with a thickness of 2000m.

The burial history is shown in figure 31, accompanied by an events system chart displaying all the erosional and depositional periods, as well as other crucial events such as the trap formation.

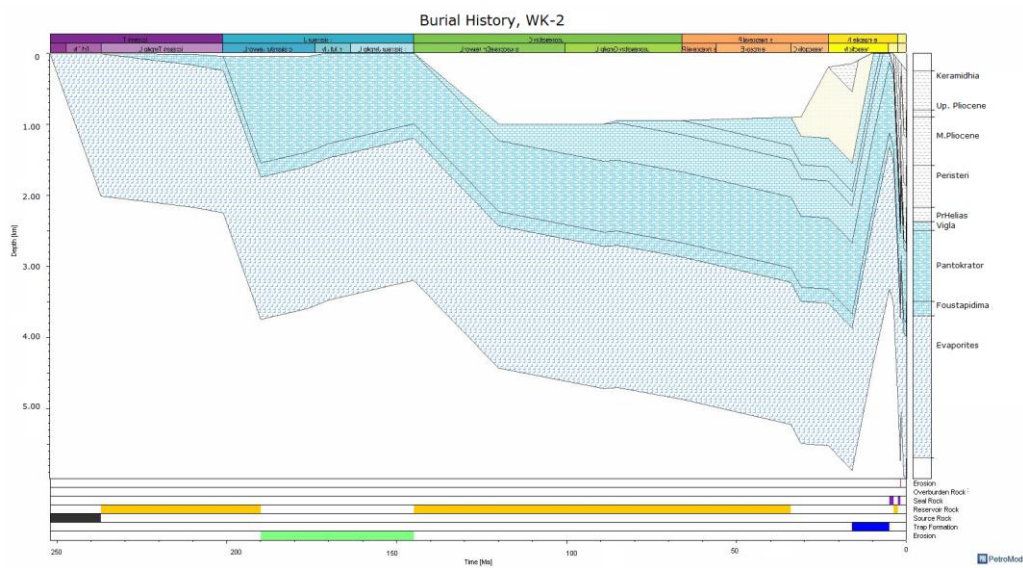


**Figure 31:** Burial history, WK-2 model.

### 7.5.2. Model input

A main deficit of this point location is the lack of maturity parameters and more specifically the lack of VR data. In order to proceed and calibrate the model in a veritable way, VR data of the clastic sequence from the WK-1 well are introduced, considering their small location distance.

Moreover, the boundary conditions are introduced in the same to WK-1 models' way. PWD is exactly the same, except the present-day depth which is 250m and SWIT is calculated from the software based on Wygrala (1989) model. Finally, paleo-HF is identical to the WK-1, with the only difference to be during the Miocene erosion, when  $50\text{mW/m}^2$  is reached with respect to the amount of the eroded sediments.

### 7.5.3. Calibration of the final model

Since the present-day HF is assumed to be  $28 \text{ mW/m}^2$  as in the WK-1 models and no other data is available, the calibration cannot be achieved in any other way rather than *erosional events' alteration*.

The present-day thicknesses of Keramidhia, Upper and Middle Pliocene formations are 520, 97 and 683m respectively. Upper Pliocene and Keramidhia fms is assumed to have been eroded after their deposition, with eroded thicknesses of 700 and 300m respectively. Important to mention is the fact that Upper and middle Pliocene fms comprise the Vounargon fm.

In this manner, paleo-conditions' calibration with respect to introduced VR values is done for the WK-2 model (figure 32), revealing a present-day minimum maturity of 0.68%Ro at the shallowest part of the evaporites and a maximum of 1.20%Ro at its deepest part.

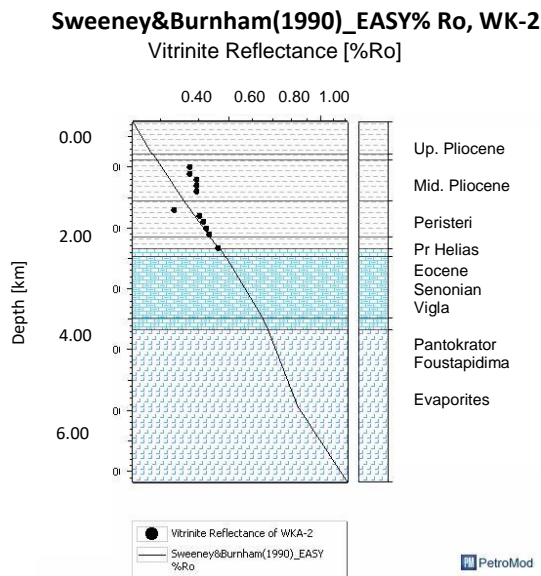


**Figure 32:** Maturity (%Ro) trend with respect to depth.

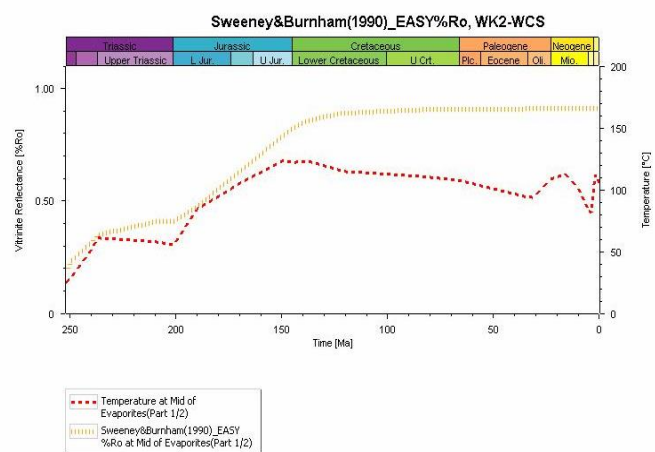


**Figure 33:** Maturity and Temperature time plots of the Evaporitic formation.

#### 7.5.4. Timing of HC generation and expulsion

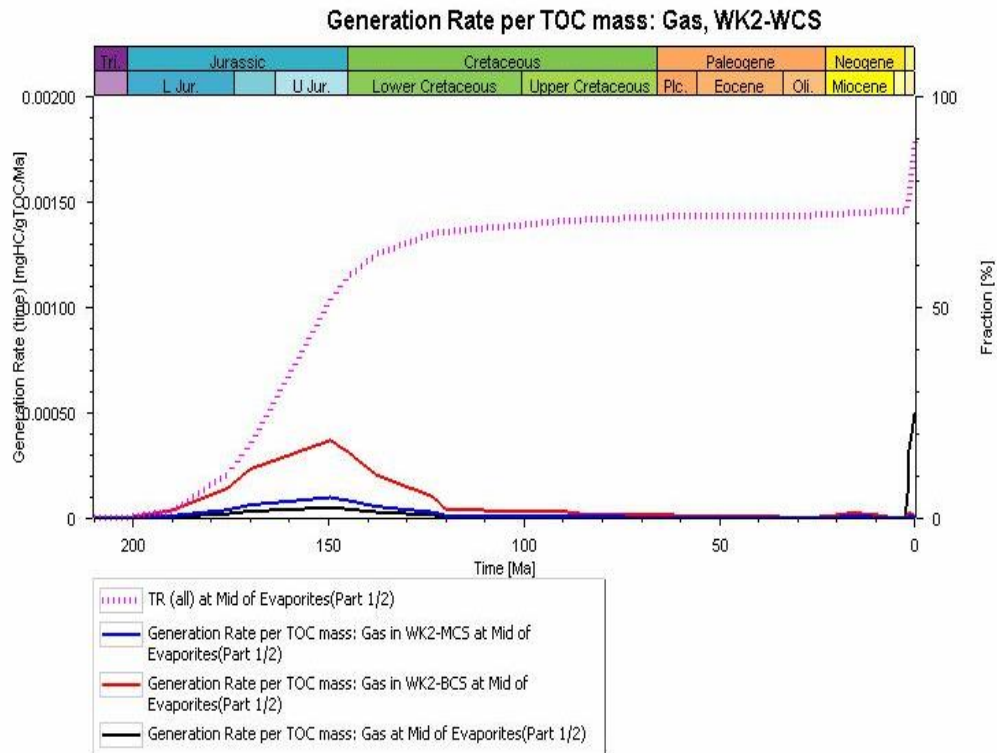
The gas generation rate is examined both for middle depth (mean expulsion onset) and maximum depth (earliest expulsion onset).

For both depths, *the first stage* of generation is restricted between 200 and 120Ma, mostly during the erosion and maximum heat flow prevalence. During this stage, regarding the deepest modelled part of the formation, the TR is around 76%, the maturity is 0.81%Ro and the temperature ranges between 92 and 120°C. The *second stage* takes place from 120 to 5Ma while the TR is around 80%, the temperature lies between 70 and 95°C and the VR is almost the same as on the first stage. The *final stage*, ranges between 5Ma to present-time. During this period, temperature rises from 85 to almost 150°C, the maturity reaches 0.94%Ro and the TR 100%.

All the aforementioned refer to the deepest part of the evaporitic section, thus to the earliest generation and expulsion phases. As far as the middle depth (1500m of the formation) is concerned, the maturation is milder while the stages have the same time ranges (figure 35). During the *first stage* the TR reaches 50%, the maturity is about 0.70%Ro and the temperature does not exceed 105°C. During the *second stage* the maturity is almost the same, the temperature ranges between 74 and 106°C and the TR is almost equal to 62%, while during the last stage the TR has reached 84% and the VR still lies in the mature phase.

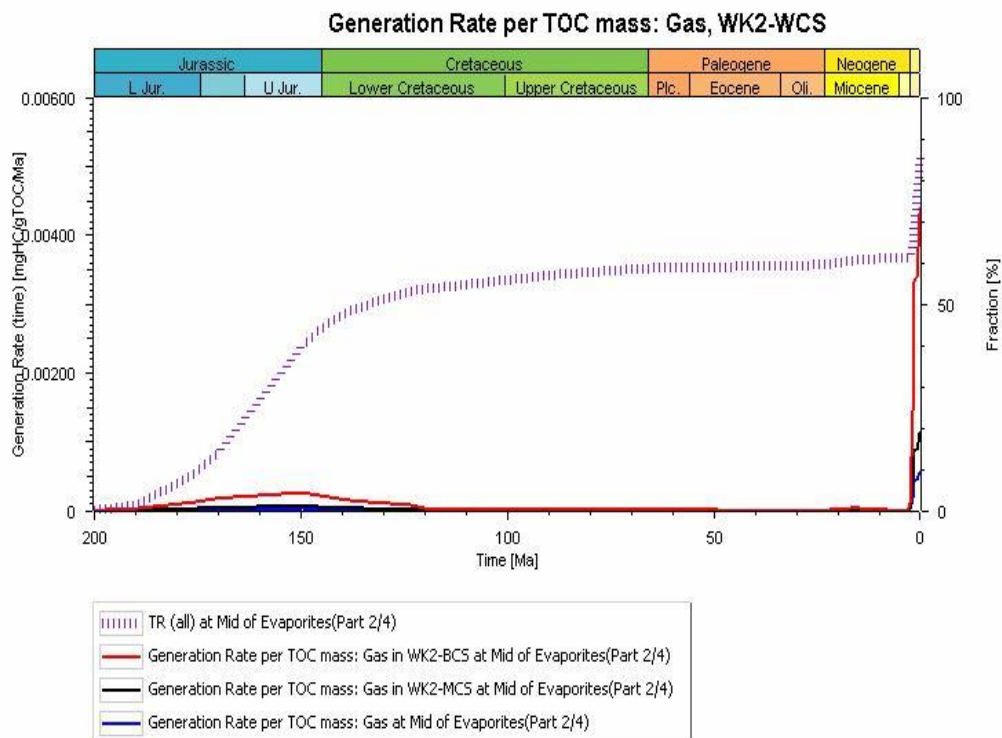
As far as the expulsion onset is concerned it is clear regarding the figures 36 to 37 that the thickness of the evaporitic formation is of major importance. The expulsion onset of the source rock's deepest part is estimated at 140Ma when the conditions are only prone to oil generation with 0.77%Ro and 120°C. At that time, entrapment of HC could not have been the case. On the other hand, gas expulsion is initiated with 82% TR, 0.87%Ro and 145°C at 1.60Ma, reaching 1.02%Ro and 158°C at present-day, illustrating a peak to late mature catagenesis phase.

As it is displayed in the following figures (figure 36 and 37), the expulsion onset is delayed in a shallower part of the formation. Still the gas expulsion onset is at 1.60Ma. At that time temperature is 136°C, the maturity is 0.78%Ro and the TR is 67%, illustrating again an early mature catagenesis stage with thermogenic gas presence.



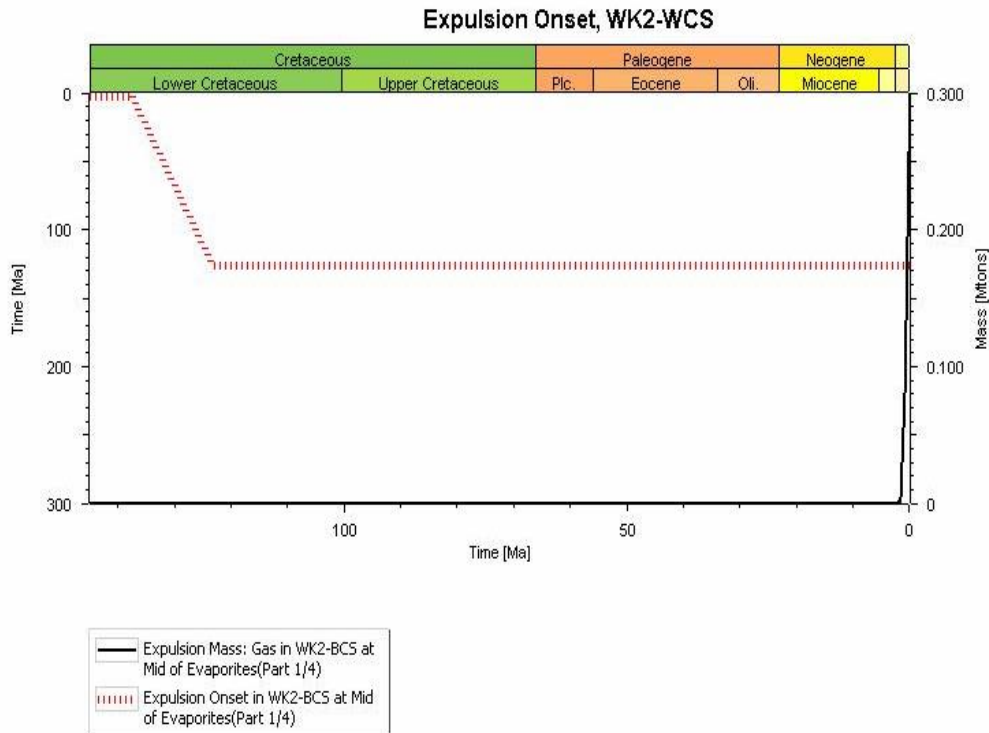
PetroMod

**Figure 34:** Gas generation rate of the deepest evaporitic part, WK-2.



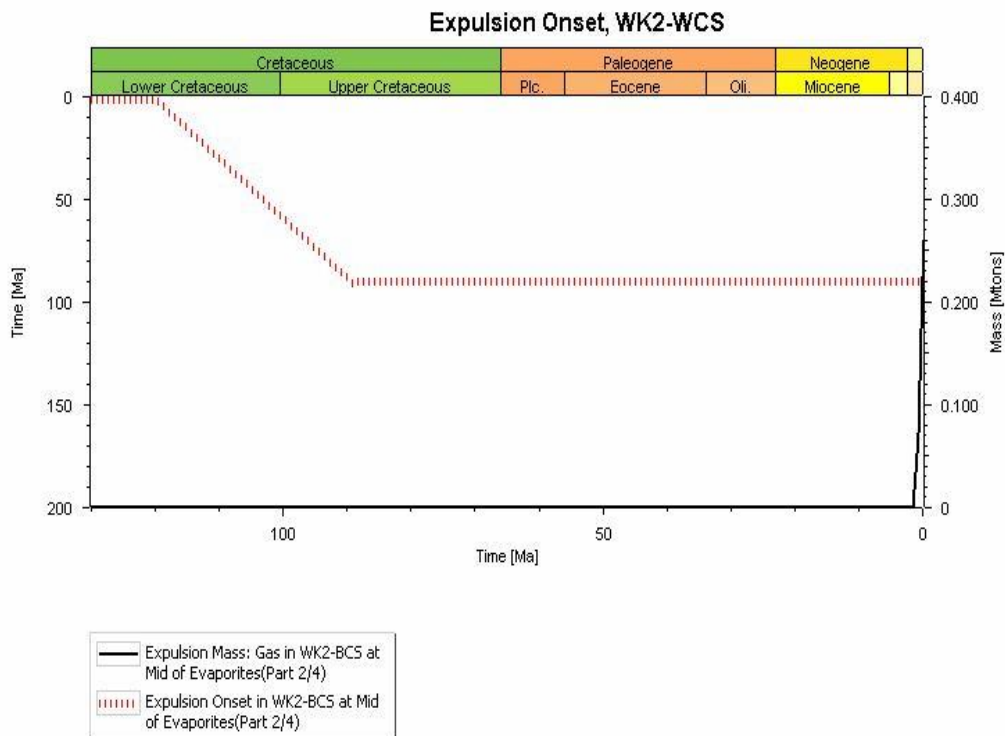
PetroMod

**Figure 35:** Gas generation rate of the middle evaporitic part, WK-2.



PM PetroMod

**Figure 36:** Expulsion onset of the deepest evaporitic part, WK-2.



PM PetroMod

**Figure 37:** Expulsion onset of the middle evaporitic part, WK-2.

## 7.6. Case study

### 7.6.1. Model frame

This case study's main purpose is the examination of both the Evaporitic and Vigla shale member source rocks, considering a thicker overburden thickness of 4000m thick flysch and 400m molasse. In previous studies (e.g. Karakitsios, 2013) it is stated that flysch's thickness exceeds 4000m in the Epirus region, comprising the main reason of this thick flysch selection. Except from the aforementioned, the general model frame is identical to the WK-1 model.

The utilized input of this model is exactly the same with the one of the WK-1 model, regarding all the available case scenarios. Thus, the burial history except the flysch's thickness is exactly the same.

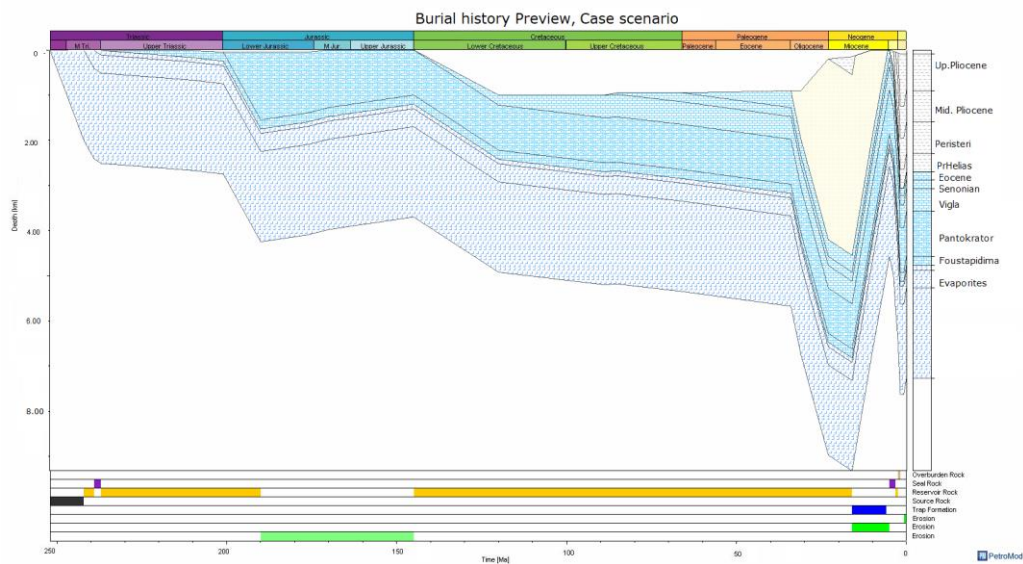


**Figure 38:** Burial history Preview, case study.

Vigla formation is separated in three parts and the middle one comprises the shale member which is dated from Albian to Cenomanian (IGRS-IFP, 1966). Moreover, a thickness of 35m is assumed with respect to Karakitsios (2007) who stated that this is the thickness of this member in the Northern Ionian zone consisting of cherty beds and shale interlayers; a lithology which is also introduced for this source rock layer.

Additionally, he introduced characteristics are a TOC content equal to 2.45% and a HI equal to 267mgHC/gTOC according to Karakitsios (2013).

A maturity depth plot is generated and further calibrated (figure 39). Thus, considering a thicker flysch deposition, the maximum VR values are 0.69% and 1.82% for the Vigla shale member and the Triassic source rock respectively, illustrating the influence of the overburden amount in the thermal maturation. This fact can be observed in figures 39 and 40, where the maturity increases abruptly during flysch deposition.

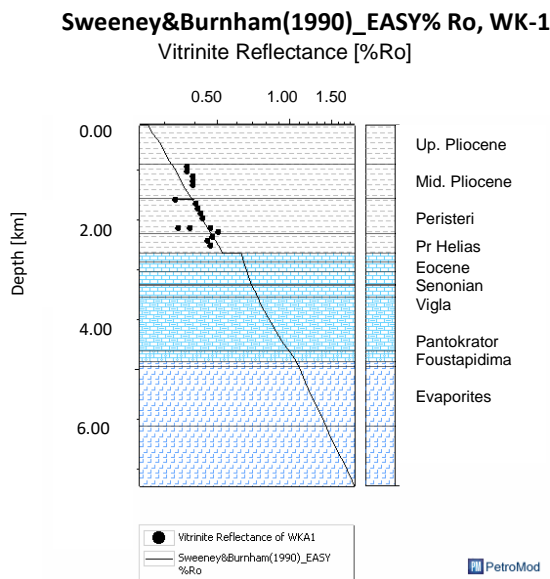


**Figure 39:** Maturity (%Ro) trend with respect to depth.

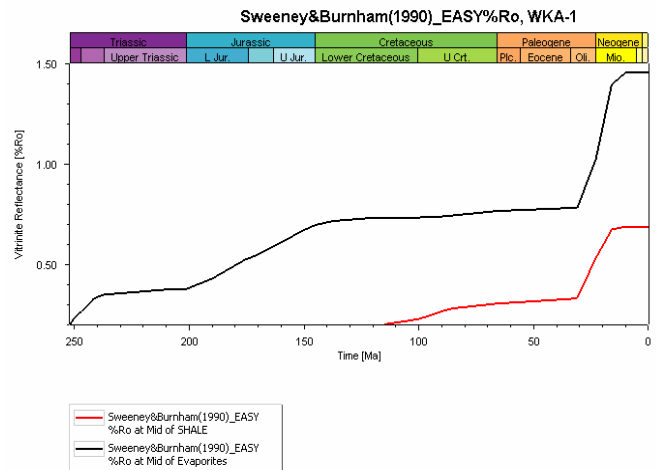


**Figure 40:** Maturity progress time plot for both evaporites and Vigla shale member.

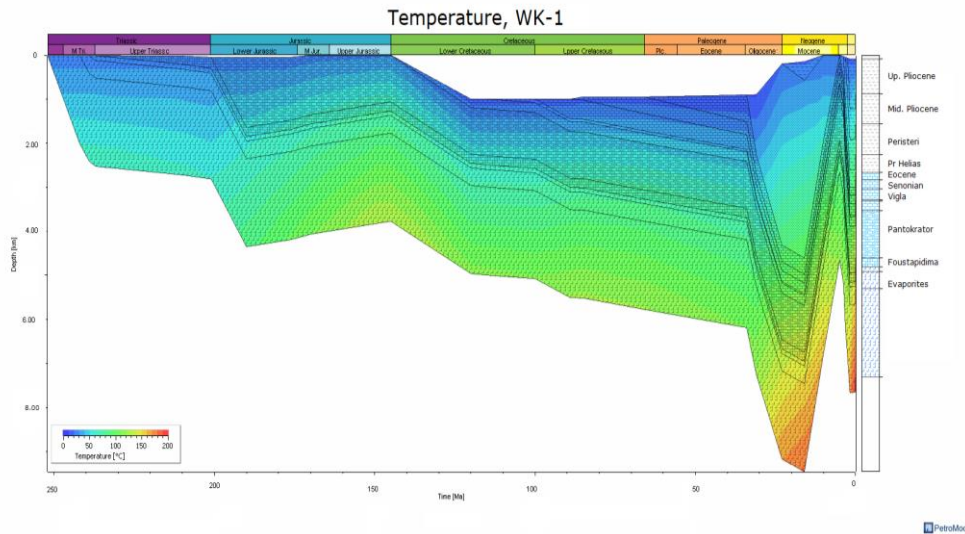


**Figure 41:** Distribution of temperature through the entire burial history.

### 7.6.2. Timing of HC generation and expulsion

In the case of a 4000m flysch and 400m molasse, the generation stages seem to be as follows when considering oil and gas prone source rocks.

Regarding a mean depth, the *first generation stage* takes place between 200 and 120Ma with a maximum TR of 47% and maturity between 0.42 and 0.73%Ro. The *second stage* lasts until 10Ma, during which the TR reaches 100% and the maturity 1.50%Ro. During this stage and more specifically around 30Ma, peak generation rate is accompanied by the initiation of gas expulsion, still only for the BCS. The *third stage* is aged between 10Ma till present time, where the TR is almost 100% and VR is more than 1.50%Ro.

In addition, the deepest part of the evaporites, in other words the earliest possible expulsion, is initiated at 170Ma. At that time, the maturity is around 0.67%Ro, the temperature is 110°C and the TR is 35%, illustrating very early catagenetic gas generation and expulsion.

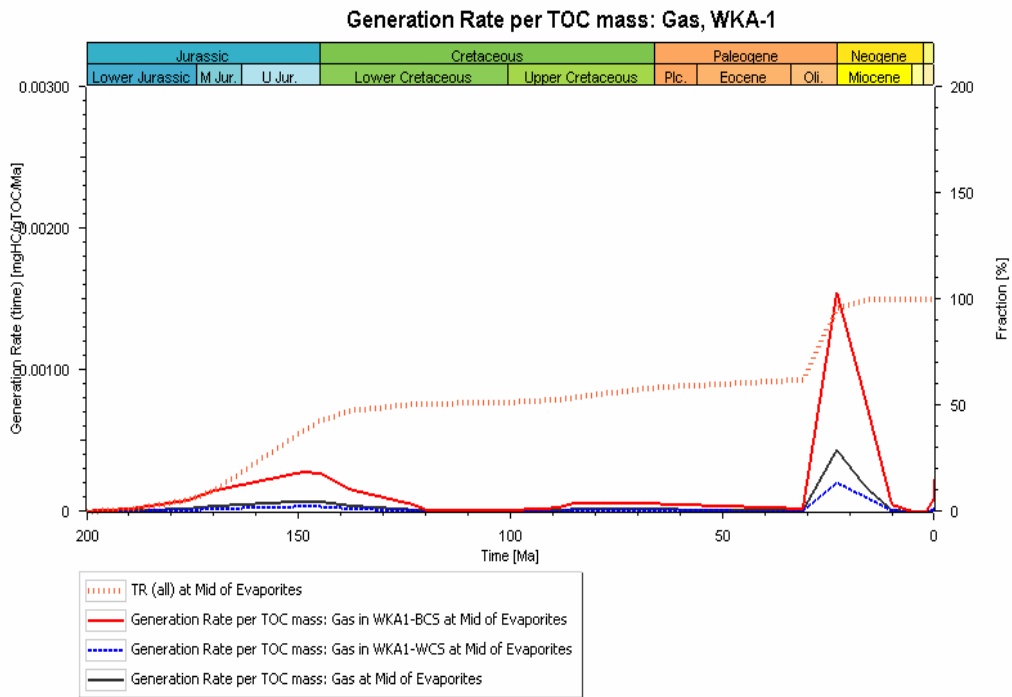
Even though a thicker flysch could be a positive effect in the HCs' generation, the WCS is still not able to expel any gas. However, around 14Ma the expulsion is initiated for the MCS with maturity around 1.50%Ro, illustrating post mature characteristics.

Utilizing *Burnham\_TIII* kinetics, generation rate has a common outline, yet with some dissimilarities. The *first stage* of generation lies between 170 and 120Ma with insignificant gas generation. During

this period TR has a maximum value of 6% and maturity of 0.75%Ro. The *second stage* lasts from 120 to 10 Ma with a maximum TR of 75% and maturity of 1.47%Ro. The *third stage* lasts from 10Ma until present time with a maximum VR of 1.58%Ro and TR of 77%.

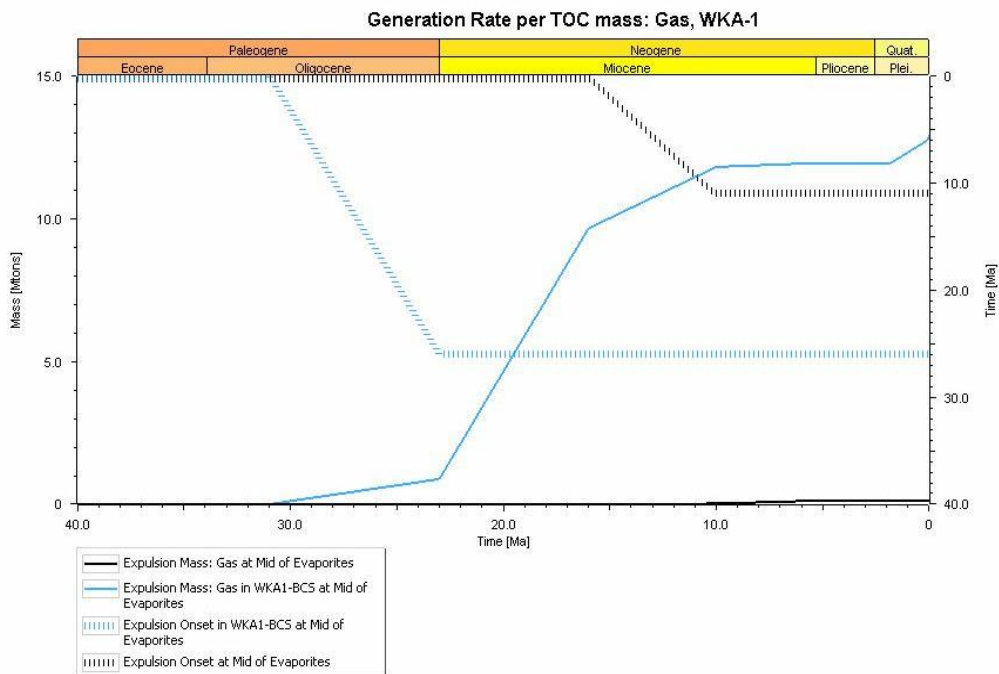
When a gas-prone kerogen is under consideration and the source rock is capable of HC generation, most probably the expulsion will begin in the first place. BCS starts expelling at 170Ma, MCS around 25Ma, yet the WCS is not able to expel any HC until present time.

In light of Vigla source rock, the expulsion onset has also never been reached. A maximum generation rate appears to be 0.004mgHC/gTOC/Ma starting from 3Ma till present-time, while the TR ranges only between 0.50% and 30%



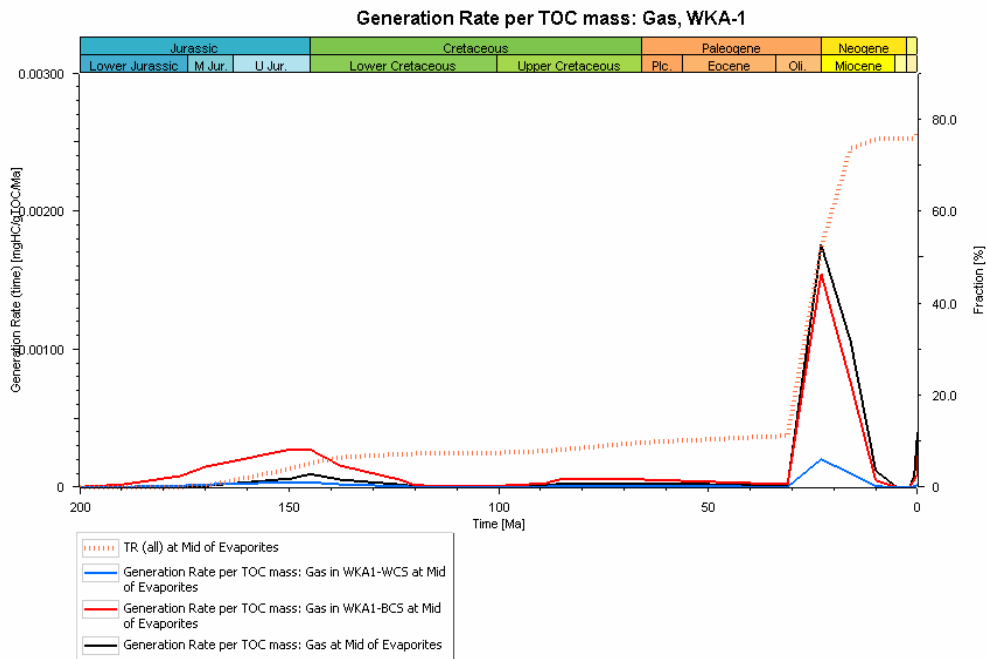
PetroMod

**Figure 42:** Generation rate of gas per TOC mass utilizing Perpper&Corvi\_TIIS and 4000m thick flysch.



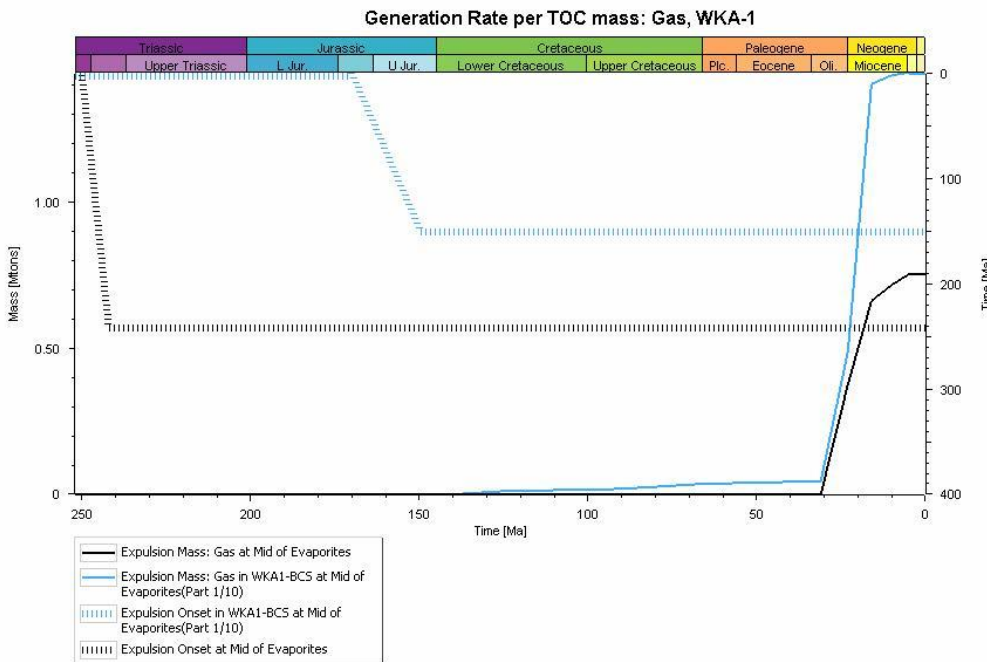
PetroMod

**Figure 43:** Gas expulsion onset, TIIS kinetics, 4000m thick flysch deposition.



PetroMod

Figure 44: Generation gas rate per TOC mass utilizing Burnham\_TIII and 4000m thick flysch deposition.



PetroMod

Figure 45: Gas expulsion onset, TIII kinetics, 4000m thick flysch deposition.

## 7.7. Discussion

Previous studies suggest a type II-S kerogen for the examined source rocks due to sulphur content. Considering the latter and given that Tmax achieves a proper calibration fit only when this kinetic model is used, type II-S generation kinetic model seems to be more representative of the real case scenario.

BCS is the only probable scenario for in situ gas generation and expulsion; still, MCS characteristics do not repel HC expulsion, although its onset is reached later with less amount of outcome. Similarly to the Vigla shale member, WCS has not been able to expel any gas yet which is probably an impact of its immaturity and poor generative potential.

### WK1

In light of a gas prone SR, the expelled gas amounts are definitely larger when compared to the type II-S kinetic model. The significant part is the gas expulsion which happens from scratch leading to its entrapment incapability.

While considering an oil and gas prone SR (type II-S), expulsion onset is reached only by the BCS. The mean gas expulsion onset is estimated at 1.80Ma, whereas the earliest expulsion at 170Ma with 0.95%Ro, 156°C, and 0.67%Ro, 110°C respectively. Present-day conditions of the mean and maximum depth are 1.25%Ro, 175°C and 1.57%Ro, 193°C respectively.

The prevailing conditions illustrate that the expelled gas ranges between the early mature (early thermogenic gas) and the postmature phase (wet gas/condensate), still in the mean case the gas has not reached the wet gas zone yet. Hence, the expelled amount of gas has a more like catagenetic-thermogenic character.

In a nutshell, the expelled HC from the deepest part of the SR could not have been entrapped, whereas the middle part's expulsion onset seems to be subsequent to the trap formation leading to the gas entrapment.

### WK2

Whereas the expulsion onset is prior to the trap formation, the gas expulsion is an ensuing event, estimated at 1.60Ma with 0.87%Ro and 144°C. In addition, the expulsion onset is later when considering a 1500m source rock or in other words a shallower part of the source rock. In this case it

is estimated at 2.50Ma, while the gas expulsion onset is again at 1.60Ma, this time with 0.70%Ro and 125°C.

According to the aforementioned, the expelled gas phase could have been trapped since the expulsion is estimated to begin several million years after the trap formation.

What is more, at present-time the maturity of the deepest part of the source rock is around 1.10%Ro with 159°C and the middle part is around 0.80%Ro with 139°C. The latter illustrates an expelled gas phase with a thermogenic character from an early to peak thermally mature source rock.

### **Case study**

It is obvious that rapid and thick paleo-deposition are the chief reasons of this sharp kerogen's transformation that takes place during the flysch deposition. The paleo-heat flow is also of vital importance, although it cannot be estimated accurately.

The maturity is increased when compared to the WK-1 models. The expulsion is estimated to begin earlier in both BCS and MCS with 0.82%Ro and 1.50%Ro and temperatures of 110°C and 164°C respectively. The onsets are at 30Ma and 14Ma, showing that their gas entrapment is not that possible.

### **Overall**

None of this models has reached the dry gas window. In the possible scenario of deeper burial or of an incident heat pulse, the maturity could have increased along with burial depth. Given that, dry gas originating from oil prone kerogen has to be sought in areas where the burial depth is bigger, or in areas associated with thrusting.

In the overall, evaporite formation turns out to uphold the previous studies which associate the existing gas in the West Katakolon with evaporitic source rocks. In the examined cases, HC could have been both entrapped and escaped depending on the source rock's thickness. A source rock of reduced thickness is more likely to start expelling at a later stage, thus enhancing the entrapment as far as these models are concerned.

Still, further analysis has to be done. Regional tectonics, a more precise paleo-HF trend and overburden paleo-thickness have to be introduced so as to achieve a result closer to the real case scena

## 7.7.1. Appendix A

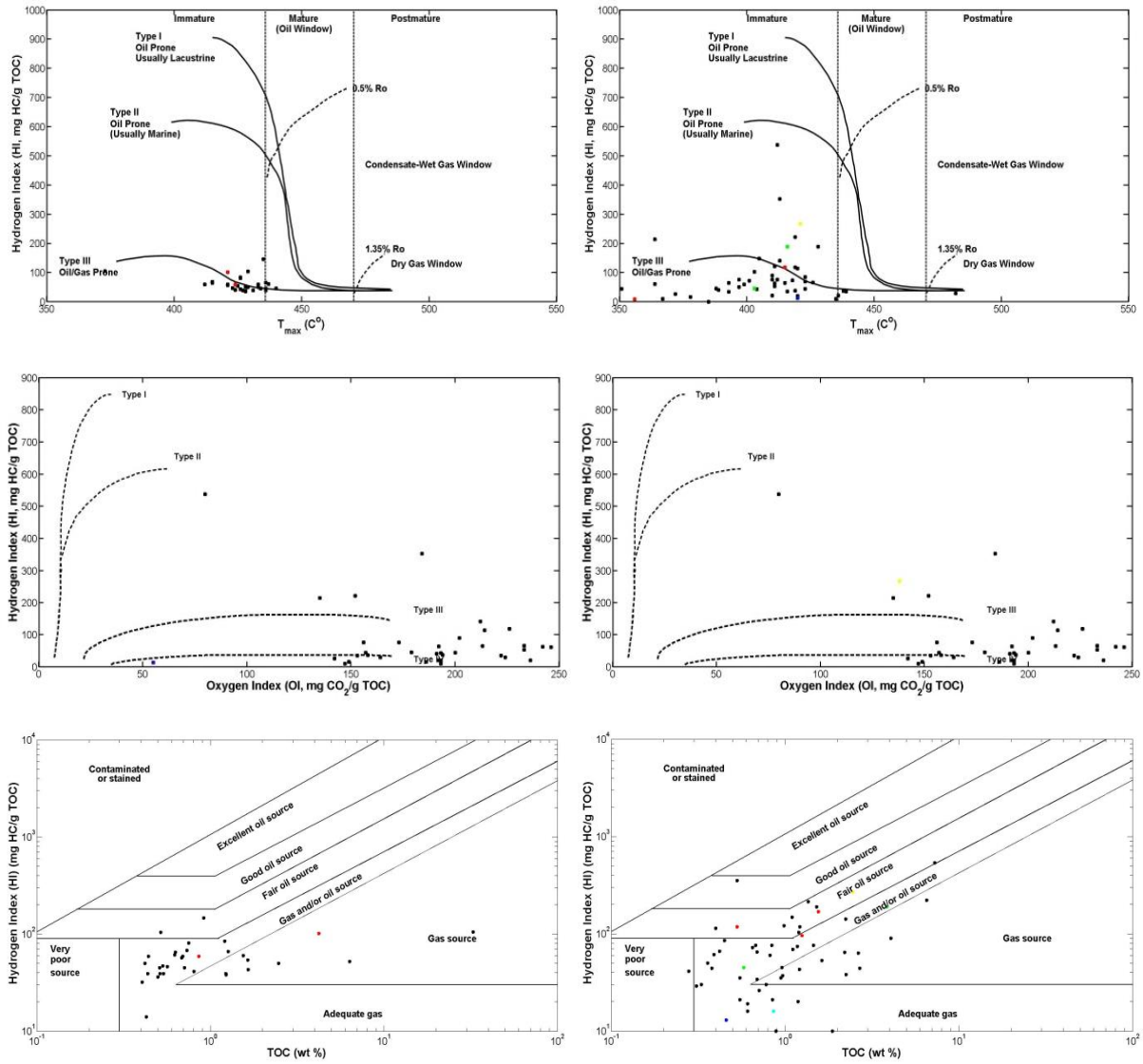


**Figure 46:** Plots indicating the hydrocarbon generation type for the onshore models (left column), offshore models (right column).

*Black dots* for both onshore and offshore models represent sample data from the obtained geochemical analyses; *Red dots* in the onshore plots indicate the outcrop Plio-Pleistocene samples which were personally analysed; *Blue dot* in the offshore plots indicates the Triassic outcrop analysed sample; *Green dots* indicate the MCS, from RE analysis and SK-1 well; *Cyan dot* indicates the BCS sample; *Yellow dot* indicates the sample characteristics of the Vigla shale member (case study).

## 7.7.2. Appendix B

Age (Ma)	Name layer/event	Depth (km)	Thickness (km)	Event type	Paleo-deposition/ Erosion		Lithology	PSE
						(km)		
0.00	Alluvial	0.000	0.040	Deposition			SST, SH, LST, CLAY	Overburden Rock
0.10	Erosion	0.040	0.000	Erosion	-0.520			
0.78	Hiatus/ Keramidhia	0.040	0.080	Hiatus/ Keramidhia	0.520		CLAY, SST, LST, SH, SLST	Reservoir Rock
1.50	Erosion	0.120	0.000	Erosion	-0.200			
1.80	Vounargo	0.040	0.412	Deposition	0.200		CLAY, COAL, LST	Seal Rock
2.20	Vounargo	0.452	0.088	Deposition			CLAY, LST, COAL	Reservoir Rock
2.28	Vounargo_Coal	0.540	0.010	Deposition			COAL, CLAY, LST	Source Rock
2.30	Vounargo	0.550	0.070	Deposition			CLAY, LST +sh	Seal Rock
2.35	Vounargo	0.620	0.275	Deposition			CLAY, LST +sh	Reservoir Rock
2.50	Vounargo	0.895	0.110	Deposition			CLST/LST	Source Rock
2.65	Vounargo	1.005	0.060	Deposition			SST, LST, CLAY	Reservoir Rock
2.75	Vounargo	1.065	0.110	Deposition			SST, CLAY, LST +coal	Source Rock
3.20	Peristeri	1.175	0.173	Deposition			CLAY, LST, SST +coal	Source Rock
3.40	Peristeri_COAL	1.348	0.010	Deposition			coal	Source Rock
3.42	Peristeri	1.358	0.100	Deposition			SST, LST +clay, coal	Source Rock
3.50	Peristeri	1.458	0.096	Deposition			LST, SST, CLAY	Seal Rock
3.60	Pr Helias	1.554	0.111	Deposition			CLAY, LST, SH +coal	Reservoir Rock
3.70	Pr Helias	1.614	0.035	Deposition			CLAY, LST, SH +coal	Source Rock
3.78	Pr Helias	1.725	0.194	Deposition			CLAY	Reservoir Rock
3.80	Pr Helias	1.760	0.129	Deposition			CLAY, LST, SH +SST, coal	Reservoir Rock
4.80	Pr Helias	1.954	0.040	Deposition			CLAY, LST, SH, +Calc, coal	Seal Rock
5.00	Erosion	2.083	0.000	Erosion	-3.700			
16.00	Molasse	2.083	0.000	Deposition	0.400		SH, SST, CLAY, CGL	
22.00	Turbidites	2.083	0.000	Deposition	1.000		SST, LST, CLAY, MARL, CGL	
34.00	Eocene	2.083	0.000	Deposition	0.400		LST, CLAY, SH	
66.00	Senonian	2.083	0.000	Deposition	0.200		LST, CLAY, SH	
89.00	Vigla	2.083	0.000	Deposition	0.500		LST, SH, CHERT, SST	
145.00	Erosion	2.083	0.000	Erosion	-0.500			
190.00	Pantokrator	2.083	0.000	Deposition	1.500		LST, SH, DOL, AHN, +GY	
201.00	Foustapidima	2.083	0.000	Deposition	0.200		LST, DOL, SH, AHN +GY	
237.00	Evaporites	2.083	2.500	Deposition			HAL, LST, CLAY, AHN +coal	Underburden Rock
252.00	Triassic							

**Table 6:** General picture of the onshore models' main input.

The well formation tops are different between the two models, yet very similar.

This input refers to the ALF-1 model, while with red are the erosion events and its characteristics of the MY-1 model.

Age (Ma)	Name top	Depth (km)	Thickness (km)	Event type	Paleodeposition/		Lithology	PSE
					Erosion (km)			
0.00	Erosion	0.087	0.000	Erosion	-0.350			
0.78	Hiatus	0.087	0.000	Hiatus				
1.80	Up. Plio (Vounargo)	0.087	0.813	Deposition	0.350		CLAY, LST, COAL	Overburden Rock
2.50	Mid. Plio (Vounargo)	0.900	0.700	Deposition			CLAY, LST, SH, SSH, COAL	Reservoir Rock
3.20	Peristeri	1.600	0.700	Deposition			CLAY, LST, SST, COAL +sh	Seal Rock
3.80	Pr Helias	2.300	0.403	Deposition			CLAY, LST, CLC, SST	Seal Rock
5.00	Erosion	2.703	0.000	Erosion	-1.600			
16.00	Molasse	2.703	0.000	Deposition	0.400		SH, SST, CLAY, CGL	
23.00	Deep sea fan	2.703	0.000	Deposition	1.000		SST, LST, CLAY, MARL, CGL	
34.00	Eocene	2.703	0.173	Deposition	0.200		LST, CLAY, SH	Reservoir Rock
66.00	Senonian	2.876	0.090	Deposition			LST, CLAY, SH	Reservoir Rock
89.00	Vigla	2.966	0.094	Deposition			LST, SH, CH +sst	Reservoir Rock
100.00	Shale member	3.060	0.030	Deposition			CH, SH	Source Rock
115.00	Vigla	3.090	0.376	Deposition			LST, SH, CH +sst	Reservoir Rock
145.00	Erosion	3.466	0	Erosion	-0.500			
190.00	Pantokrator	3.466	1.000	Deposition	0.500		LST, SH, DOL +ahn, gy	Reservoir Rock
201.00	Foustapidima	4.466	0.200	Deposition			LST, DOL, SH, +ahn, gy	Reservoir Rock
237.00	Evaporites	4.666	0.100	Deposition			HAL, LST, CLAY + ahn, coal	Seal Rock
239.00	Evaporites	4.766	0.400	Deposition			HAL, LST, CLAY + ahn, coal	Reservoir Rock
242.00	Evaporites	5.166	2.000	Deposition			HAL, LST, CLAY + ahn, coal	Source Rock
252.00	Triassic	7.166						

**Table 7:** Main input, WK-1 models

Age (Ma)	Name top	Depth (km)	Thickness (km)	Event type	Paleodeposition/		Lithology	PSE
					Erosion (km)			
0.00	Hiatus	0.250	0.000	Erosion	-0.300			
0.10	Erosion	0.250	0.000	Hiatus				
0.78	Keramidhia	0.250	0.550	Deposition	0.300		CLAY, SST, LST, SH, SLST	Overburden Rock
1.60	Erosion	0.800	0.000	Erosion	-0.700			
1.80	Up. Plio (Vounargo)	0.800	0.097	Deposition	0.700		CLAY, LST, COAL	Seal Rock
2.50	Mid. Plio (Vounargo)	0.897	0.683	Deposition			CLAY, LST, SH, SSH, COAL	Reservoir Rock
3.20	Peristeri	1.580	0.590	Deposition			CLAY, LST, SST, COAL +sh	Seal Rock
3.80	Pr Helias	2.170	0.205	Deposition			CLAY, LST, CLC, SST	Seal Rock
5.00	Erosion	2.375	0.000	Erosion	-2.400			
16.00	Molasse	2.375	0.000	Deposition	0.400		SH, SST, CLAY, CGL	Reservoir Rock
23.00	Deep sea fan	2.375	0.000	Deposition	1.000		SST, LST, CLAY, MARL, CGL	Reservoir Rock
34.00	Eocene	2.375	0.000	Deposition	0.400		LST, CLAY, SH	Reservoir Rock
66.00	Senonian	2.375	0.000	Deposition	0.200		LST, CLAY, SH	Reservoir Rock
89.00	Vigla	2.375	0.123	Deposition	0.400		LST, SH, CH +sst	Reservoir Rock
145.00	hiatus	2.498	0.000	Erosion	-0.500			
190.00	Pantokrator	2.498	0.997	Deposition	0.500		LST, SH, DOL +ahn, gy	Reservoir Rock
201.00	Foustapidima	3.495	0.200	Deposition	-0.300		LST, DOL, SH, +ahn, gy	Source Rock
237.00	Evaporites	3.695	2.000	Deposition			HAL, LST, CLAY + ahn, coal	
252.00	Evaporites	5.695						

**Table 8:** Main input, WK-2 model

## Chapter 8

### West Katakolon 2D modelling

#### 8.1. 2D model

The 2d model is created using WK-1 and WK-2 well formation tops and information from the NW-SE West Katakolon geologic cross section from Xenopoulos and Roussos (2007). This cross-section is chosen owing to its location, which depicts the entrapped formations under many assumptions, regarding the fact that the only available data are geochemical and formation tops from the WK-2 and WK-1 wells without any additional geological, structural or seismic cross-section data. Hence, it is more like a most-probable 2D scenario of the study area which has as main purpose the comparison of the maturity models, rather than a real case scenario.

Even though the 2D section has been created to display the west Katakolon offshore field as a main purpose, the created model has been calibrated using the data from the WK-1 and WK-2 wells which penetrate this cross-section.

The lithostratigraphy is created according to Xenopoulos and Roussos (2007) and Maravelis et al., (2014) combined with the above-mentioned available data. The source rock is assumed to be the whole evaporitic formation, which has a thickness of 2000m. Their characteristics and the boundary conditions of the model are the same with the final 1D WK-1 MCS model.

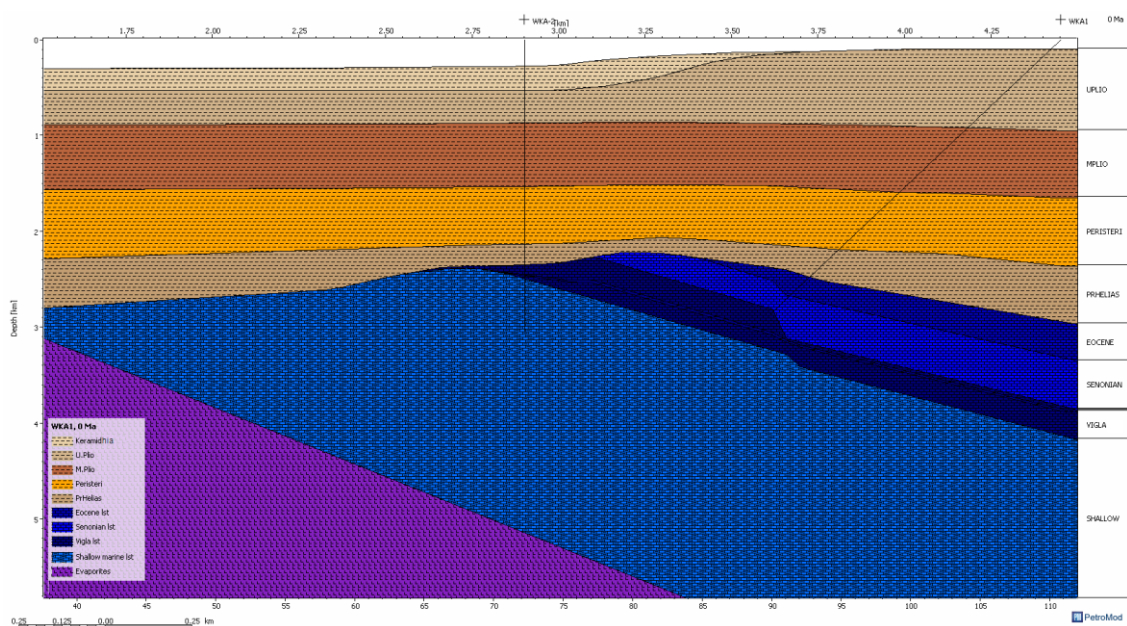


**Figure 47:** 2D model of the West Katakolon field, modified after Xenopoulos and Roussos (2007) and Maravelis et al. (2014).

As far as the deposition is concerned, it is introduced in the same sense as in the 1D model. This implies that the evaporitic formation is considered to have been deposited in situ instead of being thrust from another area, although this is a possible scenario. Thus, evaporites deposition takes place during Triassic followed by the shallow marine limestones. During 190-145Ma, 500m of the latter are eroded and the deposition continues in the same way as in the 1D WK-1 model.

Petrobuilder 2D which is a function of Schlumberger's PetroMod 2017 software was been utilised for this purpose, accompanied by the 2D Simulator and 2D Viewer. Before simulation, it is possible to visualize the 2D burial history in order to identify any inconsistencies on the geometry. During simulation, forward modelling is utilised, by simulating the deposition of each layer from bottom to top and re-compact in order to obtain the present-day geological section. Erosions are observed from 190 to 145Ma and from 16 to 5Ma, the rest time period is characterised by deposition and subsidence.

Simulation is done for generation only while taking into account Pepper&Corvi\_TIIS generation kinetic model for the encountered source rock. Owing to the lack of geological, structural and petrographic data, the outcome of the simulation is rough, yet there are some consistencies with the 1D maturity model.

The optimization value as a result of the model run which shows the geometrical consistency between the input and the modelled section is 0.023% after three simulation runs.

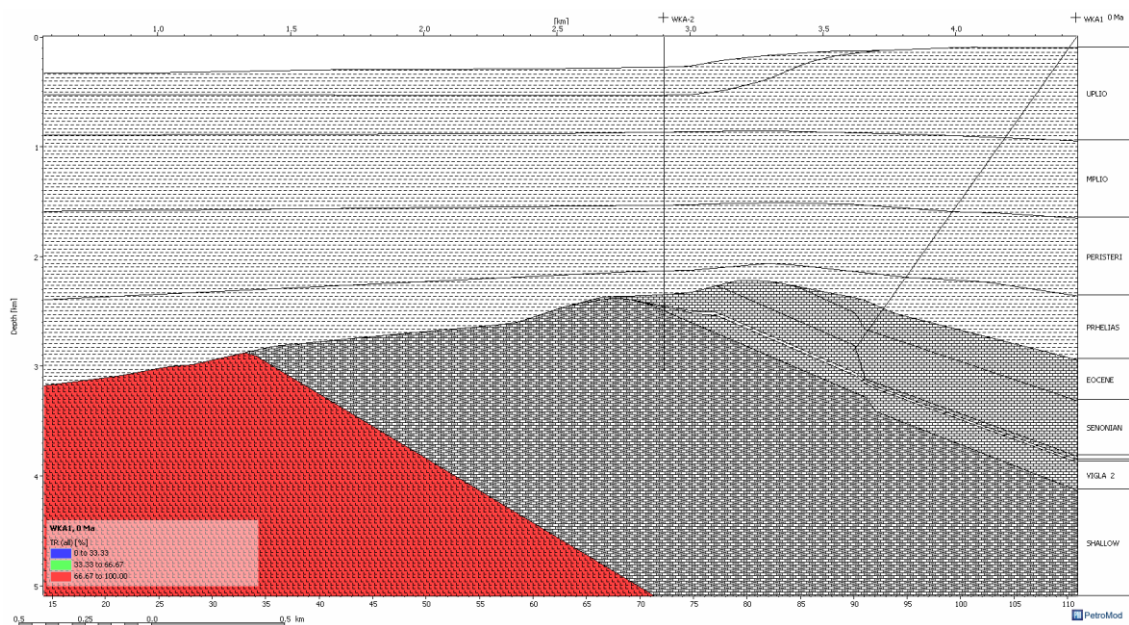


**Figure 48:** Source rock TR (%) distribution in West Katakolon offshore field.

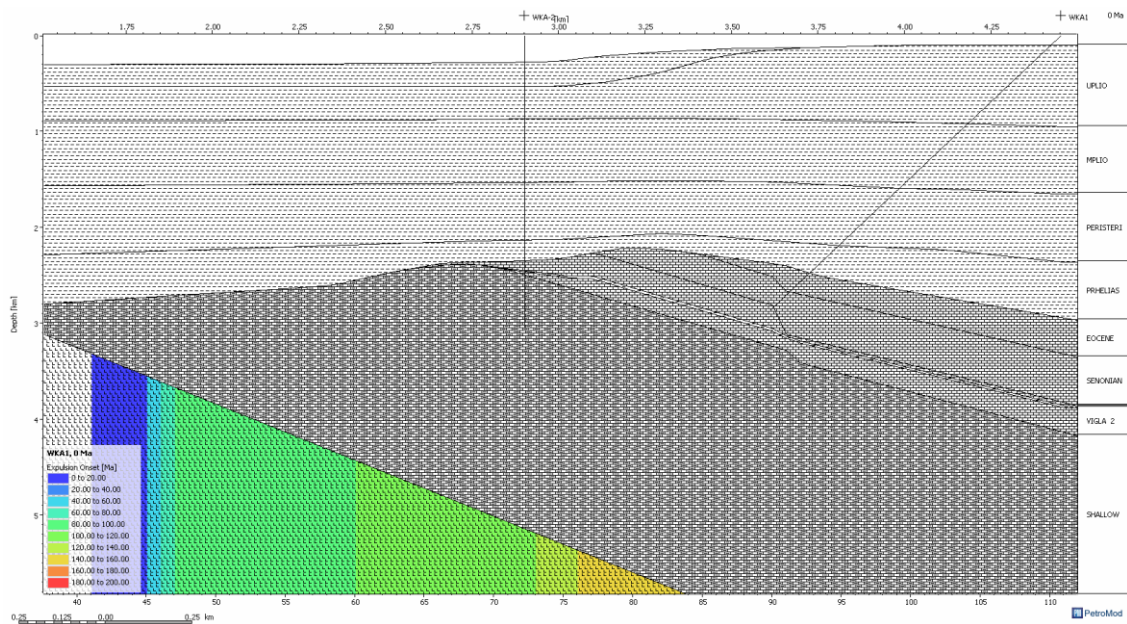


**Figure 49:** Source rock's expulsion onset in West Katakolon offshore field.

## 8.2. Discussion

Simulating in terms of generation results almost the same maturity frame to the 1D WK-1 MCS model, where a 1000m thick flysch and 400m thick molasse are considered. The evaporitic section lies in the catagenesis phase reaching also the wet gas zone at bigger depths. However, in this simulation process, evaporites seem to be more mature since the dry gas phase is present at the deepest parts of the formation.

Present-day TR (%) is almost 100% and the source rock's expulsion onset is estimated at 145Ma. Regarding the whole thickness of the SR formation, the aforementioned results are more or less in accordance with the 1D MCS results.

The observed thermal maturation in the examined cross section is in a general way in accordance with the 1D maturity model. After examining that the maturation results are congruent in the 1D and 2D models for the offshore area, the conclusion is that insignificant amounts of hydrocarbons were produced in the basin, although some of them could have probably escaped given the assistance of the regional tectonic system and the prior to the trap formation expulsion.

The available data have to be revised and re-evaluated since in terms of gas productivity the area seems to be prosperous and gas accumulation and seepage is evident. Any future work regarding the modelling of the offshore West Katakolon PS would be best served by determining the true amount of the eroded Miocene sediments, as well as the lithological properties of the present formations.

## References

- AUBOUIN, J., (1959). Contribution a l'étude géologique de la Grèce septentrionale: les confins de l'Épire et de la Thessalie, *Annales Géologiques des Pays Helleniques*, 1, pp. 1-483
- BARKER, C., 1982. Oil and gas on passive continental margins. In: Watkins, J.S., Drake, C.L. (Eds.), *Studies in Continental Margin Geology*, vol. 34. *American Association of Petroleum Geologists Memoir*, pp. 549–565.
- BERNOULLI, D. & RENZ, O. (1970). Jurassic Carbonate Facies and New Ammonite Faunas from Western Greece, *Eclogae Geologicae Helvetiae*, 63, pp. 573-607.
- BRAUN, R.L., and BURNHAM, A.K., (1987). Analysis of chemical reaction kinetics using a distribution of activation energies and simpler models: *Energy and Fuels*, v.1, p.153-161.
- BIRCH, F., ROY, R.F. and DECKER, E.R., (1968). Heat flow and thermal history in New England and New York, in *Studies of Appalachian Geology: Northern and Maritime*, p. 431, eds Zen et al, Interscience, New York
- BURNHAM, A.K., (1989). A Simple Kinetic Model of Petroleum Formation and Cracking. - Internal report of Lawrence Livermore National Laboratory
- BUSSON G., (1988). Relations entre les types de dépôts évaporitiques et la présence de couches riches en matière organique (roches-mères potentielles), *Revue de l'Institut Français du Pétrole*, 43/2, pp. 181-215. (<https://doi.org/10.2516/ogst:1988012>)
- CARSLAW, H.S. and JAEGER J.C. (1959). Conduction of heat in solids. *Oxford University Press*, Oxford, p. 510.
- C. DE GRACIANSKY, P., DE DARDEAU, G., LEMOINE, M. and TRICART, P., (1989). The inverted margin of the French Alps. Geological Society, London, Special Publications. 44. pp. 87-104. (<https://doi.org/10.1144/GSL.SP.1989.044.01.06>)
- CHRISTIANSEN F.G., PIASECKI S., STEMMERIK L. and TELNAES N., (1993). Depositional environment and organic geochemistry of the Upper Permian Ravnefeld formation source rock in East Greenland, *AAPG Bulletin*, 77, pp. 1519-1537.
- CLAYPOOL G. E., & KAPLAN I. R., (1974). The origin and distribution of Methane in marine sediments. In: Kaplan I. R. (Ed.), *Natural gases in marine sediments*, plenum Publ. Corp., New York, pp. 99-139
- CVETKOVIC, M., (2016). Modelling of maturation, expulsion and accumulation of bacterial methane within Ravneš Member (Pliocene age), Croatia onshore. *Open Geosciences*. 8, pp. 5-13. (<https://doi.org/10.1515/geo-2016-0002>)

- DE BEYUKELAER, S.M., MACDONALD, I.I., GUINASSO Jr., N.L., MURRAY, J.A., (2003). Distinct sidescan sonar, RADARSAT SAR, and acoustic profiler signatures of gas and oil seeps on the Gulf of Mexico slope. *Geo-Marine Letters* 23, pp. 177–186
- DEMBICKI, H. JR., (2009). Three common source rock evaluation errors made by geologists during prospect or play appraisals. *American Association of Petroleum Geologists Bulletin* 93, 341–356.
- DEMBICKI, H. JR., (2017). Practical Petroleum Geochemistry for Exploration and Production, Elsevier, pp. 19-60.( <https://doi.org/10.1016/B978-0-12-803350-0.00002-7>)
- DEMING, D., (1994). Overburden rock, temperature and heat flow—essential elements of the petroleum system, in L. B. Magoon and W. G. Dow, eds., The petroleum system—from source to trap: *AAPG Memoir* 60, pp. 165–186
- ENGLAND, P.C., RICHARDSON S.W., (1980). Erosion and the age dependence of continental heat flow, *Geophysical Journal International*, Volume 62, Issue 2, 1 August 1980, pp. 421–437. (<https://doi.org/10.1111/j.1365-246X.1980.tb04865>)
- ETIOPE, G., CICCIOLO, P., (2009). Earth's degassing — a missing ethane and propane source. *Science* 323 (5913), p. 478.
- ETIOPE, G., CHRISTODOULOU, D., KORDELLA, S., MARINARO, G., and PAPTAEODOROU, G., (2013). Offshore and onshore seepage of thermogenic gas at Katakolo Bay (Western Greece). *Chemical geology*, 339, pp. 115-126.
- FYTIKAS, M. D. and KOLIOS, N. P., (1979): Preliminary heat flow map of Greece. In: *Cermak, V & Rybach, L (eds.), Terrestrial Heat Flow in Europe. Springer Verlag, Heidelberg-Berlin-New York*, pp. 197-205 ([https://doi.org/10.1007/978-3-642-95357-6\\_20](https://doi.org/10.1007/978-3-642-95357-6_20))
- GELI, L., HENRY, P., ZITTER, T., DUPRE, S., TRYON, M., ÇAGATAY, M.N., DE LEPINAY, B.M., LE PICHON, X., ŞENGOR, A.M.C., GORUR, N., NATALIN, B., UCARKUS, G., ÖZEREN, S., VOLKER, D., GASPERINI, L., BURNARD, P., BOURLANGE, S., the MARNAUT Scientific Party., (2008). Gas emissions and active tectonics within the submerged section of the North Anatolian Fault zone in the Sea of Marmara. *Earth and Planetary Science Letters* 274, pp. 34–39. (<https://doi.org/10.1016/j.epsl.2008.06.047>)
- GREINERT, J., ARTEMOV, Y., EGOROV, V., BATIST, M., Mc GINNIS, D., (2006). 1300-m-high rising bubbles from mud volcanoes at 2080 m in the Black Sea: hydroacoustic characteristics and temporal variability. *Earth and Planetary Science Letters* 244, pp. 1–15 (<https://doi.org/10.1016/j.epsl.2006.02.011>)
- HERBIN, J.P., FERNANDEZ-MARTINEZ, J.L., GEYSSANT, J.R., El ALBANI, A., DECONINCK, J.-F., PROUST, J.-N., COLBEAUX, J.-P. and VIDIER, J.P., (1995). Sequence stratigraphy of source rocks applied to the study of the Kimmeridgian/Tithonian in the north-west

European shelf (Dorset/UK, Yorkshire/UK and Boulonnais/France). *Marine and Petroleum Geology* 12.

- IGRS-IFP (1966). *Etude Geologique de L'Epire (Grece Nord-Occidentale)*, Paris, Technip Editions, p. 306.
- KAMPERIS, E., IOAKIM, C., TSAILA MONOPOLIS, S. and TSAPRALIS, V., (1992). Geodynamic and palaeogeographic evolution of western Peloponnesus (Greece) during the Neogene, *Paleontologia i evolucion*.
- KAMBERIS E., RIGAKIS N., TSAILA-MONOPOLIS ST., IOAKIM CH. & SOTIROPOULOS SP., (2000). Shallow biogenic gas-accumulations in Late Cenozoic sands of Katakolon peninsula, Western Greece. Geological Society of Greece, *Special Publications*, No 9, pp. 121-138.
- KARAKITSIOS, V., (1990). Chronologie et geometrie de l'ouverture d'un bassin et de son inversion tectonique: le bassin ionien (Epire, Grece), *Memoires Sciences de la Terre, Universite Pierre et Marie Curie, Paris*, 91(4), p. 310.
- KARAKITSIOS, V., (1992). Ouverture et Inversion Tectonique du Basin Ionien (Epire, Grece). *Ann. Geol. Pays Hellen*, 35, pp. 185-318.
- KARAKITSIOS, V., DANELIAN, T & DE WEVER P. (1988). Datation par les radiolaires des Calcaires a Filaments, Schists a Posidonies superieurs et Calcaires de Vigla (zone ionienne, Epire, Grece) du Callovien au Tithonique terminal, *Comptes Rendus de l' Academie des Sciences, Paris, Series II*, 306, pp. 367-372.
- KARAKITSIOS, V. and TSAILA – MONOPOLIS, S., (1988). Donnees nouvelles sur les niveaux superieur (Lias inferieur-moyen) des Calcaires de Pantokrator (zone ionienne moyenne, Epire, Grece continenale), Description des Calcaires de Louros, *Revue de Micropaleontologie*, 31, pp. 49-55.
- KARAKITSIOS, V. & KOLETTI, L., (1992). Critical revision of the age of the basal Vigla Limestones (Ionian Zone, Western Greece) based on Nannoplankton and Calpionellids, with Paleogeographical consequences, *Proceedings of the fourth International Nannoplankton Association Conference (Prague, 1991)* (eds. B. Hamersmid and J. Young). *Knihovnika Zemniho Plynu a Nafty*, 14a, pp. 165-177
- KARAKITSIOS, V., (1995). The Influence of Pre-existing Structure and Halokinesis on Organic Matter Preservation and Thrust System Evolution in the Ionian Basin, Northwestern Greece. *AAPG Bulletin*, 79, pp. 960-980.
- KARAKITSIOS, V. and RIGAKIS, N., (1996). New Oil Source Rocks Cut in Greek Ionian Basin, *Oil & Gas Journal*, 94(7), pp. 56-59.
- KARAKITSIOS, V. and POMONI-PAPAIOANNOU, F., (1998). Sedimentological study of the Triassic solution-collapse breccias of the Ionian zone (NW Greece), *Carbonates & Evaporites*, 13(2), pp. 207-218.

- KARAKITSIOS, V. and POMONI-PAPAIOANNOU, F., (2009). Triassic subsurface evaporates and outcropping solution-collapse breccias of the Ionian zone (Western Greece). *Guide to Symposium and Field trip Evaporites: Sedimentology, Evaluation and Economic Significance (Zakynthos, 2009)*. Hellenic Sedimentological Association, pp.55-58.
- KARAKITSIOS, V., TSIKOS, H., WALSWORTH-BELL, B. and PETRIZZO, M.R., (2004). Preliminary Results on Cretaceous Oceanic Anoxic Events (OAEs) of the Ionian Zone (Western Greece). *Docum. Lab. Geol. Lyon*, 156, pp. 137-138. (<https://doi.org/10.12681/bgsg.16832>)
- KARAKITSIOS, V., TSIKOS, H., AGIADI-KATSIAOUNI, K., DERMITZOGLOU, S., CHATZIHARALAMBOUS, E., (2005). The use of carbon and oxygen stable isotopes in the study of global palaeoceanographic changes: examples from the Cretaceous sediment rocks of Western Greece, *Proc. 1st Meeting C.P.A.S., (Athens, 2005)*, *Bull. Geol. Soc. Greece*, 39a, pp. 41-56. (<https://doi.org/10.12681/bgsg.18445>)
- KARAKITSIOS, V., TSIKOS, H., VAN BREUGEL, Y., KOLETTI, L., SINNINGHE DAMSTE, J.S., JENKYN, H.C., (2007). First evidence for the Cenomanian – Turonian Oceanic Anoxic Event (OAE2 or “Bonarelli” Event) from the Ionian Zone, western continental Greece, *Int. J. Earth Sciences (Geol. Rundsch)*, 96, pp. 343-352. (<https://doi.org/10.1007/s00531-006-0096-4>)
- KARAKITSIOS, V., (2007). Studying the Carbonates from Triassic to Eocene in the Ionian Zone., *IAS 2007 25th Meeting (Patras, 2007)*, *Field Trips guide book, Field Trip P 3*, pp. 123-141
- KARAKITSIOS, V. and RIGAKIS, N., (2007). Evolution and petroleum potential of Western Greece. *Journal of Petroleum Geology* 30, pp. 197–218.
- KLAUCKE, I., SAHLING, H., BURK, D., WEINREBE, W., BOHRAMN, G., 2005. Mapping deepwater gas emissions with sidescan sonar. *Eos* 86, pp. 341–343.
- KLAUCKE, I., SAHLING, H., BURK, D., WEINREBE, W., BOHRAMN, G., BLINOVA, V., LURSMANASHVIL, N., BOHRMANN, G., (2006). Acoustic investigation of cold seeps offshore Georgia, eastern Black Sea. *Marine Geology* 231, pp. 51–67
- KOSTERS, E.C., VANDERZWAAN, G.J., JORISSEN, F.J., (2000). Production, preservation and prediction of source-rock facies in deltaic settings. *International Journal of Coal Geology* 43, pp. 13–26.
- LACHENBRUCH, A.H., (1968). Preliminary Geothermal model of the Sierra Nevada, *J. geophys. Res.*, 73, 6977.
- LACHENBRUCH, A. H., (1970). Crustal temperature and heat production: implication of the linear heat-flow relation, *J. geophys. Res.*, 75, 3291.
- MAGOON, L.B. and BEAUMONT, E.A., (2003). Search and Discovery Article #40068 Adaptation and revision for online presentation of Chapter 3, “Petroleum Systems,” by Leslie B. Magoon and Edward A. Beaumont, in *Exploring for Oil and Gas Traps*, Edward A. Beaumont and Norman H. Foster, eds., *Treatise of Petroleum Geology, Handbook of Petroleum Geology*, 1999.

- MAVROMATIDIS, A., (2009). Review of Hydrocarbon Prospectivity in the Ionian Basin, Western Greece. *Energy Sources, Part A*. pp. 619-632. (<https://doi.org/10.1080/15567030701746943>)
- MARLNELIS, F., ROUSSOS, N., RIGAKIS, N. and KARAKITSIOS, V., (2007). Structural Geology of Western Greece's fold-and-thrust belt. *Challenge our Myths: Energy Conference & Exhibition, AAPG & AAPG European Region (Athens, 2007), AAPG Field Trip, (Athens, 2007). AAPG - Hellenic Petroleum S.A, Field Tripe Guide*, pp. 1-25
- MARAVELIS, A., MAKRODIMITRAS, G. and ZELILIDIS, A., (2012). Hydrocarbon Prospectivity in Western Greece. *Oil Gas European Magazine*. 38. pp. 64-89.
- MARAVELIS, A., MAKRODIMITRAS, G., PASADAKIS, N., & ZELILIDIS, A., (2014). Stratigraphic evolution and source rock potential of a Lower Oligocene to Lower-Middle Miocene continental slope system, Hellenic Fold and Thrust Belt, Ionian Sea, northwest Greece. *Geological Magazine*, 151(3), pp. 394-413. (<https://doi.org/10.1017/S0016756813000289>)
- MILLER R. G., (1990). A paleoceanographic approach to the Kimmeridge clay formation. in Huc A. Y. (ed.), *Deposition of Organic Facies, AAPG studies in geology*, 30, pp. 13-26. (<https://doi.org/10.1306/St30517C2>)
- NAIDU, B., BURLEY, S., DOLSON, J., FARRIMOND, P., & SUNDER, V.R., & KOTHARI, V. and MOHAPATRA, P., (2017). Hydrocarbon generation and migration modelling in the Barmer Basin of western Rajasthan, India: lessons for exploration in rift basins with late stage inversion, uplift and tilting. In: *Am. Assoc. Pet. Geol. Memoir 114: Petroleum System Case Studies. American Association of Petroleum Geologists Memoirs*. 114, pp. 61-94.
- NORTH, F. K., (1985). *Petroleum geology*. Boston, Allen & Unwin.
- PAPANIKOLAOU, D., 1989. Are the Medial Crystalline Massifs of the Eastern Mediterranean drifted Gondwanan fragments? *Geol. Soc. Greece Spec. Publ.*, 1, 63-90.
- PAPANIKOLAOU, D., (1997). The tectonostratigraphic terranes of the Hellenides. Final volume of IGCP 276, *Ann. Geol. Pays Hellen.*, 37, pp. 495-514.
- PEPPER, A.S., CORVI, P.J., (1995). Simple kinetic models of petroleum formation. Part I: oil and gas from kerogen. - *Mar. Petr. Geol. Vol. 12*, No. 3, pp. 291-319.
- POWELL T. G., (1986). Petroleum geochemistry and depositional setting of lacustrine source rocks, *Marine and Petroleum Geology*, 3, pp. 200-219. ([https://doi.org/10.1016/0264-8172\(86\)90045-0](https://doi.org/10.1016/0264-8172(86)90045-0))
- RICHTER, F. M., (1986). Kelvin and the age of the earth, *J. Geol.*, 94, pp. 395-401
- RIGAKIS, N. and KARAKITSIOS, V., (1998). The source rock horizons of the Ionian Basin (NW Greece). *Marine and Petroleum Geology*, 15, pp. 593-617. ([https://doi.org/10.1016/S0264-8172\(98\)00032-4](https://doi.org/10.1016/S0264-8172(98)00032-4))

- RIGAKIS, N., (1999). Contribution to stratigraphic research on wells and outcrops of the Alpine formations in Western Greece, in relation to the petroleum generation efficiency of their organic matter, *Ph.D Thesis*, University of Athens, p. 255.
- RIGAKIS, N., ROUSSOS, N., KAMPERIS, E. and PROEDROU, P., (2001). Hydrocarbon gas accumulations in Greece and their origin. *Bulletin of the Geological Society of Greece*. 34. 1265.
- RIGAKIS, N., KARAKITSIOS, V., MARNELIS, F., & SOTIROPOULOS, S., (2013). Geological solutions concluded by petroleum geochemical data in Western Greece. *Bulletin of the Geological Society of Greece*, 47(4), pp. 2131-2143. (<https://doi.org/10.12681/bgsg.17203>)
- RICE D.D. and CLAYPOOL G. E., (1981). Generation, accumulation, and resource potential of biogenic gas. *AAPG Bulletin*, v. 65, pp. 5-25.
- SCHNEIDER, F., DUBILLE, M., MONTADERT, L., (2016) Modeling of microbial gas generation: application to the eastern Mediterranean “Biogenic Play” *Geologica Acta: an international earth science journal*, vol. 14, núm. 4, diciembre, 2016, pp. 403-417
- STEIN, C.A., (1995). Heat flow of the Earth. *Ahrens, T.J.* (ed), p. 144-158. *Global Earth physics: A Handbok of Physical Constants*. Washington: AGU.
- SWEENEY J. and BURNHAM A.K., (1990). Evaluation of a Simple Model of Vitrinite Reflectance Based on Chemical Kinetics (1). *AAPG Bulletin*. (<https://doi.org/10.1306/0C9B251F-1710-11D7-8645000102C1865D>)
- TISSOT, B.P., WELTE, D.H., (1984). *Petroleum Formation and Occurrence*. Springer-Verlag, New York. 699 p. Ungerer, P., Burrus, J., Doligez, B., Chenet, P.Y., Bessis, F., 1990. Basin evaluation by integrated two-dimensional modeling of heat transfer, fluid flow, hydrocarbon generation, and migration. *American Association of Petroleum Geologists Bulletin* 74, pp. 309–335.
- TOTTERDELL, J., I M STRUCKMEYER, H., BOREHAM, C., MITCHELL, C., MONTEIL, E. and E BRADSHAW, B., (2008). Mid–Late Cretaceous organic-rich rocks from the eastern Bight Basin: implications for prospectivity. *Symposium EABS III*. PESA. Pp. 137-158.
- TSIKOS, H., KARAKITSIOS, V., BOMBARDIERE, L., van BREUGEL, Y., SINNINGHE-DAMSTE, J., SCHOUTEN, S., FARRIMOND, P., TYSON, R.V., and JENKYNS, H.C., (2003). The Oceanic Anoxic Event (OAE) 1b in the Ionian Basin, NW Greece: organic geochemical evidence. In: *Mesozoic paleoceanography in response to palaeogeographic and palaeoclimatic forcings (Séance spécialisée SGF), (Paris, 2003) Soc. Geol. France*, 49.
- TSIKOS, H., KARAKITSIOS, V., VAN BREUGEL, Y., WALSWORTH-BELL, B., BOMBARDIERE, L., PETRIZZO, M. and JENKYNS, H., (2004). Organic-carbon deposition in the Cretaceous of the Ionian Basin, NW Greece: The Paquier Event (OAE 1b) revisited. *Geological Magazine*, 141(4), pp. 401-416. (<https://doi.org/10.1017/S0016756804009409>)

- TROSKOT-CORBIC, T., VELIC, J. and MALVIC, T., (2009). Comparison between the Middle Miocene and the Upper Miocene source rock formations in the Sava Depression (Pannonian Basin, Croatia). *Geol. Croat.*, 62(2), pp. 123-133.
- TURCOTTE, D.L. and SCHUBERT, G., (1982). *Geodynamics: applications of continuum physics to geological problems*, John Wiley, New York
- UNDERHILL, J.R., (1989). Late Cenozoic deformation of the Hellenide foreland, western Greece. *Geol Soc Am Bull* 101: p. 613–634
- VAN HINSBERGEN, D.J.J., VAN DER MEER, D.G., ZACHARIASSE, W.J. and MEULENKAMP J.E., (2006). Deformation of western Greece during Neogene clockwise rotation and collision with Apulia. *Int J Earth Sci (Geol Rundsch)*, 95: 463. (<https://doi.org/10.1007/s00531-005-0047-5>)
- WYGRALA, B., (1989). Integrated Study of an Oil field in the Southern Po Basin, Northern Italy, *Berichte der Kernforschungsanlage Jülich 2313*.
- WANGEN, M., THRONDSSEN, T., and HALVORSEN, G., (2007). The Paleo Heat Flow Contents in Vitrinite Reflectance Observations. *Mathematical Geology*, 39, pp. 491-511. (<https://doi.org/10.1007/s11004-007-9110-z>)
- WAPLES, D.W., KAMAT, H. and SUIZU, M., (1992): The Art of Maturity Modeling. Part 1: Alternative Models and Sensitivity Analysis. - *AAPG Bull.* V. 76, No. 1, pp. 47-66.